LONG-TERM SOIL-STRUCTURE INTERACTION AND DESIGN OF LARGE-SPAN FLEXIBLE CULVERTS

BY

PANAYIOTIS CHARILAOU PAPADOPOULOS

A DISSERTATION PRESENTED TO THE GRADUATE SCHOOL
OF THE UNIVERSITY OF FLORIDA IN
PARTIAL FULFILLMENT OF THE REQUIREMENTS
FOR THE DEGREE OF DOCTOR OF PHILOSOPHY

UNIVERSITY OF FLORIDA

1987

Copyright 1987

by

Panayiotis Charilaou Papadopoulos

ACKNOWLEDGMENTS

I am extremely grateful to every member of the soil mechanics group at the University of Florida whom I have had the pleasure to know. In particular I would like to thank Dr. Michael C. McVay for his direction, challenging discussions, constructive criticism and continuous involvement in every aspect of this research.

I would like to express my appreciation to Dr. Frank C. Townsend for his continuous moral, academic and technical support through the course of my study, for carefully reviewing the manuscript and for serving as chairman on the supervisory committee.

I am thankful to Dr. John L. Davidson for being an excellent teacher, carefully reviewing the manuscript and serving on the supervisory committee.

I would like to express my gratitude to Dr. Duane S. Ellifritt and Dr. Lucas Arvanitis for their cooperation and assistance, for carefully reviewing the manuscript and for serving on the supervisory committee.

I am indebted to Dr. David G. Bloomquist for his invaluable guidance, cooperation and assistance in the use of laboratory equipment and instrumentation, and for carefully reviewing the manuscript.

I would like to express my appreciation to Michael B. Woodward for his invaluable assistance, dedication and hard work throughout the experimental program, and for being a good friend and colleague.

I sincerely thank Habib Tabatabai for his guidance, dedication, assistance and friendship.

I also acknowledge the National Science Foundation, for providing financial support for this study, and Cindy Zimmerman, for her careful work in typing the manuscript.

I am greatly thankful to my fiance, Phanio Cleanthous, for her patience, dedication and assistance throughout the study and for her continuous encouragement and love.

Finally I am deeply indebted to my family for their love and support.

TABLE OF CONTENTS

Page

ACKNOWLEDGMENTS....................................iii

ABSTRACT...ix

CHAPTERS

ONE INTRODUCTION...................................1

- Purpose..1
- Objectives.......................................3
  - Improvement and Validation of Experimental Technique.................4
  - Centrifuge Study.........................4
  - Analysis of Results......................4
- Scope..5

TWO DEFINITION AND DISCUSSION OF PROBLEM...........8

- Structure Configurations.........................8
- Construction Considerations......................11
- Soil-Structure Interaction Concepts..............17

THREE LITERATURE REVIEW............................21

- Full-Scale Instrumentation Studies...............21
- Numerical Modeling...............................25
- Centrifuge Modeling..............................28
  - Centrifuge Modeling of the Underground Conduits..................28
  - Centrifuge Modeling of Consolidation Phenomena...................31
- Conclusion from Literature Review................32

FOUR ANALYTICAL THEORIES AND DESIGN PROCEDURES....34

- Analytical Theories..............................34
  - Marston's Load Theory....................34
  - Ring-Compression Theory..................41
  - Finite Element Method....................42

Design Procedures....................................42
Semi-Empirical Procedures..............42
Design Procedure by Duncan..............48

FIVE EXPERIMENTAL PROGRAM..........................51

General..51
Similitude Theory..............................52
Types of Models..........................53
Development of Similarity Conditions....54
Centrifuge Modeling............................54
Design of Experiments..........................55
Model Scale................................55
Selection of Soil Types.................56
Choice of Material Type and Size for Culvert Model.....................57
Selection of Model Geometry.............61
Construction of Culvert Model...........62
Instrumentation..........................62
Testing Program................................73
General...................................73
Test Procedure...........................74
Limitations of Experimental Program..........77
Similitude Limitations..................77
Instrumentation..........................78
Limitations of the Photographic Technique............................79
Test Procedure Limitations..............80

SIX FINITE ELEMENT ANALYSES.....................81

The Nonlinear Soil-Structure Interaction Program......................................81
The Modified Duncan Soil Model...............82
Analytical Program.............................85

SEVEN EVALUATION OF EXPERIMENTAL MODEL.............89

General..89
Finite Element Analysis........................90
Effect of Axial Stiffness...............90
Effect of Fixity of Support.............90
Centrifuge Versus Finite Element Results.....95
Axial Stresses...........................95
Bending Stresses.........................95
Centrifuge Versus Prototype Response........102
Conclusions from Validation Program.........104

EIGHT LONG-TERM SOIL-STRUCTURE INTERACTION OF SUBSURFACE LARGE-SPAN FLEXIBLE CONDUITS.....106

General.....106
Axial Stresses.....107
    Low-Profile Arch.....107
    Semicircular Arch.....107
    High-Profile Arch.....114
Bending Stresses.....118
    Low-Profile Arch.....118
    Semicircular Arch.....122
    High-Profile Arch.....126
Long-Term Axial and Bending Stresses.....126
Crown Movement.....135
    Low-Profile Arch.....135
    Semicircular Arch.....137
    High-Profile Arch.....137
Pore Pressures in the Embankment Clay.....140
    Low-Plasticity Clay.....140
    Medium-Plasticity Clay.....140
    High-Plasticity Clay.....143
Explanation of Pore Pressure Development and Dissipation.....145
Soil Displacement Vectors.....150
    Low-Profile Arch.....150
    Semicircular Arch.....155
    High-Profile Arch.....159
    Structure Deflected Shape.....159

NINE LONG-TERM SOIL-STRUCTURE INTERACTION AND DESIGN OF LARGE-SPAN FLEXIBLE ARCH-SHAPED STRUCTURES.....164

General.....164
Structure Geometry.....164
Soil Plasticity.....167
Comparison with Current Design Procedures...174
    Design Forces and Moments.....178
    Comparisons of Predictions.....178
Methodology for Predicting Long-Term Forces and Moments.....183
    General.....183
    Bending Moments.....187
Limitations of Recommended Method.....191

TEN CONCLUSION.....192

Review of Objectives.....192
Summary of Results.....192

Validation of the Model................192
Long-Term Soil-Structure Interaction...193
Deformations...........................194
Pore Pressures.........................195
Conclusions................................195
Evaluation of the Centrifuge Model.....195
Soil-Structure Interaction.............196
Design Recommendations.................197
Recommendations............................198

APPENDICES

A DIMENSIONAL ANALYSIS OF A SUBSURFACE LARGE-SPAN FLEXIBLE CONDUIT..................199

B DESIGN OF ARTIFICIAL PROTOTYPE INSTALLATION..................................207

C DATA REDUCTION.............................209

D EQUIVALENT MODEL TIME DURING THE COMPACTION OF A LIFT.........................214

REFERENCES..217

BIOGRAPHICAL SKETCH.....................................224

Abstract of Dissertation Presented to the Graduate School
of the University of Florida in Partial Fulfillment of the
Requirements for the Degree of Doctor of Philosophy

LONG-TERM SOIL-STRUCTURE INTERACTION AND DESIGN OF LARGE-SPAN FLEXIBLE CULVERTS

BY

PANAYIOTIS CHARILAOU PAPADOPOULOS

May, 1987

Chairman: Frank C. Townsend
Cochairman: Michael C. McVay
Major Department: Civil Engineering

An investigation of the consolidation effect on subsurface large-span flexible culverts via centrifuge modeling was undertaken in order to improve current perception of long-term soil-structure interaction and to provide recommendations with respect to design methods and procedures.

It has been shown that large-span flexible culverts may undergo adverse response as time progresses. In general such response is the result of a combination of consolidation of the surrounding backfill, cyclic vehicular loading and environmental factors. The influence as well as the parameters which are associated with each of the long-term effects is currently unknown. Furthermore, current design procedures do not account for adverse

response as time progresses. Therefore, in order to advance current design philosophies research efforts must be devoted in this area to obtain information concerning the long-term behavior of large-span flexible culverts which will be subsequently incorporated into design methods.

Centrifuge modeling has the advantage of accelerating the consolidation phenomenon and thus long-term studies become both feasible and economical. Furthermore, it has been successfully employed in modeling the behavior of underground structures including long-term effects.

The experimental program incorporated tests on fully instrumented culvert models and information concerning stresses and deformations in the culvert wall as well as pore pressures and displacements in the surrounding cohesive backfill were continuously monitored and recorded. Model criteria were established based on dimensional analysis and similitude. The performance of the models was validated and conferred through comparison with numerical modeling, measured field response and previous centrifuge tests.

The study focused on the effects of structure geometry and backfill plasticity to the long-term behavior of large-span flexible culverts. The response of the soil-structure system at the end of construction and as time progresses was found to be highly dependent on the above parameters.

CHAPTER ONE
INTRODUCTION

Purpose

Large-span subsurface flexible conduits are generally defined as arch-shape structures with spans ranging from 15 to 50 ft., constructed of structural-plate embedded in an envelope of engineered soil. Such structures are being successfully installed as culverts, grade separations and as a more economical alternative to traditional overpass structures. Subsurface conduits have been used by mankind from the earliest days of civilization but not until the twentieth century was an attempt made for the development of a rational design method based on scientific principles (Marston, 1930).

Because of the ease of construction, the relatively unskilled labor required and the less stringent foundation requirements, underground conduits are regarded as simple structures which have been historically designed based on semi-empirical procedures and simplified analytical theories (ring-compression theory, buckling theory). However, the behavior of a soil-culvert system is a complex interaction between the steel shell and the surrounding envelope of engineered soil.

The development of the finite element method provides a very powerful tool to investigate the soil-structure response. Validation of computer model capabilities was undertaken and correlation studies have proven the numerical characterization of an accurate representation of field behavior (Chang et al., 1980; McVay and Selig, 1982). Several investigators have used the method to study the stress and deformation behavior of underground conduits (Brown, 1967; Abel and Mark, 1973; Katona et al., 1974; Selig, 1975; Duncan, 1976b). Duncan (1979) has developed a design procedure based on finite element analyses of flexible metal culverts having various shapes, section properties and types of backfill.

Since the currently employed constitutive models are rate independent, numerical studies have focused their attention on the structural response due to the backfilling process up to the end of construction and due to vehicular live loading. Similarly, long-term full-scale instrumentation studies to monitor structural and soil response are uneconomical and require a long period of time. As a result, information concerning long-term effects is scarce and such effects are not accounted for in design. Yet, the limited long-term studies have shown that the structure may respond adversely as time progresses (Spannagel et al., 1974; Lefebvre et al., 1976; Selig et al., 1979; ENR, 1983). In general such response is the result of a combination of consolidation of the surrounding backfill, cyclic vehicular loading and environmental factors. The influence as well as the parameters involved with each one is currently unknown. The purpose of this research was to investigate the consolidation effect via centrifuge modeling with particular emphasis on structure geometry and backfill type and to provide recommendations with respect to design methods and procedures. The centrifuge is selected because of its capability to simulate field stresses in the structure as well as in the embankment soil and therefore the response of the model replicates that of the prototype if the same materials are used (Pokrovsky and Fyodorov, 1936; Schofield, 1978; Scott and Morgan, 1977; McVay and Papadopoulos, 1986). Furthermore, it has the advantage of accelerating the consolidation process (Pokrovsky and Fyodorov, 1936; Mikasa and Takada, 1973; Davidson and Bloomquist, 1980; Bloomquist, 1982; Croce, 1982) and therefore long-term studies become both practical and economical.

Objectives

The objectives of this study were divided into three main groups:

1. Improvement and validation of the experimental-modeling technique

2. Study of long-term behavior of subsurface conduits in the centrifuge
3. Analysis of results and design recommendations.

Improvement and Validation of Experimental Technique

The objectives are the following:

1. To study the effects of wall thickness and type of foundation support on the behavior of the culvert using the finite element method, to modify the established scaling laws such that modeling of these parameters will be improved and to recommend model scale
2. To perform finite element analyses of the artificial prototypes for comparison with the experimental data in order to evaluate their reliability.

Centrifuge Study

The objectives are the following:

1. To obtain experimental data which relate to the influence of soil type on the long-term behavior of subsurface conduits
2. To obtain experimental data which relate to the influence of culvert geometry on the long-term behavior of subsurface conduits.

Analysis of Results

The objectives are the following:

1. To analyze the centrifuge results with respect to the long-term behavior of a subsurface conduit

2. To validate or refute present design methods
3. To determine the significance of geometry and soil type in conjunction with long-term effects in order to provide guidelines for future culvert designs.

Scope

An extensive literature review was undertaken in order to obtain state of the art information both in terms of theory and experimental results.

The finite element analysis was utilized to study the effect of plate area on the deflected shape as well as the axial load of the structure. Two finite element analyses were performed for the same installation using different section areas of the culvert wall. A ratio of six between the two areas was used to exaggerate the problem. Furthermore, the effect of fixed support versus pinned support was also investigated. Upon completion of the study, model dimensions and material were selected based on dimensional analysis and similitude. Further finite element analyses were undertaken for the different backfill types in order to compare the end of construction results and therefore evaluate the performance of the model.

A search to obtain the necessary soils as well as laboratory testing to evaluate the properties of these soils was subsequently pursued. In order to study the effect of backfill type three types of soil were selected: a sandy clay of low plasticity, a clay of medium plasticity and a clay of high plasticity. Plasticity was established as a criterion because it can easily be determined in the laboratory and because of its relation to permeability and consolidation. In terms of structural geometry three types of arches were selected: low-profile, semicircular and high-profile. These forms of structures were expected to respond differently during construction and long-term because of the different radii of curvature involved and the resulting deflected shape.

The experimental program consisted of centrifuge tests on the model culverts. The span as well as the depth of cover over the crown of the structure was maintained the same throughout the testing for consistency. The different models were instrumented with strain gages at the springline, thrust beam and crown and with a vertical LVDT to measure crown deformations. A pore pressure transducer was also placed in the surrounding backfill in order to monitor the dissipation of pore pressure during testing. Sequins in the backfill soil were installed and a photographic technique was employed in order to measure soil and structural deformations. Centrifuge modeling of each of the different structures backfilled with each of the different soils was carried out for a total of nine tests.

Experimental results were subsequently employed for analysis of the long-term soil-structure interaction of subsurface flexible arches. The influence of geometry and backfill type were investigated. Based on the radii of curvature of the structure and the backfill's plasticity, suggested design loads were established.

CHAPTER TWO
DEFINITION AND DISCUSSION OF PROBLEM

Structure Configurations

A typical installation of a large-span flexible culvert is depicted in Figure 1. The structure is surrounded by a zone of well compacted granular soil which is commonly referred to as the structural backfill. In general a second zone of embankment fill extends from the structural fill to the boundaries of the embankment. The structure is assembled in the field of corrugated steel or aluminum structural plate of wall thickness varying from 0.10 to 0.50 in. Long-span structures may have spans anywhere from 15 to 50 ft. and backfill depths from a few feet over the crown to hundreds of feet (Selig et al., 1977; Selig, 1980). Geometrical shapes for these structures consist of circular pipes, vertical and horizontal ellipses, single or double curvature arches and pipe arches. Common long-span configurations are depicted in Figure 2. Stiffener beams or angles or concrete thrust beams are frequently used to increase the flexural stiffness of the structural plate and to transfer some of the load to the structural backfill.

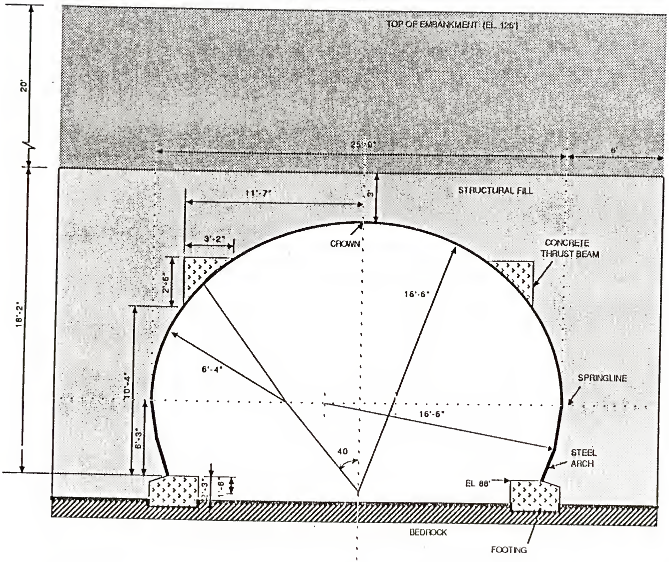

Figure 1. Typical Installation of a Large-Span Flexible Culvert

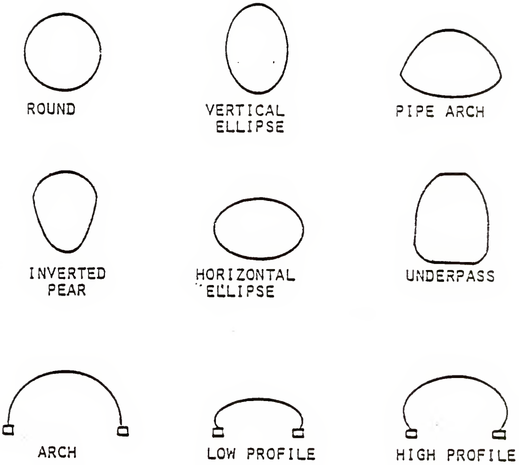

Figure 2. Common Long-Span Configurations

Construction Considerations

A most important aspect of successful large-span culvert installations is that of construction methods and compaction of the surrounding backfill soil. Particular effort must be devoted in controlling the shape of the structure while equipment is working in the near vicinity. The structure geometry must be continuously monitored to ensure that excessive structural distortion will not occur.

Construction procedures are thoroughly reviewed by Selig et al. (1977) and are divided into three major categories:

1. Excavation, Site Preparation and Foundations
2. Assembly of Long-Span Plates
3. Backfilling.

Excavation is usually necessary to create room for the structural backfill and to provide stable slopes for adequate lateral support. Depending on the type of installation, excess water is pumped out and the bedding area is cleaned. In the case of arch foundations, some reduction of the bearing area is necessary to ensure some settlement which is required to develop positive arching.

The assembly of the structural plates is usually accompanied by extensive use of cables, struts or backfill to maintain the shape. Otherwise, different manufacturers have varying requirements with respect to plate placement, alignment and contact or bolt tightening.

Selig et al. (1977) divide the compaction sequence into three major backfilling stages as shown in Figure 3. In the case of structures with invert plates adequate support must be provided in the haunch zone. This is accomplished by using gravelly materials and water jetting for compaction. The second stage involves backfilling along the sides of the structure. The material must be placed in horizontal layers, and care must be taken to maintain a symmetrical geometrical shape by compacting at the same rate on both sides. Spreading and compacting must be initiated at the farthest point from the structure and compaction equipment should travel parallel to the axis of the culvert. Although some peaking of the crown (2%) at this state is encouraged, excessive peaking must be avoided. Concrete thrust beams are poured as soon as the level of the backfill reaches the bottom of the thrust beams. Manufacturers recommend special procedures at this stage according to the different design features that they use (Selig et al., 1977). The next stage begins when the backfill reaches the top of the crown. At this point the equipment should travel from the thrust beams towards the abutments. Then using a light dozer, material must be placed over the crown and compacted using a vibratory roller starting away from the structure and crossing over

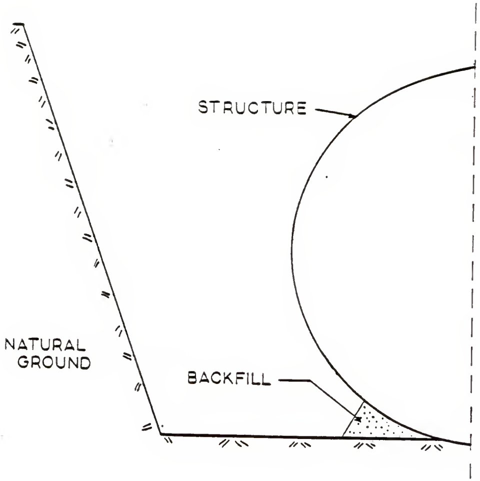

(A)

Figure 3. Backfilling Stages: (A) Backfilling Under the Haunch; (B) Backfilling of the Sides; (C) Backfilling Next to the Thrust Beams; (D) Backfilling Over the Top

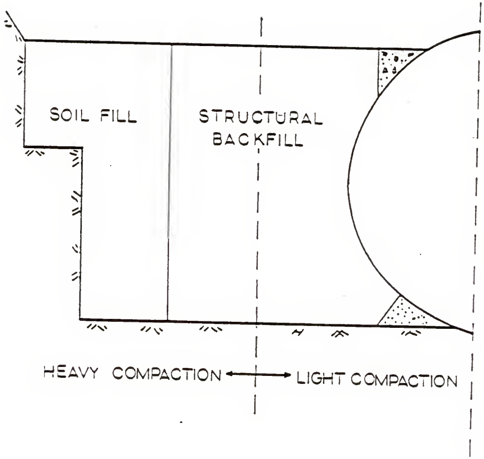

(B)

Figure 3--continued.

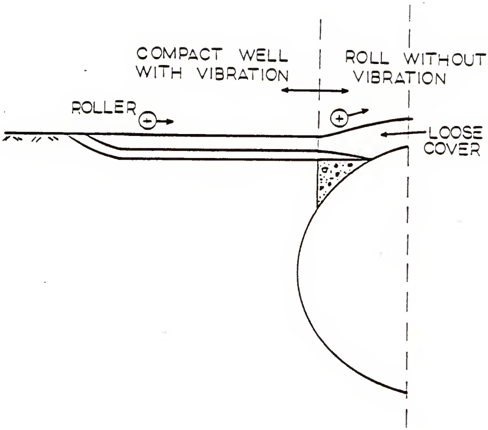

(c)

Figure 3--continued.

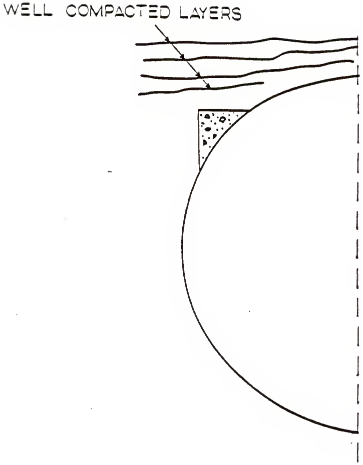

(D)

Figure 3--continued.

the top to the opposite side in a continuous pass. Backfill over the top must be compacted without vibration but as the height of cover over the crown increases this region should diminish. In all three stages excessive construction equipment must be avoided in the vicinity of the structure and continuous monitoring must be provided to prevent excessive distortion of the shape.

Soil-Structure Interaction Concepts

Soil-structure interaction problems generally develop in those cases of foundation engineering where stresses and displacements in the structural element and in the surrounding soil medium are interrelated in a complex manner. In the case of flexible culverts the corrugated steel plate has little stiffness to support the load by itself and the surrounding soil is utilized as a deformation restraining element. As the backfill is placed and compacted, the sides of the culvert move inward while the crown rises. The trend is reversed as soon as placement of soil starts above the crown. The sides of the culvert move outward, the adjacent soil develops passive resistance which prevents further outward movement and the soil lateral pressure increases above the at-rest value. Therefore, "the overburden pressure is redistributed" to the adjacent soil columns (Luscher and Hoeg, 1965; Selig, 1980). Similarly, the soil provides a form of lateral bracing. Since it forces the structure to buckle in higher modes, it increases its resistance to buckling. This aspect of soil-structure interaction was recognized by Luscher and Hoeg (1965) and defined as "deformation restraint." It is, therefore, evident that since neither the structure nor the the soil can support the loads individually they act in unison. The degree of load transfer between each load bearing element is primarily a function of the geometry and flexibility of the structure compared to the surrounding soil medium (Leonards and Wu, 1981). The behavior of a soil-structure system which causes load transfer and pressure redistribution from the structure to the soil and vice versa is defined as "arching." Arching is the most important soil structure interaction concept and has been studied by several investigators (Marston, 1930; Voellmy, 1937; Terzaghi, 1943; Abbott, 1967; Lefebvre et al., 1976). Arching can be either positive (active) or negative (passive). Positive arching is the redistribution of the load on the structure, due to the overlying soil column, to the surrounding soil such that the stress at the crown of the structure is less than the overburden pressure (Figure 4A). In negative arching the load on the structure is larger than the weight of the overlying soil column (Figure 4B). The degree of arching can be quantified with the formula

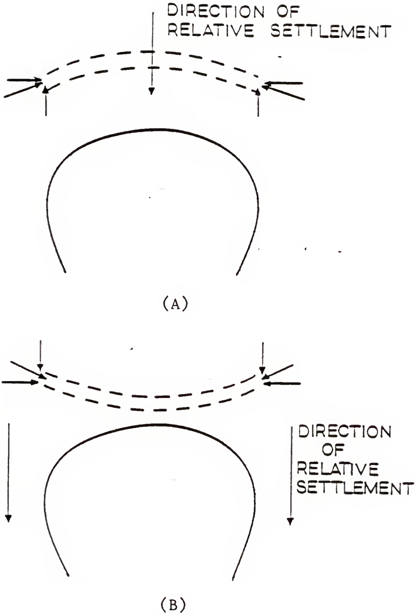
DIRECTION OF RELATIVE SETTLEMENT
(A)
DIRECTION OF RELATIVE SETTLEMENT
(B)

Figure 4. Types of Arching: (A) Positive Arching and (B) Negative Arching

$$A = 1 - \frac{\sigma_{cr}}{\sigma_v}$$

where σ_{cr} = Crown normal stress

σ_v = Overburden stress.

Since the type and extent of load transfer between the structure and the surrounding soil are primarily attributed to relative deformations, the structure geometry and flexibility as well as soil plasticity and compressibility become critical parameters of the system. Most importantly, settlement and consolidation of the soil masses are directly associated with load distribution and the long-term structural integrity of subsurface metal culverts.

CHAPTER THREE
LITERATURE REVIEW

A literature review was undertaken as part of the investigation and also to enhance our perception of the trend in current research, its abilities and limitations. The literature on the subject is very extensive; therefore, the context of this chapter was selected to provide a sample of work in the following areas:

1. Full-scale instrumentation studies
2. Numerical methods
3. Centrifuge modeling.

Full-Scale Instrumentation Studies

Marston (1930) performed studies on concrete, cast iron and corrugated metal pipes. Spangler (1973) monitored the installations for 21 years. In general the load on the corrugated metal culvert was 35% less and more uniform than the other two pipe-types which carried approximately the same load with the same distribution. Based on the fact that arching persisted even after all finite relative movements have ceased, Spangler suggested that not only relative movement but also tendency for such movement can cause arching.

Results from three full-scale instrumentation studies were reported by Selig (1975). The installations were long-span flexible culverts. The instrumentation on the Kettle Creek culverts consisted of inductance coil strain sensors. Readings were taken periodically until 3 1/3 years after the completion of the embankment which showed that although the distribution of the strains remained the same, the magnitude increased significantly. Volumetric strains as much as 4.4% were measured in the surrounding soil. In the case of the Thunder Bay culvert a relief slab was employed since the height of fill was only 10% of the span. The study included measurements of soil strains and earth pressures in the vicinity of the structure as well as deflections of the structure itself. The springline moved inward at the early stages of backfilling. When backfilling started over the crown, the trend was reversed but outward movement was significantly prevented by temporary struts wedged inside the structure to carry some of the soil load. The structure moved further out after the struts were removed. The effect of truck loading was also investigated and was proven to be insignificant. The Port Dover culvert was instrumented with soil sensors and horizontal soil extensometers. In this case long-term strain measurements suggested that the crown was settling while the thrust beams were pushing into the backfill.

Displacements, earth pressures and stresses in the structural wall were measured by Lefebvre et al. (1976) on a large-span flexible culvert. The culvert span was 51 ft. covered by 44 ft. of fill. The height of the arch was 26 ft. The instrumentation revealed that the springline moved 2 in. inward while the crown moved 4 in. upward during placement and compaction of the backfill. Once the fill was placed over the crown, the behavior was reversed. Approximately 50% of the upward movement at the crown and 60% of the inward movement at the springline subsisted to the end of construction. Monitoring of the earth pressures around the periphery of the structure showed that immediately over the crown the pressure was 25% of the overburden indicating a high degree of arching. Bending strains showed little increase during filling over the crown while axial strains increased significantly at the same stage.

The Newtown Creek culvert (Selig et al., 1979) was a 26-ft. span arch with a 23-ft. compacted-soil cover serving as a highway crossing in Bucks County, Pennsylvania. The culvert was built from corrugated steel plates assembled in the field. Two longitudinal reinforced concrete thrust beams were also formed and cast. The structure was instrumented with weldable strain gages for strain measurements which were converted to axial and bending stresses in the culvert wall. Deflections as well as soil strains were also monitored. The structure was pushed inward at the sides during backfilling and the crown deflected upward. The process reversed as soil was placed over the top but the crown was 0.5 in. over its original height at the end of construction. Axial stresses increased at the springline 4 months after the end of construction. Bending stresses varied irregularly but the maximum values were on the order of the axial stresses. The vertical soil pressure in the structural backfill at the springline was considerably in excess of the overburden pressure at the end of construction. The horizontal pressure at the same location was approximately 30% of the vertical. In general the measurements showed that negative arching occurred in 4 months.

Beal (1982) reported field measurements on a long-span aluminum culvert which carries Van Campen Creek in the town of Friendship, New York. The structure was constructed of aluminum corrugated plates with stiffening ribs. The span was 28.5 ft. and the rise 17 ft. 10 in. Displacements and strains of the culvert wall were monitored. Measurements showed that backfill placement resulted in distortion of the shape. In general live-load stresses were small compared to dead-load stresses. Most importantly, design estimates of moment were less than the actual values whereas estimates of thrust were greater.

Numerical Modeling

Brown et al. (1968) performed finite element analyses of underground flexible culverts, incorporating elastic models. The study included numerical modeling of sequential construction. Comparisons of normal stresses at select locations around the periphery of the culvert showed good agreement between the predicted and measured values.

Duns and Butterfield (1971) used the finite element method to analyze underground flexible pipes. Material models were elastic. It was concluded that bending moment in the culvert wall is dependent upon the Young's modulus of the surrounding medium. A nonlinear analysis showed that the thrust varied linearly with fill height while the value at the springline was 20% higher than the overburden pressure indicating negative arching.

The Nonlinear Soil-Structure Interaction Program (NLSSIP) was developed by Duncan (1976a). The program models flexible installations. It incorporates modeling of incremental construction and utilizes the modified Duncan nonlinear soil model.

Katona et al. (1976) formulated another finite element program for the analysis of culverts. The CANDE (Culvert Analysis and Design) which utilizes either of the following soil models in the analysis: linear elastic, overburden-dependent and extended Hardin. They reported that predictions of the program were in good agreement with field measurements on underground rigid and flexible conduits.

Duncan (1976b) illustrated the use of the finite element method in the analysis of the Bell's station culvert in California in order to evaluate the possibility of impending failure due to excessive deformations. He found very good agreement between the theoretical and measured deflection. He also concluded that the structure was performing satisfactorily.

Chang et al. (1980) analyzed a long-span corrugated metal culvert using the finite element method. They found major discrepancies between the measured and predicted behavior in the early stages of construction. However, the numerical prediction was good after the backfill reached crown level. They concluded that the method could provide reasonable predictions of culvert performance.

McVay (1982) performed a critical evaluation of numerical modeling of buried conduit installations. Different soil models were used in the analysis and the results were compared with measured field response to evaluate their suitability. Good agreement was observed between predicted (modified Duncan model) and measured field behavior. The study also revealed that simulation of sequential construction is very important in modeling underground conduits and that agreement between measured and predicted results was achieved without considering interface slip. Finally, compaction wings and thrust beams were found to provide no beneficial effect to justify their use.

Leonards et al. (1985) used a modified version of CANDE to study the performance of buried metal conduits with particular emphasis on the following: different soil models, different interface conditions, importance of the placement of soil in sequence, yielding and buckling of the conduit wall and applications of analysis to practice. They concluded that results are strongly affected by the type of soil model used in the analysis. They suggested that the behavior of the numerical model is also sensitive to interface conditions and that results with fully bonded surfaces are often unrealistic. Another aspect of great importance according to the study is that of construction sequence. The response of the model was found to be very sensitive to the details of soil placement. Initiation of yielding in the conduit walls during construction is not necessarily detrimental, the authors suggested, since it can result in a favorable redistribution of soil pressures. However, buckling of the metal plate was found to be an important failure mode and further research effort in this area was recommended.

Centrifuge Modeling

Centrifuge Modeling of the Underground Conduits

Pokrovsky and Fyodorov (1969) studied the distribution of radial and tangential earth pressures on the periphery of a pipe buried in trenches of varying widths and depths. The backfill soil was clay at a moisture content of 25% and dry sand. They reported maximum radial pressures at the crown and invert and minimum at the springline. They also reported upward tangential pressures around the periphery of the pipe with a maximum at the springline.

Ovesen (1971) investigated the effect of wall thickness on unreinforced concrete pipes. The backfill was uniform dense sand. The centrifugal acceleration level was increased until cracks were registered in the pipe wall. In general thicker pipes cracked at lower acceleration levels than thin-walled pipes indicating that the rigidity of the pipe determines the amount of load transfer on the pipe.

Larsen (1977) investigated the validity of centrifuge testing in soil-structure interaction applications such as buried conduits. He also performed parametric studies by varying the conduit wall thickness, the density of the sand and the geometry of the trench. Radial and tangential earth pressures were measured using miniature load cells embedded in the pipe wall. Larsen concluded that centrifuge modeling is an accurate representation of field behavior. Based on the test results he suggested that the loads on the pipe vary linearly with fill height and that for trench widths less than 1.25H any decrease in trench width causes a substantial decrease in both the vertical and horizontal loads. He also found that wall thickness is a very important factor in determining the amount of load transfer on the pipe. Finally he concluded that agreement between model tests and Marston's theories was on the whole good.

Trott et al. (1984) compared centrifuge modeling of a flexible pipe to a full-scale prototype. Comparisons were made with respect to strain distributions, sustainable loads and structure deflections. They observed appreciable variation in the behavior of the pipes due to differences in the placement and compaction of the sand in the model and the prototype. The placing and compacting of the sand in the prototype produced much higher strains accompanied by appreciable crown deflection in contrast to the model installation which produced negligible effects. However, the distributions of strains measured on the prototype and model pipes for similar applied surface loading configurations were generally in good agreement. A comparison of the behavior under central strip loading and eccentric loading showed good agreement in the distribution of bending stresses but revealed some discrepancies with respect to hoop stresses at the crown.

Takada et al. (1984) performed two series of centrifugal model tests on underground pipes in dry sand with sheet piling. The first series measured normal and tangential stresses on a rigid pipe and the second measured bending moments of a flexible pipe. The study showed significant increases of the normal stress at the crown and invert of the rigid pipe during sheetpile extraction. Normal stress at the crown reached a peak when the lower ends of the sheetpile reached the crown level. In the case of the flexible pipe the bending moment increased remarkably at the start of the first sheetpile extraction and then slightly decreased at the end. They concluded that the behavior of the models was very similar to that of a prototype installation observed in a field test.

McVay and Papadopoulos (1986) investigated the validity of centrifuge modeling of long-term effects due to consolidation on large-span flexible culverts. The study incorporated in-flight simulation of the construction sequence. Tests were performed at different acceleration levels and culvert strains and deformations as well as soil strains and pore pressures were continuously monitored. Results were compared with field information from a selected prototype. In general the correlation between model and prototype was excellent. Pore pressure development and dissipation were observed during construction and long-term as a consequence of compaction and self-weight consolidation. Thrust and bending stresses increased substantially and vertical downward movement of the crown continued as time progressed. The study concluded that centrifuge modeling is an excellent method of simulating prototype long-term response.

Centrifuge Modeling of Consolidation Phenomena

Mikasa and Takada (1973) studied the consolidation process in the centrifuge. They employed the technique of modeling the models. Samples of remolded marine clay were accelerated to 50, 100 and 200 multiples of the earth's gravity. Measurements were made of initial and final solid's contents as well as of the time required to achieve a particular solids content. They concluded that the scaling relationship between times at different gravities was

$$tg_1 = \frac{(g_2)^2}{(g_1)^2} tg_2$$

where g_1 = acceleration level 1

g_2 = acceleration level 2

tg_1 = time to achieve a particular value of solids content at acceleration level 1

tg_2 = time to achieve the same value of solids content at acceleration level 2.

Croce (1982) utilized centrifuge modeling to evaluate consolidation theories. He also applied the technique of modeling the models to verify the scaling relationship between diffusion time in the centrifuge and that in the prototype. Based on the degree of settlement calculated from the height of the model, as well as excess pore water pressure dissipation, he concluded that the scaling relationship for diffusion time is

$$tm = tp/n^2$$

Conclusion from Literature Review

1. Research has progressed towards full-scale instrumentation studies, numerical and centrifuge modeling in order to improve understanding of the principles which govern soil-structure interaction of buried conduits.
2. Full-scale instrumentation studies have shown increased stresses and deformations of flexible conduits as time progresses.
3. The finite element method can be used for predicting the end of construction soil-structure interaction but it is currently incapable of handling long-term effects.

4. Centrifuge modeling has been successfully used in modeling the behavior of underground conduits and the consolidation phenomenon.
5. Centrifuge modeling has been successfully employed in modeling long-term effects on underground large-span, flexible arch-shaped structures.

CHAPTER FOUR
ANALYTICAL THEORIES AND DESIGN PROCEDURES

Analytical Theories

Current design methods have been based primarily on empirical methods and simplified theoretical concepts. Most of the theoretical work deals with the determination of the load on the conduit assuming that shear planes develop in the overlying soil mass. Selection of conduit section is then determined based on compression, buckling and deflection criteria. The most widely utilized design philosophy is that suggested by White and Layer (1960) which has come to be known as the "ring-compression theory," while the most extensive and generalized method of determining loads on underground conduits was developed at the Iowa State University by Marston (1930). Although most of Marston's theory applies to rigid conduits it is reviewed here for completeness.

Marston's Load Theory

The basic soil-structure interaction concept utilized by the theory is that of arching which assumes that shear planes develop in the soil mass such that load transfer occurs between the soil and the conduit. Marston's load theory considers basically four classes of conduit installations (Figure 5) for the purpose of load computation. Ditch conduits are installed in relatively narrow excavations in undisturbed soil backfilled with soil. A positive projecting conduit is installed with its top projecting above the ground surface and then covered with an embankment. Negative projecting conduits are installed in shallow ditches in undisturbed soil and then covered with loose uncompacted soil. Finally, imperfect ditch conduits are installed such that their top projects from the ground surface but are then covered with compacted soil at the sides and loose soil at the top.

The theory assumes that the shear stress on the sides of the overlying soil prism is proportional to the vertical stress such that

$$T = Kf\ \sigma v \qquad (1)$$

where $K = \tan^2 (45-\phi/2)$

$f = \tan\phi$

σv = average vertical stress on the section

such that the load on rigid ditch conduits is of the form

$$Wc = Cd\ \gamma\ b^2 \qquad (2)$$

where Cd is a load coefficient whose value depends on the material type and the ratio of the height of fill to the

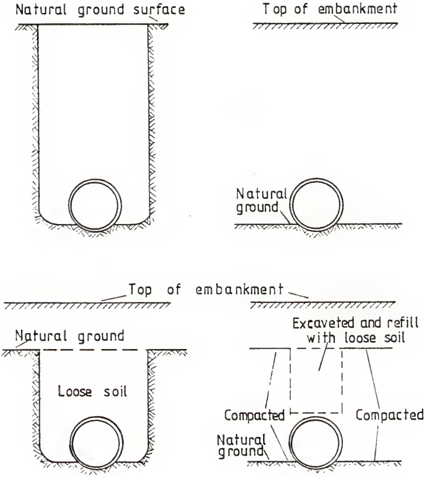

Figure 5. Classes of Conduits Considered by Marston

actual width of a parallel-sided ditch. In the case of a sloping sides ditch the width of the ditch at the crown or slightly below the crown is used.

For projecting conduits shearing can take place up to a certain plane which is defined as a horizontal plane above which no shearing will occur due to addition of a uniform soil layer and therefore the soil prisms over and adjacent to the conduit will settle equally above this plane. The distance between the top of the conduit and this plane is called the height of equal settlement. Although normally the settlement of a prism under its own weight is a function of the characteristic properties of the material and the height of the prism, in this case the exterior prisms transfer some of their weight through shear to the interior prism thereby increasing the downward force. As a result the summation of deformations in the interior prism increases and the height at which these deformations become equal to those of the exterior prisms is the height of equal settlement (Spangler, 1941). Since the magnitude and direction of relative movements determine the load transfer on the conduit, the location of the plane of equal settlement is important. Based on the assumption that the compressibility of the material is constant, the height of equal settlement is a function of the projection ratio, the settlement ratio, the width of the pipe and the material properties of the soil. The projection ratio is defined as the ratio of the vertical projection of the pipe above the ground to the width of the pipe. The settlement ratio is defined by the equation

$$r_{sd} = \frac{(S_m + S_g) - (S_f + dc)}{S_m} \qquad (3)$$

where S_m = Compression strain of the side prisms of height RpBc

S_g = Settlement of the natural ground surface adjacent to the conduit

S_f = Settlement of the conduit into its foundation

dc = Shortening of the vertical height of the conduit.

Once the height of equal settlement is determined, the coefficient Cd in equation 2 above is computed from the equilibrium of forces acting on the soil prisms above the pipe. Since there is no rational method for computing R_{sd}, it is usually determined from previous experience or recommended values.

Flexible conduits generally deflect more than rigid conduits; therefore, they are expected to carry less load. For the case of a flexible pipe in compacted backfill such that it provides the same resistance as the pipe itself, Spangler (1941) suggests the following modification of equation 2:

$$W = C_d \gamma B_d^2 (B_c/B_d) = C_d \gamma B_d B_c \tag{4}$$

Furthermore, it is recognized that since flexible conduits generally fail by deflection rather than yielding or rupture of the wall, it is necessary to have a theoretical prediction of the expected deflection. Based on a number of field experiments on flexible culverts, the following conclusions were made:

1. The load on the pipe is as determined from Marston's theory.
2. The pressure distribution on the pipe is as shown in Figure 6.
3. Deflections can be estimated with the formula developed by Spangler (1941):

$$\Delta x = D_e \frac{K W_c \nu^3}{EI + 0.016 E' \nu^3} \tag{5}$$

where Δx = horizontal deflection of the pipe

D_e = deflection lag factor (depends upon the quality of backfill; 1.25 recommended for design purposes)

K = a bedding constant; values range from 0.110-0.083 depending on bedding angle

W_c = load per unit length

ν = mean radius of pipe

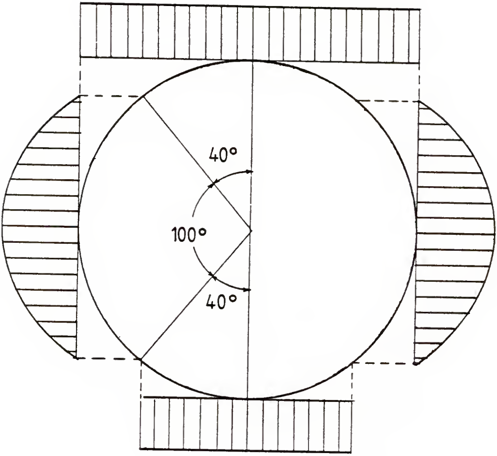

Figure 6. Pressure Distribution on Flexible Pipe

E = modulus of elasticity of the pipe material

E' = modulus of soil reaction.

Ring-Compression Theory

The ring-compression theory is a simple concept which provides an estimate of the load carrying capacity as well as the mode of behavior of the pipe. According to ring-compression theory the structural wall behaves primarily as a membrane; thus bending moments are insignificant. The pressure on the culvert wall is equal to the overburden pressure. The axial thrust is given by the equation

$$T = Pv * D/2 \tag{6}$$

where Pv = Magnitude of the pressure due to the dead load of the soil

D = Effective width of the pipe.

Estimates of the compressive force are used for design considerations.

A basic difference between the two theories as they apply to flexible culverts is with respect to design criteria. According to Marston and Spangler deflection will generally control design whereas White and Layer (1960) impose strength criteria with respect to compressive stress in the pipe wall.

Finite Element Method

The finite element method is currently the most reliable analytical tool for many applications and the soil-structure interaction of underground conduits is certainly one of them. The mechanics of the method have been described elsewhere (Zienkiewicz, 1977). Among the characteristics of an installation that can be modeled by the method are the geometry of the structure, the material properties, backfilling effects due to incremental construction and frictional slippage of soil-structure interfaces. Correlation studies have proven the method to be reliable (Chang et al., 1980; McVay and Selig, 1981) and a design procedure has been developed which is based exclusively on finite element analyses (Duncan, 1979).

Design Procedures

Semi-Empirical Procedures

The design of underground flexible culverts is based upon the concept of ring-compression theory. Live loads, due to highway or railroad loadings, are assumed to be distributed through the earth fill as uniform pressures superimposed on the dead load pressures and are most commonly determined by Boussinesq's formula (Armco, 1958; AISI, 1967). Despite the assumption of ring-compression behavior (i.e., bending moments are not critical), stiffness requirements are applicable for practical handling and installation. Handling stiffness is defined by a flexibility factor. Deflection control is also applicable and is measured with the Iowa formula.

Thus conventional design procedures of corrugated metal culverts involve criteria with respect to the following failure modes:

1. Compression failure
2. Buckling failure
3. Seam compression failure
4. Failure due to excessive deflection.

Duncan (1976a) summarized the acceptable values of the above criteria as shown in Table 1. Design factors for the American Iron and Steel Institute (AISI) and American Association of State Highway and Transportation Officials (AASHTO) were also summarized by Selig (1985) and are presented in Tables 2 and 3. In general the structural design process consists of the following steps:

1. Selection of the backfill density to be expected in the field
2. Determination of the total pressure acting on the steel based on applicable load factors
3. Computation of the compression force in the pipe wall
4. Determination of the required thickness
5. Checking of minimum handling stiffness
6. Checking of bolted seam requirements
7. Checking of corner bearing pressure if necessary.

Table 1
Conventional Design Methods for Corrugated Pipes and Pipe Arches from Duncan (1976)

	AASHO (1969)	USDOT (1970)	AISI (1971)
Design Load	$T = (\gamma H+LL)\frac{D}{2}$	$T = \gamma H \frac{D}{2}$	$T = K(\gamma H+LL)\frac{D}{2}$ for $H \geq D$ $T = (\gamma H+LL)\frac{D}{2}$ for $H<D$
Wall Compression Criterion	$T \leq \frac{f_y A}{2}$	$T \leq \frac{f_y A}{2}$	$T \leq \frac{f_y A}{2}$
	$T \leq \frac{f_b A}{2}$	$T \leq \frac{f_b A}{2}$	$T \leq \frac{f_b A}{2}$
Wall Buckling Criterion	$f_b = \frac{12E}{(\frac{kD}{r})^2}$	$f_b = \frac{12E}{(\frac{kD}{r})^2}$	f_b is less than the AASHO and USDOT value for k=0.22 and higher than the value for
k=0.44			
Seam Compression Criterion	$T \leq \frac{P_u}{4}$	$T \leq \frac{P_u}{3.33}$	$T \leq \frac{P_u}{2}$

Table 1--continued.

	AASHO (1969)	USDOT (1970)	AISI (1971)
Deflection Criterion	Pipes: $\Delta \leq 5\%$ of diameter Pipe arches: no restriction	Circular pipes: $\Delta \leq 5\%$ of diameter Vertically elongated pipes: $\Delta \leq 10\%$ of diameter	No restriction. Usually does not control wall thickness.
Flexibility Factor	$D^2/EI \leq$ limiting values which depend on type of corrugation and metal.	Same as for AASHO.	Same as for AASHO.

Note: A = area of pipe wall
D = diameter of pipe
E = Young's modulus of pipe material
f_b = buckling stress
f_y = yield stress
H = height of fill over culvert
K = load coefficient; values vary with density of backfill; $K=0.86$ for fill compacted to 85% of maximum dry density in standard AASHO compaction test
k = buckling coefficient; $k=0.22$ for good backfill, $k=0.44$ for poor backfill
LL = live load on pipe due to traffic (in pressure units)
P_u = ultimate seam strength (force/length)
r = radius of gyration of pipe wall
T = axial load in pipe wall (force/length)
Δ = vertical deflection
γ = unit weight of soil

Table 2
Summary of AISI Design Factors for Ordinary Structural Plate Conduits

Factor	1967	1971	1983
Largest span (ft)	25	25	50
Factor of safety			
Wall yield			
Arch	?	4	2.7
Other	2	2	2
Wall buckling			
Arch	?	4	2.7
Other	2	2	2
Seam strength			
Arch	?	4	2.7
Other	4	2	2
Flexibility factor[a]			
Arch	0.02	0.02	0.026
Pipe arch	0.02	0.02	0.03
Other	0.02	0.02	0.02
Span (ft.)/cover (ft.)[b]			
Round	21/34	26/35	26/35
Arch	-	26/18	26/27

Note: ? = value unknown.

[a] Inches per pound for 6- x 2-in. corrugation with steel.
[b] From maximum height-of-cover tables.

Table 3
Summary of AASHTO Design Factors for Ordinary Structural Plate Conduits

Factor	1969	1977	1978	1981	1983
Factor of safety					
Wall yield	?	?	2	2	2
Wall buckling	2	2	2	2	2
Seam strength	4	3	3	3	3
Flexibility factor[a]					
Arch	?	?	?	0.03	0.03
Pipe arch	?	0.03	0.03	0.03	0.03
Other	0.02	0.02	0.02	0.02	0.02

Note: ? = value unknown.

[a] Inches per pound for 6- x 2-in. corrugation with steel.

Design Procedure by Duncan

Based on a series of finite element analyses of long-span flexible culverts, Duncan (1979) proposed a simple design procedure for deep and shallow cover conditions. The procedure is applicable to structures with or without stiffening ribs but does not apply to structures which employ horizontal ribs and fin plates to stiffen the upper part of the structure.

The analyses showed that the load carried by these structures exceeds the weight of the overburden soil and that the ring-compression forces can be approximated with the following equation for design purposes:

$$P = Kp1\ \gamma\ S^2 + Kp2\ \gamma\ HS + Kp3\ LL$$

where P = maximum axial force in culvert in kips

γ = unit weight

S = span

H = cover depth

LL = live load

$Kp1, Kp2, Kp3$ = coefficients determined from figures. The prediction of the axial force from this formula is in general 30-40% higher than ring-compression theory; therefore, a lower factor of safety is appropriate. A value of 1.5 is recommended.

With respect to bending moments it was found that they can be related to the relative stiffness of the backfill by means of a dimensionless ratio defined as follows:

$$Nf = Es\ S^3/EI$$

where Nf = flexibility number

Es = secant modulus of backfill soil

S = span

E = Young's modulus for the culvert

I = moment of inertia per foot of culvert.

Bending moments can be approximated from the equation

$$M = Rb\ (Km1\ \gamma\ S^3 - Km2\ \gamma\ S^2H)$$

where M = maximum bending moment due to backfill loads

Rb = moment reduction factor which varies with rise to span ratio

Km1,Km2 = moment coefficients determined from figures.

For conditions of shallow cover, where moments due to live loads are important, the moment should be increased at the quarter point by the following:

$$\Delta ML = RL\ Km3\ S\ LL$$

where dML = additional moment due to live load
RL = reduction factor for live load moment
Km3 = live load moment coefficient.

The dividing point between shallow cover and deep cover occurs when the height of backfill over the crown is such that H/S = 0.25. For such a case a factor of safety against development of a plastic hinge should also apply. It can be calculated from the following formula:

$$F_p = 0.5\ \frac{P_p}{P_1}\left\{\sqrt{\left(\frac{M_1}{M_p}\right)^2\left(\frac{P_p}{P_1}\right)^2 + 4} - \left(\frac{M_1}{M_p}\right)\left(\frac{P_p}{P_1}\right)\right\}$$

where P = axial force
Pp = fully plastic axial force
M = bending moment
Mp = fully plastic moment.

The procedure has been used to design several successful metal culverts and comparisons of field behavior with finite element results show good correlation (Duncan, 1979).

CHAPTER FIVE
EXPERIMENTAL PROGRAM

General

Reduced-scale models have been extensively used in geotechnical research and design. In general a geotechnical model is a reduced-scale structure built according to laws of similitude such that when tested its behavior may be correlated to that of a real prototype, an artificial prototype or an idealized numerical characterization (James, 1972). The technique of investigating the behavior of a system through modeling involves the very important aspects of theoretical similitude and experimental stress analysis. Theoretical similitude specifies the requirements for geometry, materials, loading and interpretation of the results such that correlation between model and prototype can be achieved. Establishing similitude stipulations requires extensive insight into the problem under investigation and in particular to the parameters that influence prototype and model behavior. On the other hand the broad field of experimental stress analysis provides with the equipment, methods and procedures to measure loads, stresses, strains, deformations, pressures and any other quantity such that the behavior of a system can be investigated.

Similitude Theory

Dimensional analysis and Buckingham's pi theory (1914) are the basis of modeling today. According to dimensional analysis, any aspect or law of nature can only be described by a mathematical formulation which is dimensionally homogeneous. In other words the governing expression must be valid in any consistent system of units. Furthermore any such expression can be expressed in the form

$$F(X_1, X_2, X_3, \ldots, X_n) = 0$$

where (X1,X2...Xn) are the physical variables.

According to Buckingham any dimensionally homogeneous equation expressed in the above form can also be reduced to

$$f(\Pi_1, \Pi_2, \Pi_3, \ldots, \Pi_m) = 0$$

where the pi terms are dimensionless products of the physical variables. Since f is only a function of dimensionless parameters, it does not depend on the magnitudes of the measures used to characterize the Xi parameters. Thus a necessary condition for similitude between a prototype and a reduced-scale model is that the pi terms are equal and the functionals f are identical for the two physical systems. The form of the functional relationship between the dimensionless products would have to be determined by experiments which would involve subsequent variation of the ratios in the form of a parametric study.

Types of Models

Depending on the objectives of modeling, models can be classified as research, instructional, or design models (Sabnis et al., 1983). Research models which are used to derive generalizations with respect to the behavior of a structural system, or to provide data such that a theory may be substantiated, require simulation of every stipulation set by the modeling theory with respect to materials, geometry, boundaries, even construction and erection procedures. The degree of sophistication in the case of design models varies depending upon the information that the designer wants to derive from the model. Finally, instructional models require much less accuracy as they are usually used to demonstrate a theoretical concept.

Although it is well recognized that research and design models require simulation of all the details involved, it is not always possible to satisfy all similitude requirements. The engineer has to be able to recognize which of these requirements are of first order priority to the behavior of the model. Sabnis et al.

(1983) describe three types of models based on the level of similarity with the prototype. A true model is one which is completely similar with the prototype. An adequate model is one which does not satisfy some of the stipulations set forth by similitude theory because it can be proved that they are not of first order priority. A model that does not satisfy important modeling requirements is a distorted model.

Development of Similarity Conditions

Dimensional analysis and similitude stipulations as they apply to centrifuge modeling have been extensively discussed by others (Pokrovsky and Fyodorov, 1969). The complete dimensional analysis of a culvert is presented in Appendix A.

Centrifuge Modeling

In geotechnical problems one of the controlling parameters is the nature of the soil and its characteristics. In a reduced-scale model, modeling the complex behavior of soil is practically impossible. The need to maintain similitude of stress and strain deems the necessity of modeling the engineering properties of soil. As a result the same soil must be used in the model and prototype. Furthermore, the problem is accentuated by the need to simulate the geostatic stresses since the primary loading configuration is self weight. In a gravity representation the geostatic stresses will be small and the stress state in the medium will not be represented. Therefore, in order to achieve similitude between model and prototype the same soil must be used in an artificial gravitational field such that the self weight will be increased. A convenient gravitational field is that due to circular motion which can be adjusted with angular velocity and can be achieved in a centrifuge. In such representation the geostatic stresses in the model and prototype are the same (Pokrovsky and Fyodorov, 1936, 1968, 1969). Moreover the diffusion process is accelerated and consolidation phenomena occur faster such that long-term studies become both practical and economical.

Design of Experiments

Model Scale

Based on the results from the correlation study by McVay and Papadopoulos (1986) it was concluded that there was no scale effect distorting the centrifuge results. Therefore, the selection of model scale was based primarily on the capacity of the centrifuge container vessel. In particular the size of the model was such that the soil would extend at least half the span on both sides and that the height of cover above the crown would be sufficient to be considered deep. Finally, the largest possible size that would satisfy the above restrictions was selected in order to make the instrumentation process easier and to avoid having a very small model compared to the grain size of the surrounding soil. Therefore, a model scaling factor of 55 was applied throughout the experimental program.

Selection of Soil Types

Since the thrust of the research reported herein was to study the long-term consolidation effects of cohesive soils on subsurface large-span culverts, the selection of soil type was a critical aspect of the investigation. Emphasis was devoted in selecting soils that are representative of the backfill types that are commonly used in the field. On the other hand distinct differences between the properties that most critically affect the consolidation process were also desirable such that any variation between the responses of the soil-structure systems under study would be significant enough to enable the investigation to draw definite conclusions concerning the effects of different soil properties. Therefore, it was concluded that the study should include soils of low and medium plasticity which are commonly used in the field, as well as a high-plasticity soil which would accentuate the consolidation effect and would bound the range of long-term effects. Plasticity was established as a criterion on the following justification:

1. It is a property that has been directly or indirectly related to permeability and consolidation by other investigators.
2. It can be easily determined in the laboratory and in the field and therefore it provides a simple criterion to be used in design.

The properties of the backfill soils which were selected based on the above reasoning are depicted in Table 4.

Choice of Material Type and Size for Culvert Model

The dimensional analysis of the culvert has shown that if the same material is used between the model and prototype, then the area per unit length of the model relates to that of the prototype by the following expression:

$$A_m = \frac{A_p}{n}$$

where A_m = model area

A_p = prototype area

n = scale factor

and the moment of inertia per unit length by the expression:

$$I_m = \frac{I_p}{n^3}$$

Table 4
Backfill Properties

	Low-Plasticity	Medium-Plasticity	High-Plasticity
Maximum Dry Density	18.69 119 pcf	17.28 110 pcf	[illegible] 81 pcf
Optimum Moisture Content	13%	13%	36%
Liquid Limit	21%	33%	71%
Plastic Limit	15%	17%	40%
Plasticity Index	6%	16%	31%

13[illegible] 126.4 12[illegible]6

21.44 19.87 [illegible].5

where I_m = model moment of inertia per unit length

I_p = prototype moment of inertia per unit length.

However, in order to satisfy the above requirement an extremely thin plate would be necessary which would have to be corrugated to the prototype shape. Although such a similarity would be highly desirable, it is nearly impossible to be achieved. However, it has been suggested (Duncan, 1979; McVay, 1982; Papadopoulos, 1985; McVay and Papadopoulos, 1986) that the deflected shape of large-span culverts is primarily controlled by the bending stiffness rather than axial stiffness of the culvert. Although flexible culverts support the load mainly in axial compression, the amount of load transferred to the culvert is determined by the deflected shape. Therefore, similitude of the bending stiffness is more important for the purpose of this study which investigates the long-term degree and type of load-transfer between the structure and the surrounding soil. Similitude of bending stiffness requires that

$$\frac{E_m I_m}{C_m} = \frac{E_p I_p}{C_p n^2}$$

where E_m = model Young's modulus

E_p = prototype Young's modulus

C_m = model distance from neutral axis to outside fiber

C_p = prototype distance from neutral axis to outside fiber;

therefore, the load transfer in the model correlates to that of the prototype by the expression:

$$P_m = \frac{P_p}{n}$$

where P_m = model axial load

P_p = prototype axial load,

which results in the following relationship for bending moments:

$$M_m = \frac{M_p}{n^2}$$

where M_m = model moment

M_p = prototype moment,

and the following relationship for bending strain:

$$E_{bm} = E_{bp}$$

where E_{bm} = model bending strain

E_{bp} = prototype bending strain.

In order to satisfy the above relationship an aluminum plate of thickness 0.025 in. was used. This size of plate results in the following relationship for axial stresses in the structural wall:

$$\sigma_{a,p} = \frac{nP_m}{A_p}$$

where $\sigma_{a,p}$ = prototype axial stress.

Although similitude is violated with respect to axial stiffness, the model is adequate since it was shown that the effect of axial strain is small to the degree and type of load transfer.

Selection of Model Geometry

Selection of the different geometries to be used in the study was based on the following criteria:

1. The models should simulate representative artificial prototypes.
2. The different shapes should incorporate the same span and the same height of cover such that any differences in the response would come due to variations of the radii of curvature and not due to the different overburden weight.
3. The structures should have different rise-to-span ratios which would be used as the varying parameter. The three most commonly used shapes for long-span structures are the low-profile, semicircular and high-profile arches. The low-profile and high-profile arches have a larger radius of curvature at the crown than the

semicircular. The high-profile arch has a shorter radius of curvature in the vicinity of the thrust beam and then the radius increases to that at the crown. The selected artificial installations to be modeled by this study are depicted in Figures 7-9.

Construction of Culvert Model

The culvert model was made out of an aluminum plate 0.025 in. thick, such that the bending stiffness would be simulated and the axial stiffness would not deviate significantly from similitude requirements. The plate was cold rolled at the University of Florida machine shop in order to obtain the appropriate curvature. Delicate care was taken in order to obtain a symmetrical shape with uniform cross section along the axis of symmetry and in order to avoid kinks and potential plastic hinges in the metal.

Instrumentation

In view of the nature of the long-term soil-structure interaction problem as it applies to large-span culverts (i.e., increased stresses and deformations) it was decided that the response of the culvert models could be best described in terms of stresses, strains and deformations of the structure as well as pore pressures in the backfill which would give a qualitative and quantitative indication of the consolidation phenomenon that would take place. As a result the selected instrumentation consisted of strain

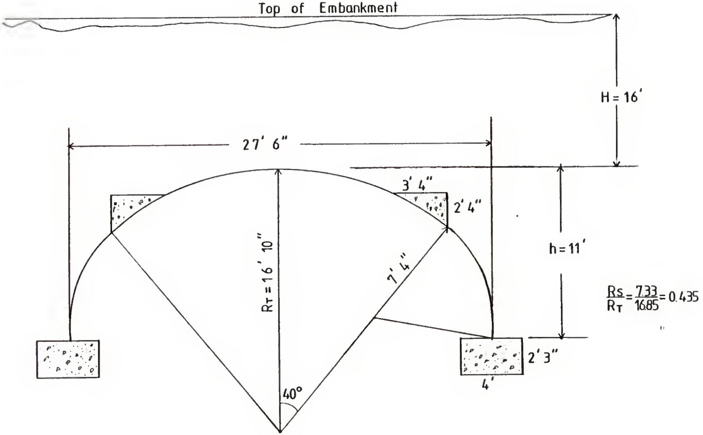

Figure 7. Low-Profile Arch

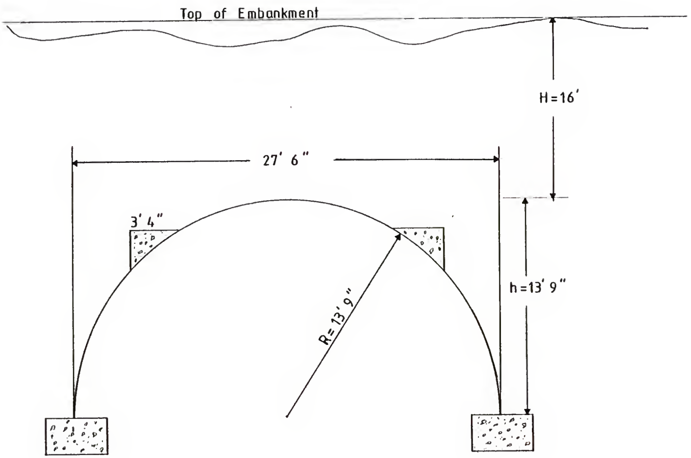

Figure 8. Semicircular Arch

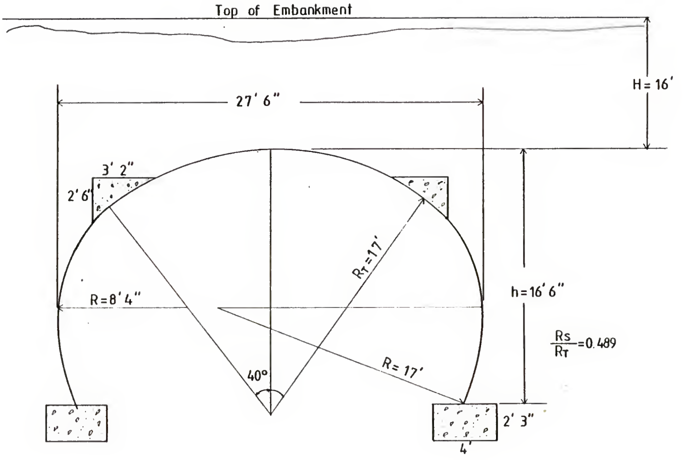

Figure 9. High-Profile Arch

gages mounted on the periphery of the culvert wall, a linear variable differential transformer (LVDT) to measure deformations of the crown, a pore pressure transducer to monitor the pore pressure of the backfill at the springline level and sequins in the soil in order to employ the photographic technique by Avgherinos (1969).

Strain gages. Electrical resistance strain gages were mounted in pairs around the periphery of the culvert models. Since any effects due to nonsymmetrical deformation of the culvert were not to be investigated, it was assumed that stresses and deformations of each side would be the same. Similarly, since the shape and loading of these structures approximate a plane strain condition, it was assumed that every section would behave similarly. Therefore, strain gages were mounted at the springline, thrust beam and crown locations as shown in Figures 10-12. Three sections were instrumented to provide redundancy and to account for possible wear. Gages were epoxied to the inside and outside of the culvert wall at the same location. The arrangement of the gages in this manner permitted the measurement of bending and axial strain at each location. Since three locations were instrumented at three sections nine pairs were required for a total of 18 gages. Micromeasurements fully encapsulated constantan precision strain gages designated as

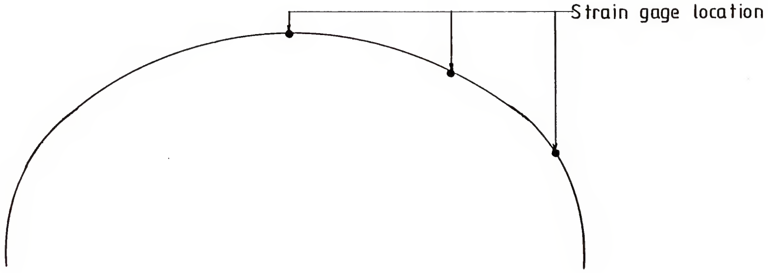

Figure 10. Strain Gage Locations, Low-Profile Arch

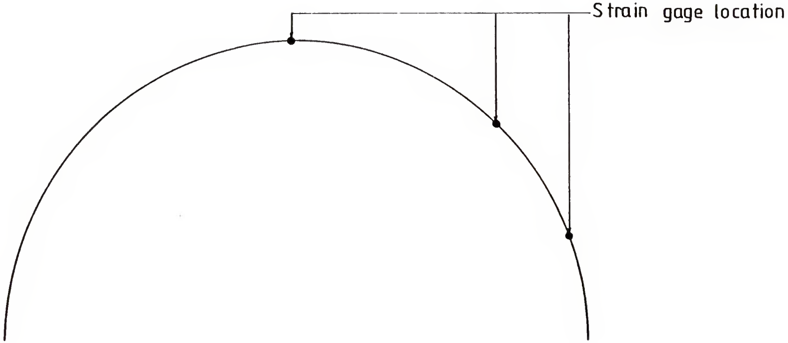

Figure 11. Strain Gage Locations, Semicircular Arch

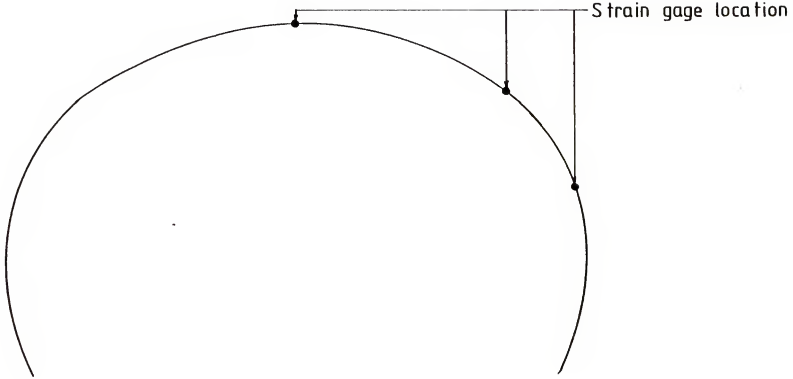

Figure 12. Strain Gage Locations, High-Profile Arch

WA-06-125AD-120 option LE were used which provided a resistance of 120 ohms and a gage factor of 2.04, self-temperature compensation, four integral high-endurance lead ribbons and a backing and encapsulation matrix consisting of a high-temperature epoxy phenolic resin system reinforced with glass fiber.

Linear variable differential transformer. This type of transformer is an excellent device for converting a mechanical displacement into an electrical signal. The displacement is transmitted to a core which moves relative to a set of coils such that an electrical output is produced across the coils. An LVDT with a Schweitz Transducer Indicator (Figure 13) which was calibrated prior to installation was used to measure crown deformations. The LVDT was mounted between the culvert model and the bottom of the container as shown in Figure 14.

Pore pressure transducer. A Druck miniature 1-bar PDCR-81 transducer with a Doric Transducer Indicator 420 calibrated prior to installation was used to measure pore pressures in the cohesive backfill. A similar device has been successfully used in earlier studies by Morris (1979) and McVay and Papadopoulos (1986).

Photographic technique. In order to measure soil strains in the backfill the photographic technique as described by Avgherinos (1969) was employed. A grid was

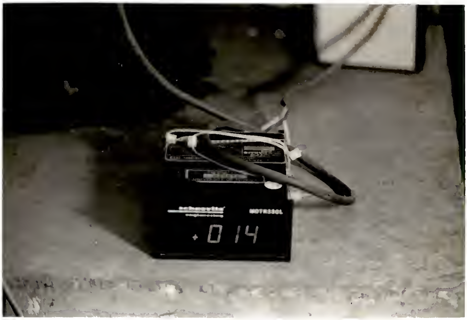

Figure 13. Schweitz Transducer Indicator

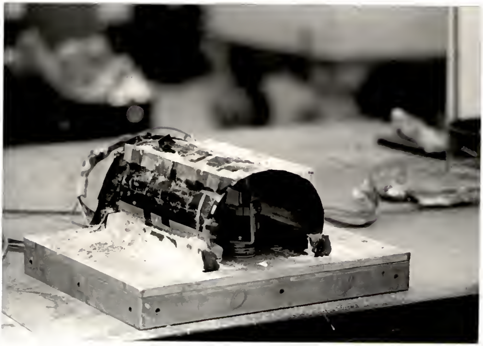

Figure 14. Linear Variable Differential Transformer

drawn on the inside of the plexiglass plate and straight pins with flat heads were placed across the top of each lift of backfill. In order to measure structure deformations the edge of each culvert facing the transparent side of the container was marked with black stripes. Displacements were calculated by measuring the relative displacements of the pins on successive photographs. A Swiss Kern DSR-1 device which is accurate to one micron was used to measure the relative movements of the markings. This effort was greatly limited by the fact that photographs could only be taken after the centrifuge had been spun and therefore some rebound of the backfill and of the elastic structure due to reduced overburden weight was bound to occur. Although the technique did not allow for exact measurement of soil strains and structure deformations, it revealed the trend of soil movement as well as an approximate deflected shape for each culvert geometry.

Testing Program

General

Nine centrifuge tests were performed on flexible metal culverts. The investigation incorporated variation of structure geometry and variation of backfill type. All tests incorporated the same testing procedure, the same instrumentation and the same centrifugal acceleration.

Test Procedure

Once a model was built and instrumented, it was mounted on the removable bottom plate of the container (Figure 15). High strength epoxy was used for the attachment in order to prevent any lateral movement of the model at the supports and to simulate the rigidity of the prototype foundations. The bottom plate was then bolted on the swinging vessel inside the centrifuge and all wires from the various transducers were taped on the sides of the container and brought out through the top. The wires were then connected to the centrifuge slip rings and signals were carried out through them to the data acquisition systems (Figure 16). Since it was recognized at the outset that the construction process significantly affects culvert behavior, the construction of the embankment was part of the centrifuge test. As a result the test procedure typically consisted of the following steps:

1. accelerating the culvert model and recording initial readings from all instruments while spinning at test acceleration level
2. placing the first lift of structural backfill as well as embankment soil on both sides simultaneously and compacting using hand tamping
3. accelerating the centrifuge to test acceleration level and take a reading from all instruments

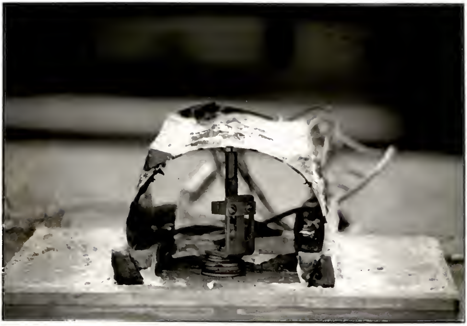

Figure 15. Culvert Model

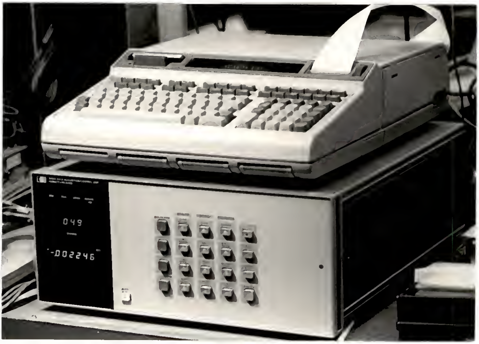

Figure 16. Data Acquisition System

4. installing the pore pressure transducer at the end of construction of the first lift (care was taken to ensure that the porous stone was saturated and that it was covered with muddy, fully saturated soil)
5. placing sequins in the backfill
6. placing the next lift and repeating steps 3 and 5
7. attaching the thrust beams on the culvert once the embankment reached the appropriate height
8. placing the rest of the embankment repeating steps 2, 3 and 5 until the fill reached the appropriate height
9. accelerating to the test acceleration level for as long as it was necessary in order for pore pressures to dissipate while taking readings from all instruments at regular intervals.

The total test duration was typically 10 hours for the low-plasticity clay, 14 hours for the medium-plasticity clay and 20 hours for the high-plasticity clay. No compaction was carried over the crown in order to simulate the light compaction that occurs in the prototype.

Limitations of Experimental Program

Similitude Limitations

As was mentioned earlier similitude is violated with respect to axial stiffness of the culvert wall. In fact the axial stiffness of the model is twice that of the prototype. However, it has been shown that the model is an adequate one since the load on the structure is primarily controlled by the bending stiffness. In order to further support this point a finite element analysis was carried out with different axial stiffnesses of the culvert wall to investigate its effect. Results from this analysis are presented in the next chapter.

A second similitude limitation is that of modeling the fixity of the support. In prototype installations there exists a bolted connection between the culvert plate and the supporting channel. This type of support, although usually modeled as a pin, has some moment capacity but cannot be characterized as fixed. This intermediate type of fixity was difficult to achieve in the model but emphasis was devoted in the micro concrete supports to allow for some rotation. This effect was also investigated with the finite element analysis and results are presented in the next chapter.

Instrumentation

Instrumentation on the culvert model and in the surrounding backfill was limited by the number of the centrifuge slip rings. Repeatability of strain-gage results was provided by the three instrumented sections on the culvert wall. Since the complete bridge was not assembled on the rotating member with possibilities of electrical noise due to changes in the resistance of the slip-rings, strain-gage redundancy was deemed necessary. Electrical noise was also controlled by a hardware noise filter in the data acquisition system. The number of LVDTs and pore pressure transducers was limited to one of each with no redundancy. However, these transducers work with larger voltages and any effects of slip-ring resistance changes on their measurements are minimized.

Limitations of the Photographic Technique

As was mentioned earlier the primary limitation of the technique which was incorporated in this case was the fact that successive photographs were not taken during centrifuge spinning due to safety precautions and instead were taken after the centrifuge came to a stop. Although rebounding undoubtedly occurred, some permanent deformations did remain to provide evidence with respect to the tendency of soil movement. The photographic technique also assumes that surface pins displace in the same manner as the soil throughout the model. This assumption has been extensively examined by Arthur and Roscoe (1965) who compared strains from radiographs of internal lead shot markers with strains of surface markers. The overall agreement was very good. Other errors due to the photographic technique had been also discussed by Endicott (1970), Beasley (1973) and Larsen (1977). These errors limit the accuracy of the method to displacements greater than 1 mm (Larsen, 1977).

Test Procedure Limitations

It is obvious that this procedure does not model the stress path history of the prototype soil since it involves a loading-unloading pattern due to continuous accelerations and deccelerations in the centrifuge which are not encountered in the field. However, this investigation is not concerned with failure conditions in the soil. The study concentrates on the consolidation phenomenon which is primarily dependent on void ratio. Void ratio will in general continue on the same path of void ratio versus vertical stress curve after unloading and reloading of a drained sample (Lambe and Whitman, 1969). Furthermore, most of the consolidation takes place during the long-term phase of the test which is continuous throughout. It is, therefore, likely that the type and degree of consolidation of the model embankment at the end of a test did not deviate from that of the prototype.

A similar limitation of the test procedure occurs with respect to the metal structure as well, since it encounters a loading cycle which does not occur in the prototype. However, as long as the loads remain within the elastic range the deflected shape of the structure will not be significantly affected. Furthermore, no fatigue problems may arise since the loading-unloading cycles are limited.

CHAPTER SIX
FINITE ELEMENT ANALYSES

The method of finite elements was employed in order to evaluate the adequacy of the model. In particular the effect of the axial stiffness of the culvert as well as the importance of the degree of fixity at the support to the response of the soil structure system was investigated. Furthermore, results from the finite element analyses were used for comparison with the experiment results.

The Nonlinear Soil-Structure Interaction Program

The Nonlinear Soil-Structure Interaction Program (NLSSIP) developed by Duncan (1976b) was employed in the analysis. The program was designed for use on flexible conduits. The culvert structure is modeled as a series of straight beam elements connected at common nodes with horizontal, vertical and rotational degrees of freedom. The program calculates shear and axial forces, bending moments and deflections at each node on the structure. The soil properties are modeled using the modified Duncan or the linear elastic models, and the continuum is modeled with triangular or quadrilateral subparametric elements with two degrees of freedom with respect to vertical and horizontal displacements at each corner node. The program incorporates incremental construction and backfill elements are divided into level layers placed one at a time thus simulating the placement of backfill around and over the structure. A typical finite element mesh is depicted in Figure 17.

The Modified Duncan Soil Model

The nonlinear stress-strain soil behavior is approximated by a hyperbola as suggested by Kondner (1963) and Kondner and Zelasko (1963). The equation of the hyperbola is of the following form:

$$(\sigma_1-\sigma_3) = \frac{E}{(\frac{1}{E_i}) + \frac{E}{(\sigma_1-\sigma_3)ult}}$$

where Ei = initial tangent modulus

$(\sigma 1-\sigma 3)$ult = asymptotic stress difference.

Since the actual stress difference at failure is less than the asymptotic value, a correction factor is introduced:

$$R_f = \frac{(\sigma_1-\sigma_3)f}{(\sigma_1-\sigma_3)ult}$$

Janbu (1963) proposed a relationship between Ei and σ_3 expressed as follows:

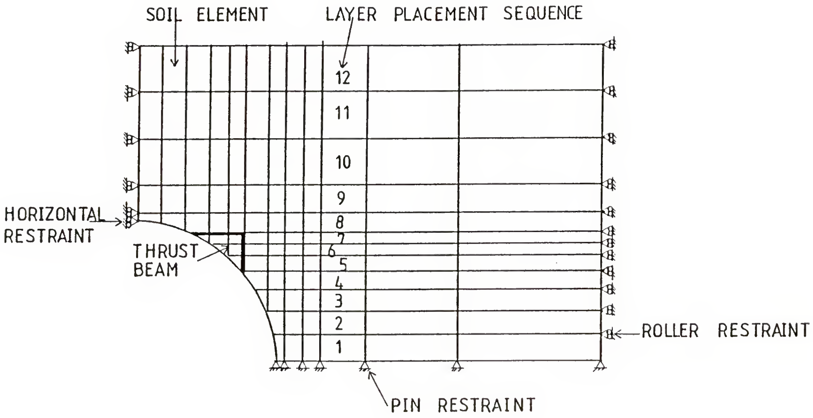

Figure 17. Typical Finite Element Mesh

$$E_i = K\,P_a\left(\frac{\sigma_3}{P_a}\right)^n$$

where P_a = atmospheric pressure

K,n = experimentally determined constants.

Duncan et al. (1980) combined the hyperbolic relationship above, the proposed expression by Duncan and the Mohr-Coulomb strength criteria to form the following relationship for the tangent Modulus:

$$E_t = \left[1 - \frac{R_f(1-\sin\phi)(\sigma_1-\sigma_3)}{2c\cos\phi + 2\sigma_3\sin\phi}\right]K\,P_a\left(\frac{\sigma_3}{P_a}\right)^n$$

The following equation was also incorporated in the model in order to account for the variation of the angle of internal friction with confining pressure:

$$\phi = \phi_0 - \Delta\phi\log_{10}\left(\frac{\sigma_3}{P_1}\right)$$

where ϕ_0 = angle of internal friction for σ3 equal to Pa

= reduction in φ for 10-fold increase in σ3.

The model assumes that the bulk modulus is independent of stress difference and dependent upon the confining pressure as follows:

$$B = K_b\,P_a\left(\frac{\sigma_3}{P_a}\right)^m$$

where $K_{b,m}$ = experimentally determined constants.

Duncan et al. (1980) proposed the values shown in Table 5 to be used in cases where experimental data are not available (low- and medium-plasticity soils).

Analytical Program

The installation was modeled as shown in Figure 17. Only half the installation was considered assuming that the structure, backfill and boundary conditions were symmetrical. The bottom boundary was placed at the top of the footings. The right boundary was placed more than three spans away from the structure. The soil nodes at the bottom boundary were restrained against both horizontal and vertical displacements whereas the nodes of the two vertical boundaries were restrained against horizontal displacements and rotation. Straight beam elements modeled the structure and triangular or quadrilateral isoparametric elements modeled the surrounding soil. Backfill layers were placed incrementally to simulate the sequence of construction. The values for the parameters in the analysis were selected from Duncan et al. (1980), except for the high plasticity clay and they are depicted in Table 5. The properties shown in Table 6 were used for structural plate representation. They were selected from the Republic Steel Sectional Plate Handbook based on the recommended design procedure (Appendix B).

Table 5
Modified Duncan Soil Model Parameters

Parameter	Low-Plasticity	Medium-Plasticity	High-Plasticity
K	150	90	70
n	0.6	0.45	0.4
R_f	0.7	0.7	0.7
K_b	75	80	250
m	0.5	0.2	0.2
ϕ	33	30	30
$\Delta\phi$	0	0	0
γ lb/in.^{3}	0.0625	0.0625	0.0625

Table 6
Prototype Culvert Material Parameters

Steel Corrugated Plate 5-gauge, 2 in.; 6 in. corrugations	
Young's Modulus, E (psi)	= 29,000,000
Moment of Inertia, I (in.^{4}/in.)	= 0.1269
Cross Sectional Area, A (in.^{2}/in.)	= 0.2666
5-Gage Plate Thickness, T (in.)	= 0.218
Distance from Neutral Axis to Outer Fiber C (in.)	= 0.1068

The analytical program involved variation of the axial stiffness of the culvert by reducing the area of the wall. A reduction factor of six was selected. Furthermore, the installation was also analyzed using a structure support with all three degrees of freedom restrained.

CHAPTER SEVEN
EVALUATION OF EXPERIMENTAL MODEL

General

The technique as well as the procedures which are employed in the experimental program reported herein have been extensively validated through comparison with measurements of a field installation (McVay and Papadopoulos, 1986) and excellent agreement has been observed. However, due to the modeling limitations with respect to axial stiffness and fixity of support which were mentioned in the previous chapter and in order to improve current perception of their importance in large-span culvert behavior, a study utilizing the finite element method was undertaken which incorporated variation of these parameters and comparison of the results. Furthermore, since the experimental model incorporated a new modeling feature (modeling of the bending stiffness rather than the moment of inertia), further validation of the centrifuge results was undertaken through comparison with results from the finite element analysis and results from the previous centrifuge study (McVay and Papadopoulos, 1986).

Finite Element Analysis

Effect of Axial Stiffness

The effect of axial stiffness with respect to load transfer on the structure is depicted in Figures 18 and 19. Figure 18 depicts the axial load distribution (all values are compressive) around the periphery of the culvert wall as predicted by the finite element analysis for the actual area of the wall and for a reduced area by a factor of six. It is evident that the load distribution is practically the same with the reduced area carrying slightly less load as expected. Similarly the bending diagram (inside tension is positive) for the two cases is practically the same (Figure 19) which asserts previous evidence (Duncan, 1976b; McVay, 1982; McVay and Papadopoulos, 1986; Woodward, 1986) that the load transfer to the structure is primarily controlled by the bending stiffness and not the axial stiffness.

Effect of Fixity of Support

Figures 20 and 21 depict the influence of a fixed support versus a pinned support with respect to axial load and bending moment distribution. Axial load is practically the same for the two cases (Figure 20). The bending moment diagram is slightly affected and some difference exists primarily in the vicinity of the support. However, since the two cases of completely fixed and pinned supports represent the two extremes with relatively small variation

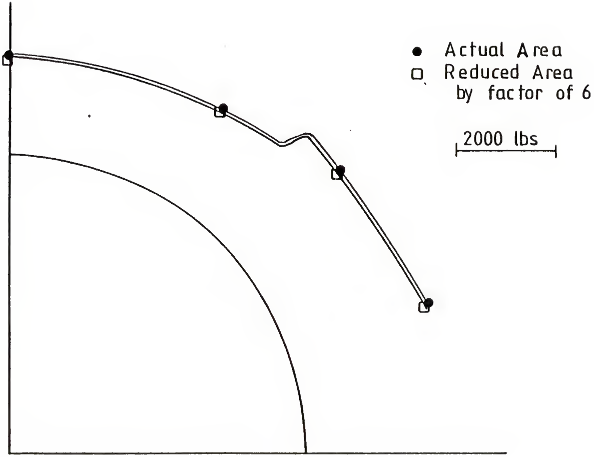

Figure 18. Effect of Area Reduction on Axial Force

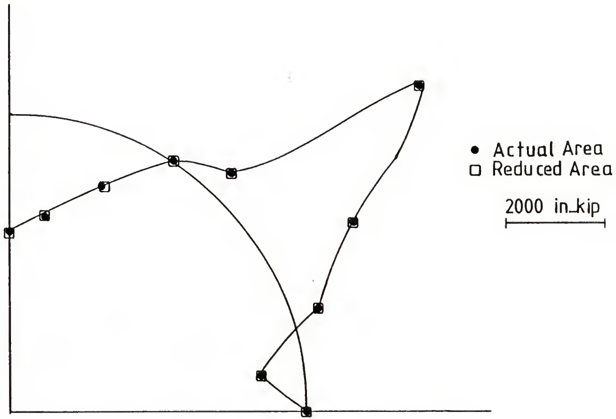

Figure 19. Effect of Area Reduction on Bending Moment

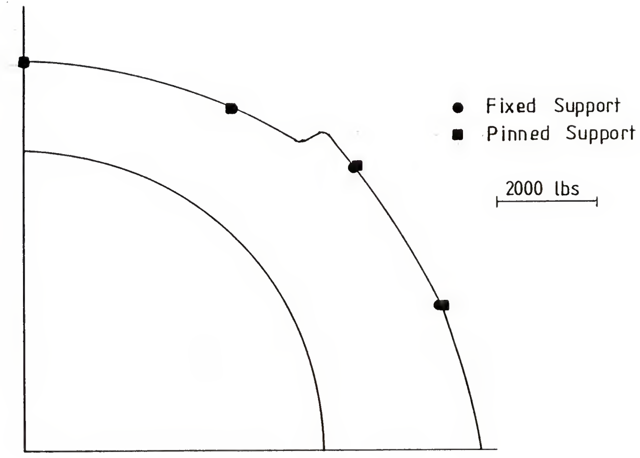

Figure 20. Effect of Fixity of Support on Axial Force

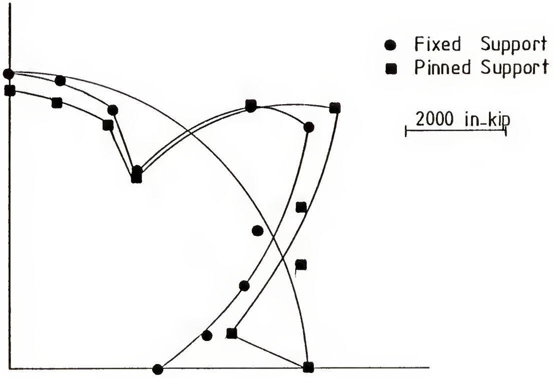

Figure 21. Effect of Fixity of Support on Bending Moment

in the distribution of bending moment, it can be concluded that slight variations from the exact prototype support conditions can be tolerated.

Centrifuge Versus Finite Element Results

The comparison between centrifuge and finite element analysis is undertaken in terms of axial stresses and bending stresses for the semicircular arch.

Axial Stresses

Figures 22, 23 and 24 depict prototype axial stresses as predicted by the two methods for the low-, medium- and high-plasticity clays. (All axial stresses are compressive.) Although in the case of the low-plasticity clay the centrifuge axial stress at the crown and thrust beam is slightly higher, in general the agreement between the two methods is excellent. The axial stress increases uniformly from the crown towards the springline. The finite element method suggests that the thrust beam causes an increase in axial stress in the wall below it rather than transferring load to the surrounding soil.

Bending Stresses

Bending stress diagrams are depicted in Figures 25, 26 and 27 for the three embankment soils (inside tension is positive). As expected the shape of the bending diagram is very complex for all cases. A bending stress concentration develops in the vicinity of the thrust beam. The

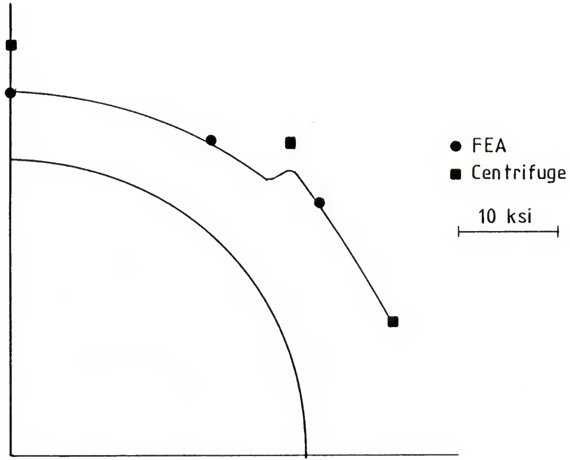

Figure 22. Axial Stresses, Backfill of Low-Plasticity

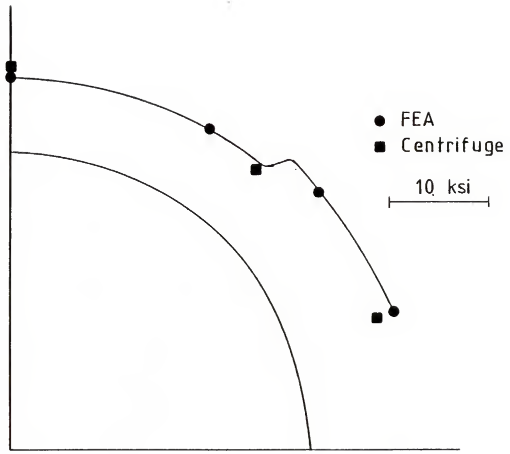

Figure 23. Axial Stresses, Backfill of Medium-Plasticity

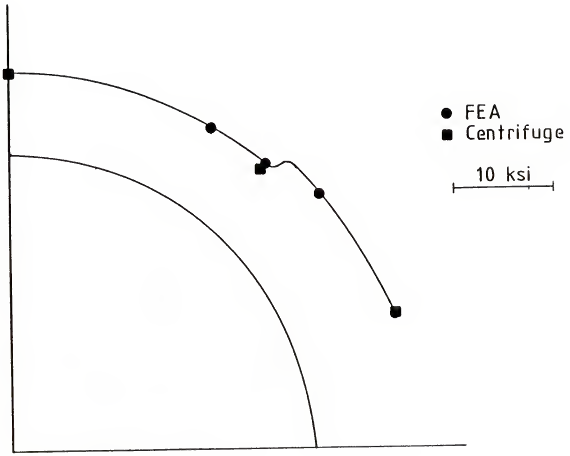

Figure 24. Axial Stresses, Backfill of High-Plasticity

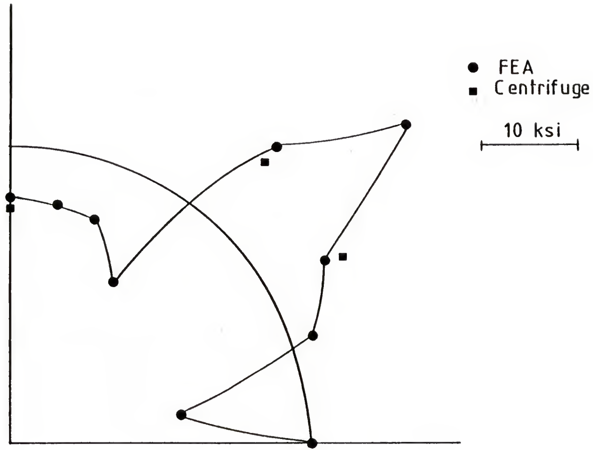

Figure 25. Bending Stresses, Backfill of Low-Plasticity

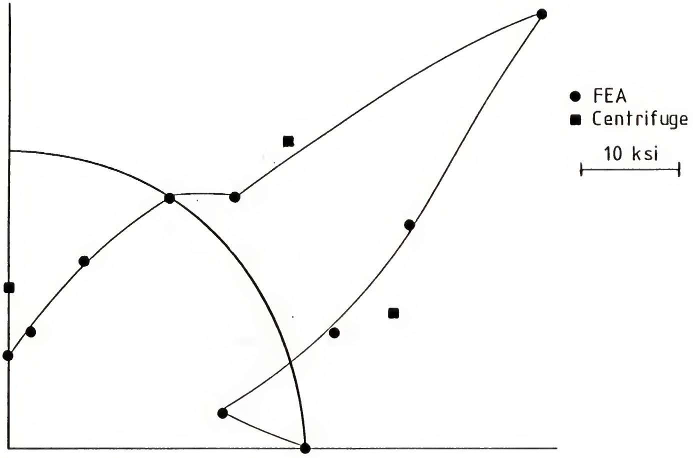

Figure 26. Bending Stresses, Backfill of Medium-Plasticity

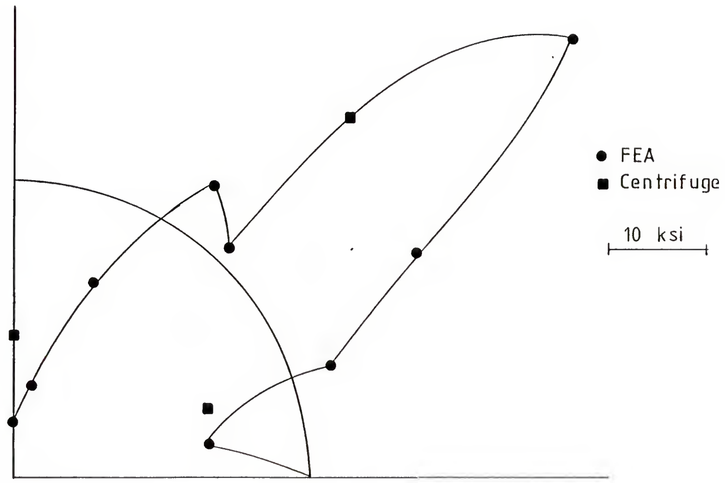

Figure 27. Bending Stresses, Backfill of High-Plasticity

semicircular-arch structure deflects inward at this location and outward at the crown. Bending stresses at all locations increase with increasing plasticity of the soil. Despite the fact that the instrumented locations in the experimental study were limited and definition of the complete bending stress distribution is not possible by this method, the overall agreement between bending stresses at select locations as predicted by the centrifuge and the complete bending diagram as predicted by the finite element method is very good.

Centrifuge Versus Prototype Response

Centrifuge results from this study concerning the high-profile arch in medium-plasticity clay are compared with results from a previous correlation study (McVay and Papadopoulos, 1986) of a large-span culvert of similar geometry and soil characteristics. Comparison is made with respect to axial stress and bending stress distribution. All values are measured with reference to the values obtained when the backfill reached the top of the crown; therefore, they do not represent the actual stresses in the culvert wall. This type of presentation was deemed necessary because results from the prototype study as reported by Selig et al. (1979) were presented in this manner. Depicted in Figure 28 are axial stresses around the periphery of the culvert wall as predicted by this

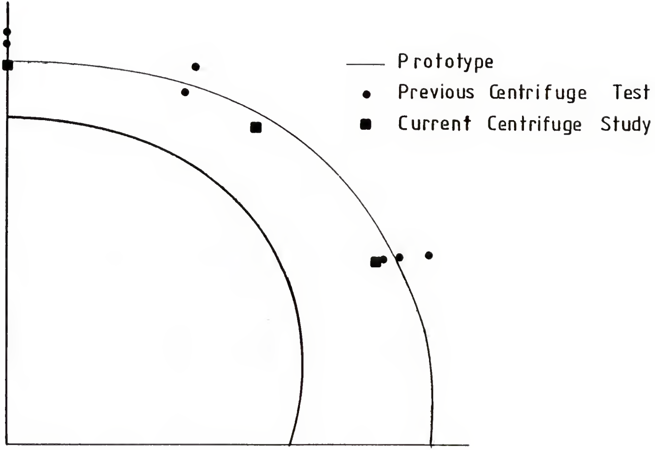

Figure 28. Comparison of Axial Stress (Scale: 1" = 10 Ksi)

centrifuge test series, the previous centrifuge investigation and the prototype field installation study. Inspection of results shows the correlation to be very good, with the test from the current study falling within the range of previous centrifuge results and in agreement with prototype behavior. Similarly, bending stresses at the instrumented locations agree well with the complicated structural bending diagram (Figure 29).

Conclusions from Validation Program

The parametric study, using the finite element method, has shown that any slight deviations from dimensional analysis and similitude (with respect to axial stiffness and connection type at the support) can be tolerated without significant losses in the accuracy of the method and, therefore, the experimental model is adequate. Furthermore, comparisons between centrifuge test results with numerical predictions as well as previous centrifuge tests and prototype behavior have shown very good agreement which confirms the conclusion from the preceding correlation study that modeling in the centrifuge is an excellent technique of duplicating field response.

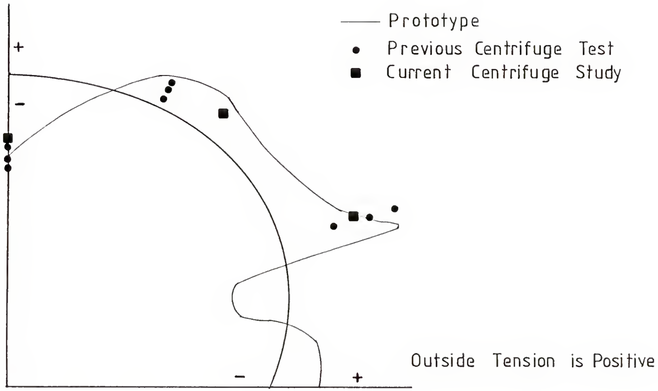

Figure 29. Comparison of Bending Stress (Scale: 1" = 10 Ksi)

CHAPTER EIGHT
LONG-TERM SOIL-STRUCTURE INTERACTION OF SUBSURFACE LARGE-SPAN FLEXIBLE CONDUITS

General

A description of the long-term behavior of large-span flexible conduits as predicted by the experimental program is presented in this chapter. The response of the system is defined on the basis of circumferential bending and axial stresses, crown deformations, pore pressures in the embankment soil and soil displacement vectors. Processing of the data from electronic acquisition systems is presented in Appendix C.

The investigation is primarily concerned with time effects due to consolidation; therefore, the measured quantities are plotted with respect to time or comparisons are made between values at different time frames. The term "long-term," as it is used herein, implies a condition of approximately constant pore water pressure which indicates that most of consolidation has taken place and the system has reached a stable state.

For convenience, since the presentation is of comparative nature, it has been chosen to describe each aspect of soil-structure interaction separately.

Axial Stresses

Axial compression in the structure wall is considered the primary load carrying mode for underground conduits. Figures 30 through 38 depict axial compressive stresses at the end of construction (EOC) and long-term (LT) conditions around the periphery of the culvert wall for the nine tests considered.

Low-Profile Arch

Maximum axial compression for the low-profile arch occurs at the springline for the three clays considered (Figures 30, 31 and 32). In general axial compression uniformly decreases from springline to the crown for the medium- and high-plasticity clays (axial stress at the crown for the low-plasticity clay is not available due to strain-gage malfunction) and the trend shows that a similar variation occurs for the low-plasticity clay as well (Figure 30). Axial stresses in general decrease with increasing soil plasticity for this shape.

A comparison between end of construction and long-term indicates minimal variations for all clays. In particular for the low-plasticity clay (Figure 30) long-term axial stress slightly increases whereas for the other two classes it decreases.

Semicircular Arch

Figures 33, 34 and 35 give the axial stress at select locations around the periphery of the semicircular arch for

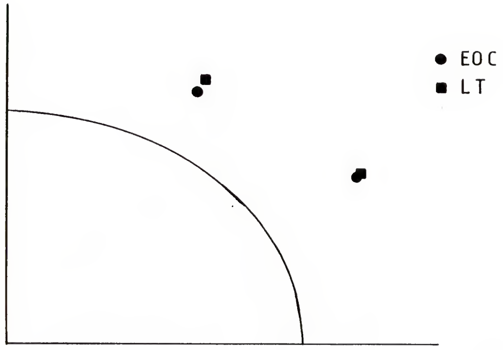

Figure 30. Axial Stress, Low-Plasticity Clay (Scale 1" = 10 Ksi)

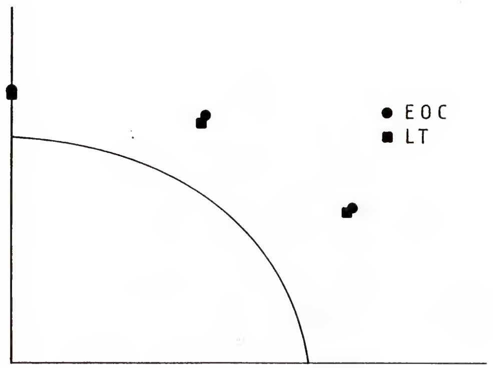

Figure 31. Axial Stress, Medium-Plasticity Clay (Scale 1" = 10 Ksi)

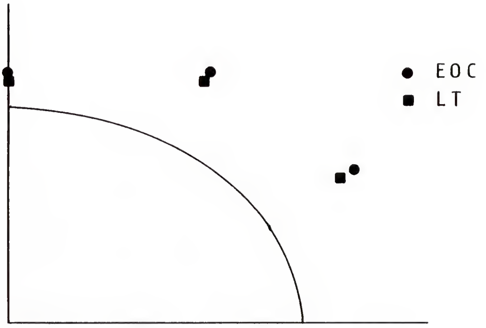

Figure 32. Axial Stress, High-Plasticity Clay (Scale 1" = 10 Ksi)

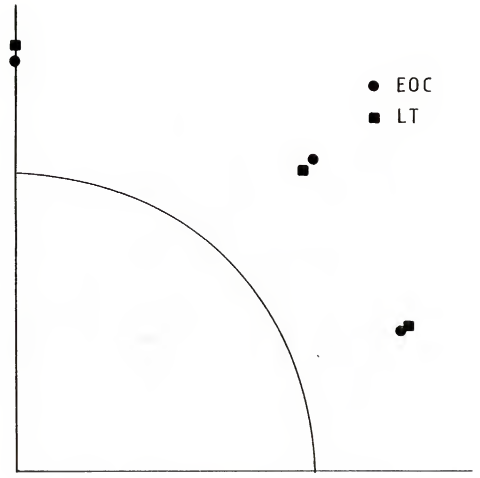

Figure 33. Axial Stress, Low-Plasticity Clay (Scale 1" = 10 Ksi)

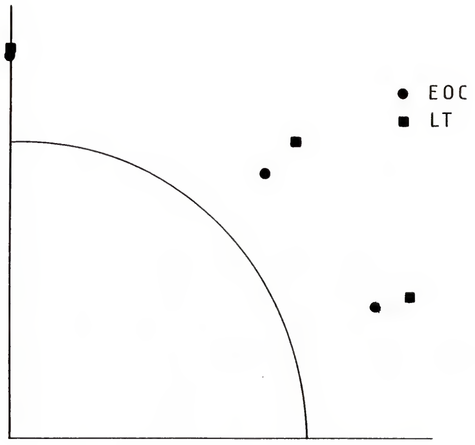

Figure 34. Axial Stress, Medium-Plasticity Clay (Scale 1" = 10 Ksi)

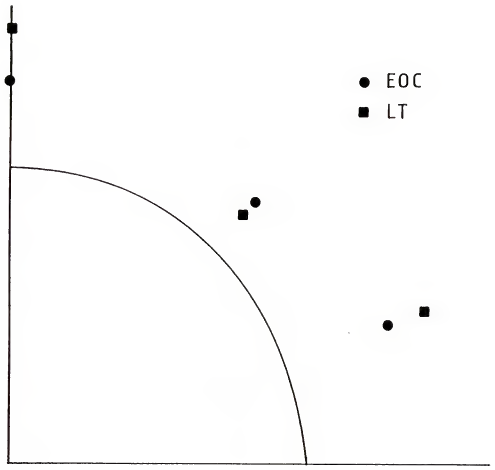

Figure 35. Axial Stress, High-Plasticity Clay (Scale 1" = 10 Ksi)

the low-, medium- and high-plasticity clays, respectively. The axial stress distribution is uniform for the low- and medium-plasticity clays whereas for the high-plasticity clay a decrease of axial stress is observed at the thrust beam location. In general end of construction stresses decrease with increasing plasticity, a phenomenon which has been observed for the low-profile arch as well.

Long-term stresses in general increase at the crown and springline and decrease at the thrust beam location for this shape. The net change in axial stress increases with increasing plasticity. In particular the increase in axial stress at the crown for the high-plasticity clay is approximately 50%.

High-Profile Arch

In general axial stresses in the high-profile arch (Figures 36-38) increase from the crown towards the springline in a similar manner as in the low-profile arch. End of construction stresses decrease with increasing plasticity of the backfill for this structure as well.

Long-term stresses increase at the springline and decrease at the thrust beam and crown for the low-plasticity clay. For the other two clays axial stresses increase at the crown and springline and decrease at the thrust beam location similarly to the response of the semicircular arch.

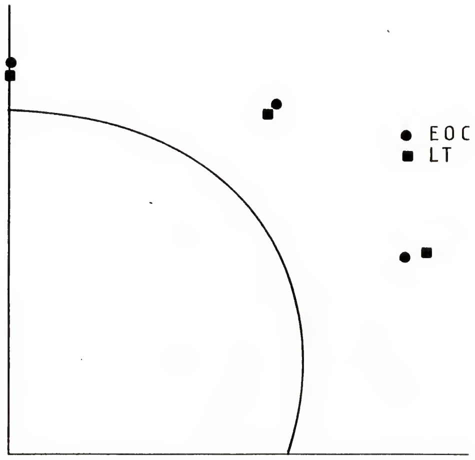

Figure 36. Axial Stress, Low-Plasticity Clay (Scale 1" = 10 Ksi)

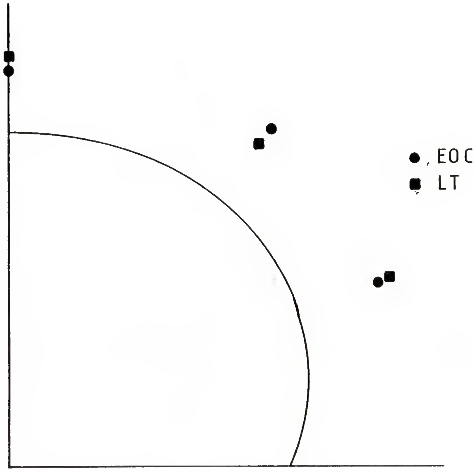

Figure 37. Axial Stress, Medium-Plasticity Clay (Scale 1" = 10 Ksi)

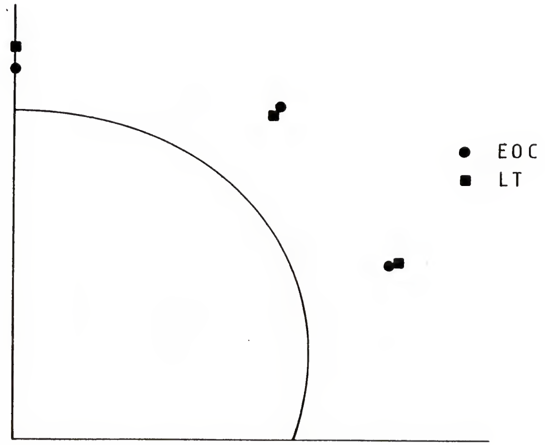

Figure 38. Axial Stress, High-Plasticity Clay (Scale 1" = 10 Ksi)

Bending Stresses

Figures 39 through 47 depict bending stresses at the end of construction and long-term conditions. (Tension on the outside is positive.) For completeness the approximate deflected shape as implied by the bending diagram is also presented.

Low-Profile Arch

The low-profile arch moves inward at the springline and outward at the thrust beam and crown at the end of construction for the low-plasticity clay (Figure 39). The long-term bending stresses do not vary significantly, indicating that the deflected shape does not change.

The medium-plasticity clay causes the structure to deflect inward at the springline and outward at the thrust beam locations (Figure 40). The crown is approximately in its original position. Long-term bending stresses indicate further downward movement at the crown and outward movement at the thrust beam and springline locations.

Figure 41 depicts bending stresses for the high-plasticity clay. The structure moves inward at the springline and crown and outward at the thrust beam location. Bending stress reverses (tension on the outside) at the springline after consolidation (long-term) and a 100% increase in bending is observed at the crown.

In general bending stress at the crown is controlled by soil plasticity. The low-plasticity clay causes tension

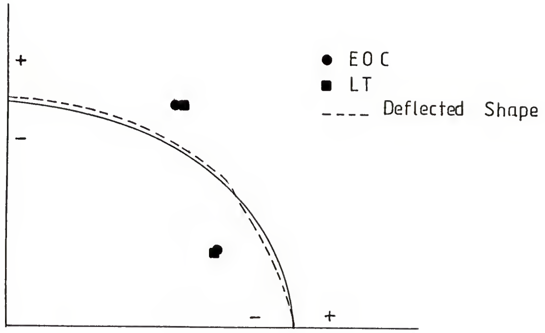

Figure 39. Bending Stress, Low-Plasticity Clay (Scale 1" = 10 Ksi)

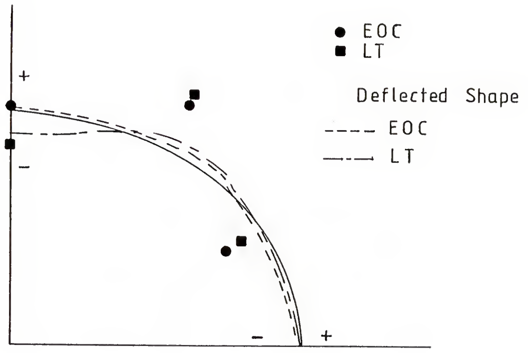

Figure 40. Bending Stress, Medium-Plasticity Clay (Scale 1" = 10 Ksi)

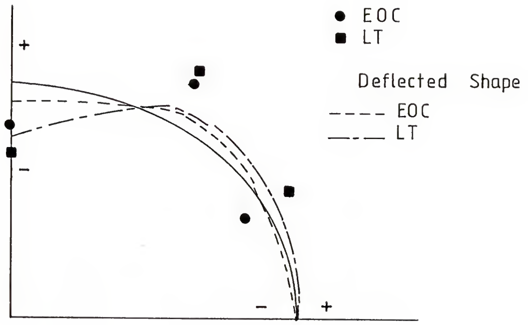

Figure 41. Bending Stress, High-Plasticity Clay (Scale 1" = 10 Ksi)

on the outside, the medium-plasticity clay causes less tension on the outside and the high-plasticity clay causes tension on the inside at the end of construction. Similarly, the net change in bending stress at a particular location after consolidation increases with increasing soil plasticity. However, the trend at the springline is to move outward after consolidation, causing less inside tension or tension on the outside.

Semicircular Arch

The semicircular arch (Figures 42-44) provides a distinctly different bending pattern from that of the low-profile arch. In this case the structure moves inward at the thrust beam location, causing inside tension. For the low- and medium-plasticity clays the springline also moves inward while the crown moves upward. The structure in the high-plasticity embankment moves outward at the springline causing a sudden reversal of curvature at the thrust beam location and therefore large bending stresses.

Bending stresses increase significantly in the long-term condition. The high-plasticity clay provides the most critical condition with stresses at the crown and thrust beam locations over 20 Ksi. The long-term increase in bending stress is approximately 20% at the thrust beam and 35% at the crown. In general the net change in bending stress increases with increasing plasticity.

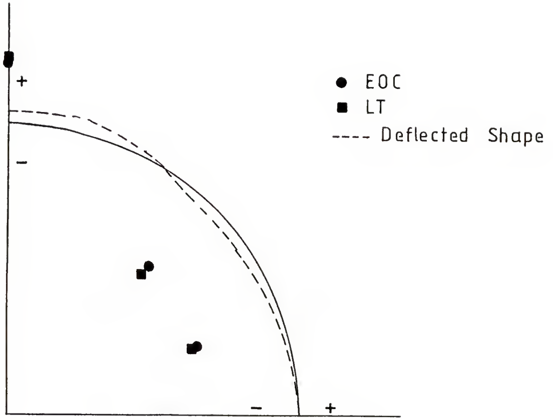

Figure 42. Bending Stress, Low-Plasticity Clay (Scale 1" = 10 Ksi)

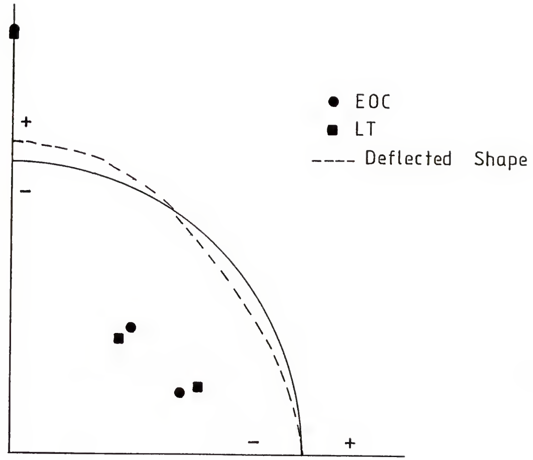

Figure 43. Bending Stress, Medium-Plasticity Clay (Scale 1" = 10 Ksi)

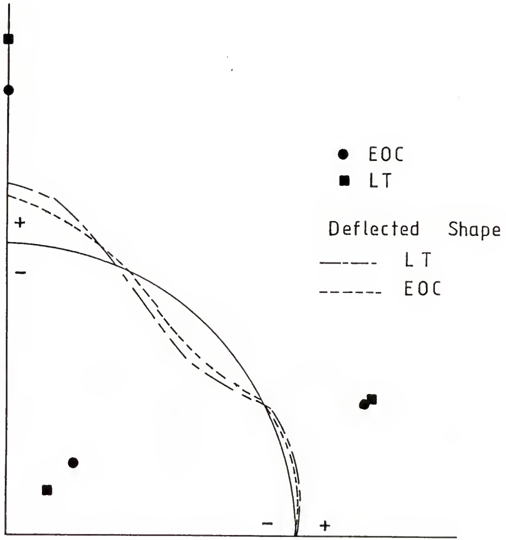

Figure 44. Bending Stress, High-Plasticity Clay (Scale 1" = 10 Ksi)

High-Profile Arch

Figures 45, 46 and 47 present the bending stress distribution for the high-profile arch. The end of construction behavior of this shape is very similar to that of the semicircular arch. Tension on the inside at the springline and thrust beams and tension on the outside at the crown. The highest bending stress value occurs at the thrust beam.

Unlike the semicircular arch, however, long-term crown bending stress reverses sign indicating downward crown movement. Thus thrust beam bending stresses decrease in the case of low- and medium-plasticity clays. The structure in high-plasticity embankment soil deflects outward at the springline and downward at the crown. Bending stresses at these locations do not change in magnitude from corresponding stresses at the end of construction but they do change in sign. The highest bending stress (15 Ksi) occurs at the thrust beam location.

Long-Term Axial and Bending Stresses

Presented in Figure 48 is the variation of axial stress at the springline with time for the three structures in the high-plasticity clay. Model time of 20 minutes represents EOC. During construction axial stress increases and then continues as time progresses. However, the increase does not continue to the end of long-term. This

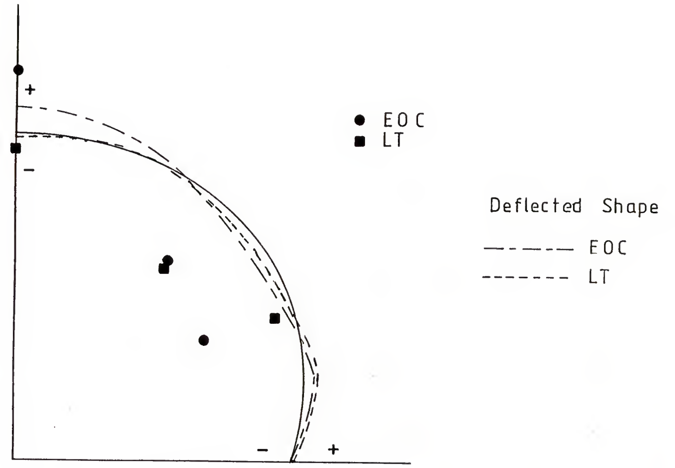

Figure 45. Bending Stress, Low-Plasticity Clay (Scale 1" = 10 Ksi)

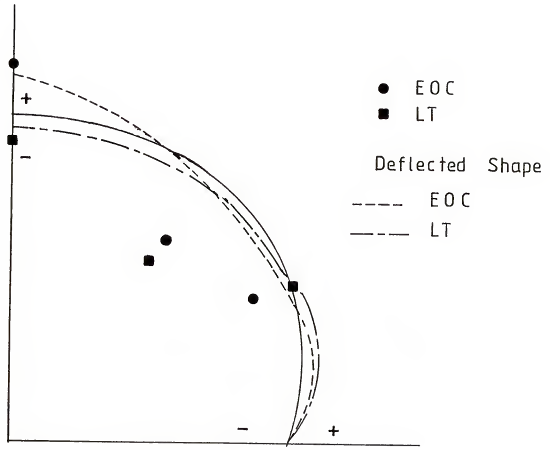

Figure 46. Bending Stress, Medium-Plasticity Clay (Scale 1" = 10 Ksi)

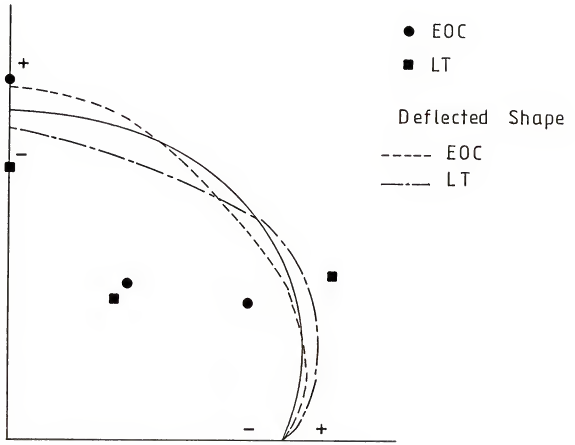

Figure 47. Bending Stress, High-Plasticity Clay (Scale 1" = 10 Ksi)

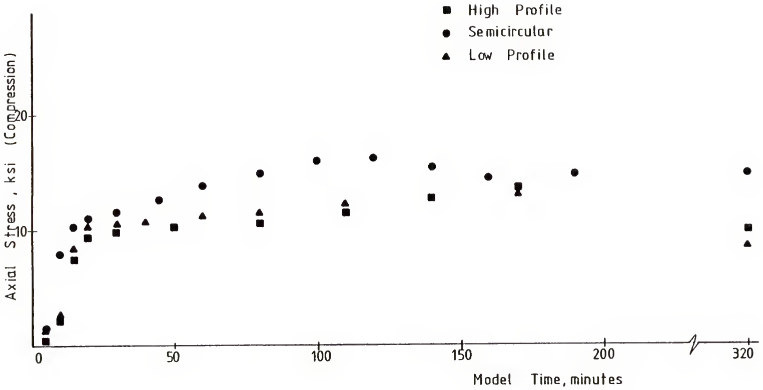

Figure 48. Variation of Springline Axial Stress with Time for the Semicircular Arch

is probably due to excessive increase in bending moment at the location of the thrust beam which distorts the shape at that location and therefore load is not transferred efficiently to the springline location. Figure 49 depicts the variation of axial stress at the springline of the semicircle for the three clays considered. It is evident that axial stress becomes constant for the low-plasticity soil and later for the medium-plasticity soil. Furthermore, axial stress does not decrease as time progresses since excessive distortion of the shape does not occur.

Figure 50 presents the variation of bending stress with time for the three structures considered in the high-plasticity soil. Examination of the figure reveals that the long-term behavior agrees quite well with the earlier discussion. In the case of the semicircular arch, the wall is continuing to move inward and bending stress increases. The high-profile arch exhibits similar behavior as the semicircle; however, due to subsidence of the crown the distorted shape is reduced and thus bending stress does not increase significantly. The low-profile arch develops tensile stresses on the outside of the culvert due to continuous downward crown movement (discussed later). Finally, Figure 51 depicts bending stresses at the thrust beam location of the semicircular arch for the three clays considered. Bending stress increases with soil plasticity,

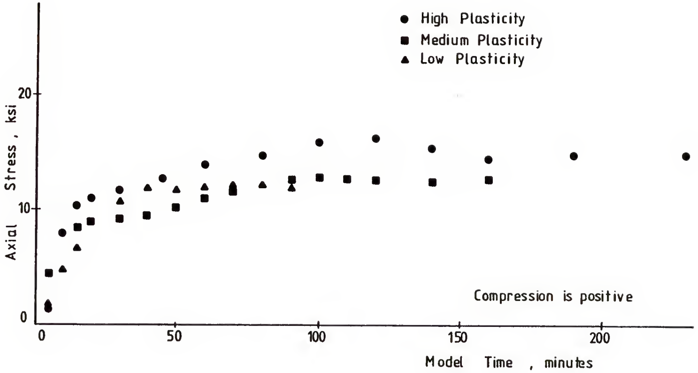

Figure 49. Variation of Springline Axial Stress with Time for High-Plasticity Embankment Soil

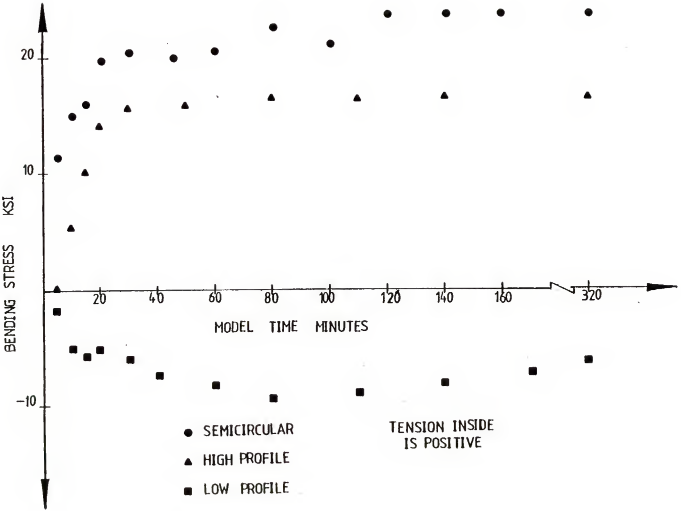

Figure 50. Variation of Bending Stress at the Thrust Beam Location with Time for the Semicircular Arch

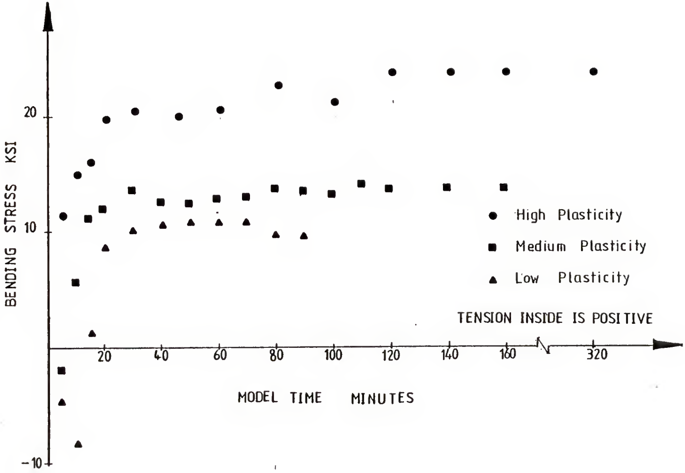

Figure 51. Variation of Bending Stress at the Thrust Beam Location with Time for High-Plasticity Embankment Soil

as expected. Furthermore, the low- and medium-plasticity soils reach equilibrium sooner.

Crown Movement

Figures 52, 53 and 54 present the crown deformation with respect to model time for the low-profile, the semicircular and the high-profile arches, respectively. The 20-minute time frame corresponds to the end of construction (Appendix D).

Low-Profile Arch

Inspection of the results shows that the crown moves upward during backfilling against the sides and downward during backfilling over the top (Figure 52). Downward movement continues as time progresses. The magnitude of upward and downward movement, however, is controlled by the plasticity of the backfilling material. The low-plasticity clay causes the crown to move 0.25 in. upward and then allows a very slight amount of downward movement. On the contrary the high-plasticity material forces the crown to move 0.5 in. upward and then is squeezed back to allow approximately 0.8 in. of downward movement until the completion of embankment consolidation. As expected the behavior of the structure in medium-plasticity soil is bounded by the two extremes.

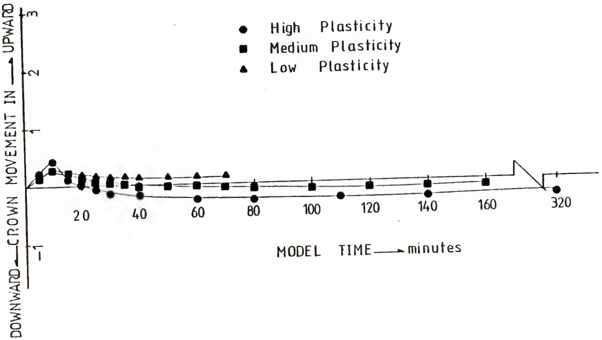

Figure 52. Crown Movement of the Low-Profile Arch

Semicircular Arch

Figure 53 depicts the crown movement of the semicircular arch for the three clays considered. The behavior is similar to the low-profile arch during construction of the embankment. The structure moves upward as soil is placed against the sides and then downward as soil is placed over the top. However, the trend reverses again as soon as construction is complete and the crown moves upward as the embankment soil consolidates. In general the crown rises to a higher location at the end of consolidation than at the time when the backfill reaches crown level during construction. The height to which the crown rises is proportional to the plasticity of the clay. In general the less plastic soils start the rising path earlier and reach a stable height sooner.

High-Profile Arch

The behavior of the high-profile arch is depicted in Figure 54. The general trend is very similar to that of the low-profile structure. This structure, however, is experiencing larger deformations than both of the previous structures. The magnitude of deformations increases with increasing plasticity. Although it appears that the culvert in the medium-plasticity embankment reaches a lower height at the end of long-term, the net downward movement (highest point to lowest point) is larger for the high-plasticity clay.

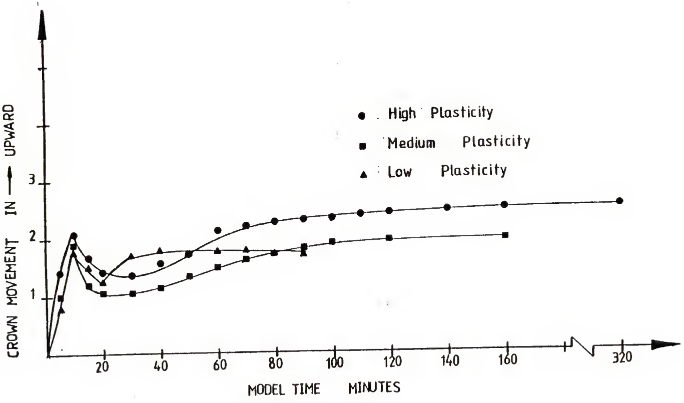

Figure 53. Crown Movement of the Semicircular Arch

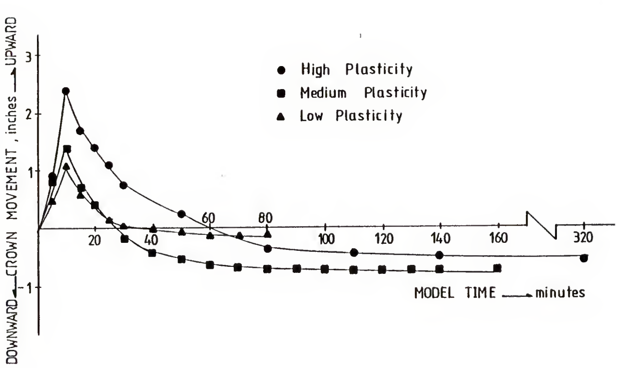

Figure 54. Crown Movement of the High-Profile Arch

Pore Pressures in the Embankment Clay

Pore pressures in the embankment fill are presented in Figures 55, 56 and 57. Pore pressure development and dissipation as time progresses is primarily controlled by the soil characteristics but structure geometry is also an important factor.

Low-Plasticity Clay

Figure 55 depicts pore pressures from two of the geometries in the low-plasticity clay. Results from the test of the semicircular arch were erratic.

The peak value occurs at the end of construction since all of the load due to the overburden soil is immediately transferred to the soil columns of low compressibility next to the structure. Pore pressure then dissipates until it reaches a stable value. Pressures in the case of low-profile arch are in general lower due to the less overburden weight (Figure 55) but also because this shape deflects less under load; therefore, less load is transferred to the soil columns.

Medium-Plasticity Clay

Results from tests in this type of embankment soil are presented in Figure 56. Pore pressures from the test of the high-profile arch were erratic.

In this case the peak occurs later than the end of construction since the more compressible soil causes some of the load to be taken by the structure. The structure

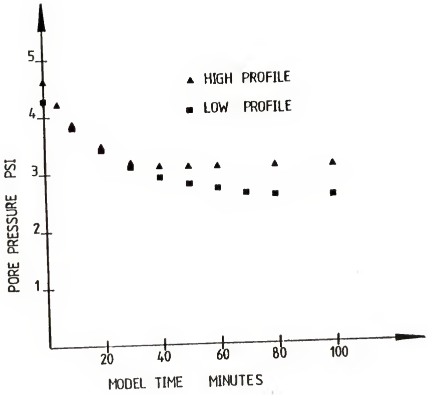

Figure 55. Pore Pressures in Low-Plasticity Clay

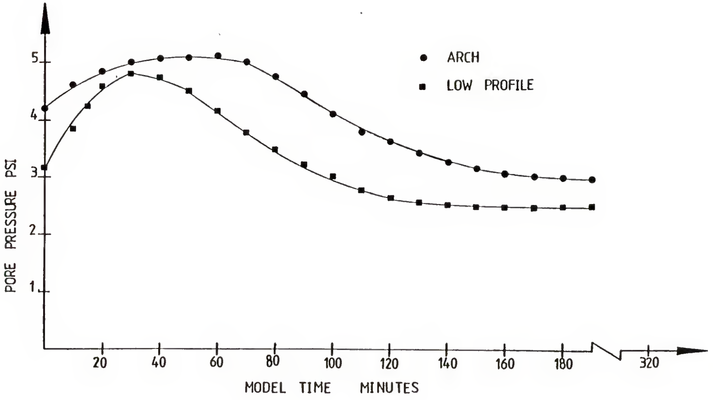

Figure 56. Pore Pressures in Medium-Plasticity Clay

deflects under load and therefore further arching occurs toward the soil columns which causes the excess pore pressure to rise. This cycle continues to occur until the maximum value is reached followed by dissipation to a constant pore pressure. The peak occurs faster for the low-profile arch since this shape is associated with less deflection than the others. In general pore pressure values are lower for the low-profile arch due to the same reasons that were mentioned in the case of low-plasticity clay.

High-Plasticity Clay

Figure 57 presents pore pressures in the high-plasticity clay for the three geometries. Pore pressure rises very gradually to a constant value. It is evident that due to the high compressibility of this type of soil load transfer from the structure occurs very slowly. In fact load transfer from soil to the structure occurs as consolidation takes place and then, as the structure deflects, load is transferred back to the soil columns to cause further increase of pore pressure. As a result, a clear dissipation curve is not evident since these processes (development of excess pore pressure and dissipation) occur simultaneously (explained later).

The final pressures are highest for the high-profile arch and lowest for the low-profile arch since the embankment in the case of the former requires a larger

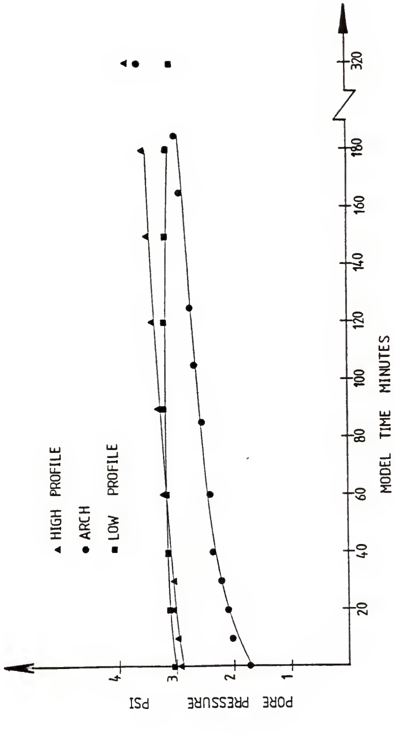

Figure 57. Pore Pressures in High-Plasticity Clay

volume of embankment soil and therefore contains a larger volume of water.

Explanation of Pore Pressure Development and Dissipation

Pore pressure development and dissipation in the case of complex soil-structure interaction deviates from consolidation of a semi-infinite soil medium. In particular pore pressure development is affected by the arching effect and the degree of load transfer between the structure and adjacent soil columns.

An explanation of pore pressure distribution with time is offered in Figures 58 through 61. The gradual increase in hydrostatic pressure (Figure 58) is due to the fact that as the gravitational field increases, soil and water particles move towards the bottom of the container until all voids are filled. Void ratio decreases and the soil gradually becomes saturated (development of pore pressure). Furthermore, as soil is placed during the construction of the model embankment, further decrease in void ratio occurs. Thus, hydrostatic pressure is assumed to rise linearly during a centrifuge test due to the energy input from the artificial gravitational field, and the rate of increase will depend on the permeability of the soil.

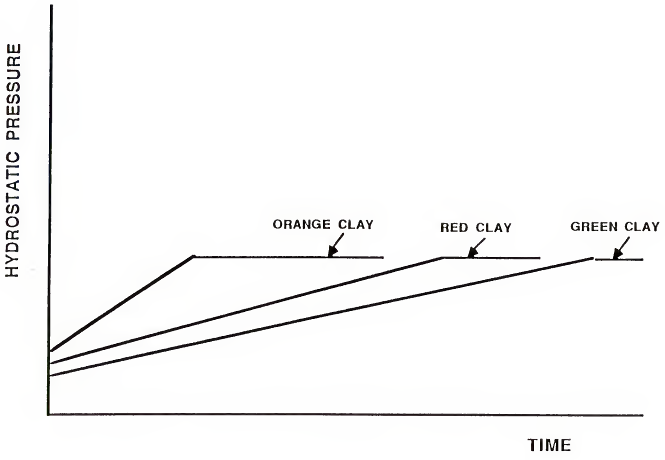

Figure 58. Variation of Hydrostatic Pressure with Time

The excess pore pressure as depicted in Figures 59, 60 and 61 is related to soil compressibility and permeability. The low-plasticity clay, for instance, is the least compressible of the backfill materials and therefore it carries most of the load due to its own weight in the soil columns adjacent to the structure. Thus, excess pore pressure peaks immediately after placement of the last lift of soil. However, as time progresses, pore pressure dissipates quickly, due to the high permeability of the soil, into the structural backfill (coarse sand) and bottom sand layer in the container.

The more compressible soils do not carry all of their own weight immediately but transfer some to the structure. As time progresses the structure deflects, the crown moves downward and thus load is transferred back to the soil columns (positive arching). Therefore, excess pore pressure gradually increases. Meanwhile dissipation of pore pressure occurs into the drain areas. Thus development and dissipation of pore pressure occur simultaneously (Figure 60). The lines which connect the dots (Figure 60) indicate in a graphical manner the combined effect of pore pressure dissipation and development due to load transfer, which produce a smooth curve. In the case of a highly compressible soil of low

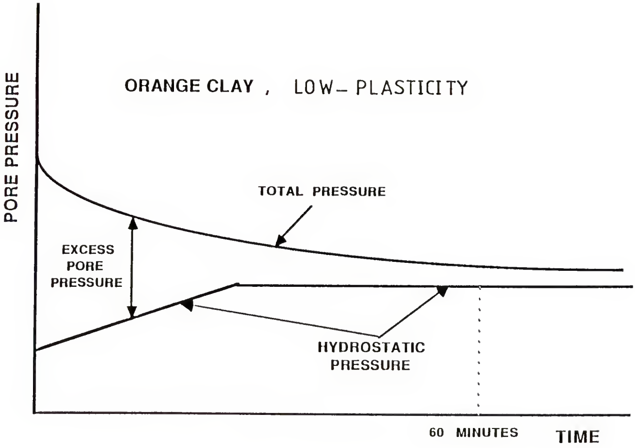

Figure 59. Pore Pressure Development and Dissipation, Orange Clay

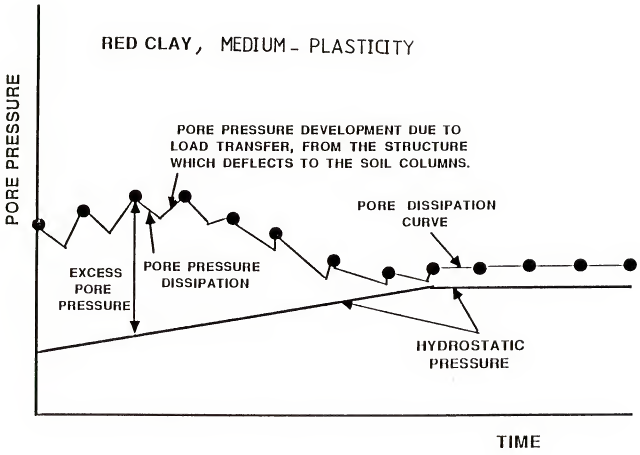

Figure 60. Pore Pressure Development and Dissipation, Red Clay

permeability, this process is very slow and it produces a smooth curve which is gradually rising (Figure 61).

Soil Displacement Vectors

Although soil displacements are generally a function of soil compressibility, in the case of soil interacting with a structure, the problem becomes very complex and structural behavior is also a controlling factor.

In order to emphasize the soil-structure interaction effect it has been chosen to present soil movement in terms of displacement vectors. The vectors indicate the direction and approximate magnitude of the displacement of a soil grain with reference to its location at the end of construction.

Low-Profile Arch

Figures 62, 63 and 64 depict soil displacement vectors around the low-profile arch as determined by the photographic technique. In general downward movement decreases in the higher layers. Lateral movement is also larger at the lower layers and at locations closer to the structure. Downward movement is larger in the lower layers because it is primarily attributed to settlement and consolidation which increases with increasing overburden weight. Similarly, lateral movement is larger closer to the structure since it is the outcome of the soil structure

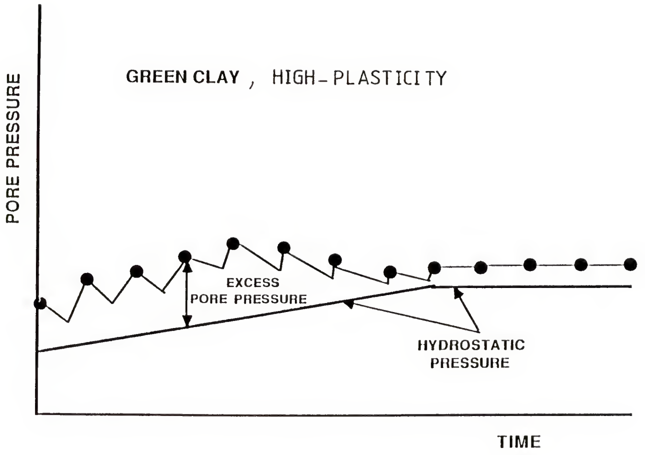

Figure 61. Pore Pressure Development and Dissipation, Green Clay

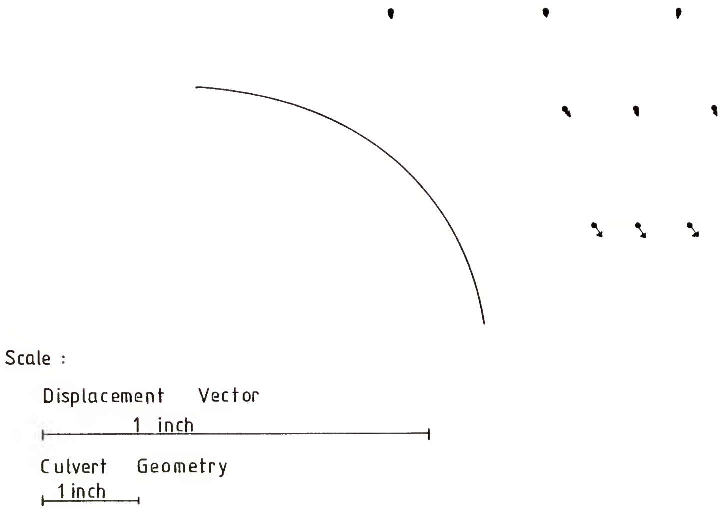

Figure 62. Soil Displacement Vectors, Low-Plasticity Soil

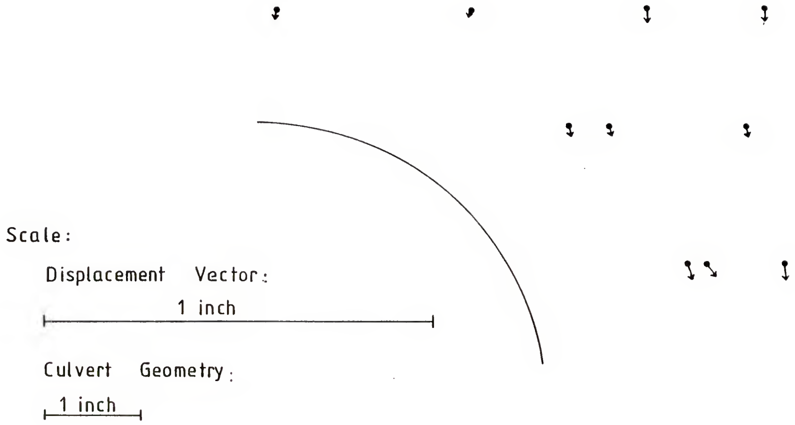

Figure 63. Soil Displacement Vectors, Medium-Plasticity Soil

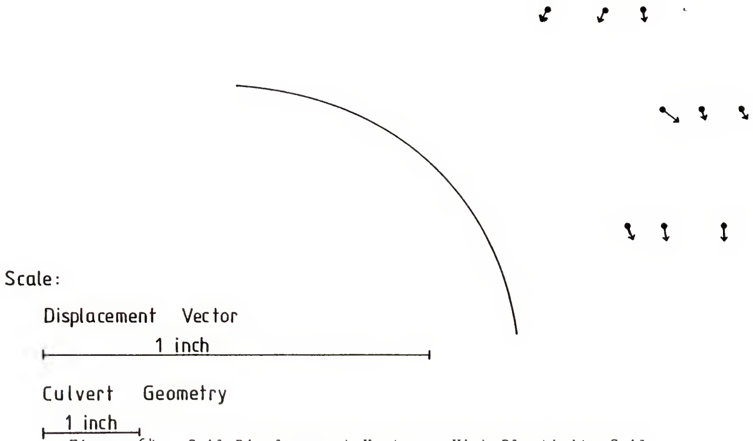

Figure 64. Soil Displacement Vectors, High-Plasticity Soil

interaction effect which is more evident closer to the structure.

In the case of low-plasticity clay, soil particles move as if they were pushed away from the structure at the springline and thrust beams whereas very little lateral movement takes place at the soil layer just over the crown. This type of soil displacement can be easily explained when compared to the deflected shape of the low-profile arch as time progresses. In general the springline and thrust beams move outward, whereas there is very small downward movement at the crown.

The soil behavior is similar as plasticity increases although the magnitude of displacements increases. Clay particles in the layer just over the crown which are closer to the structure seem to move towards the center of the embankment whereas distant particles move away from the structure (Figures 62 and 63).

Semicircular Arch

The displacement vectors (Figures 65-67) indicate soil movement towards the structure at the thrust beams and away from the structure at the springline. These results are compatible with the deflected shape of the structure as time progresses. Soil particles over the crown experience very small downard movement and in the case of medium- and high-plasticity clays upward movement. Downward movements

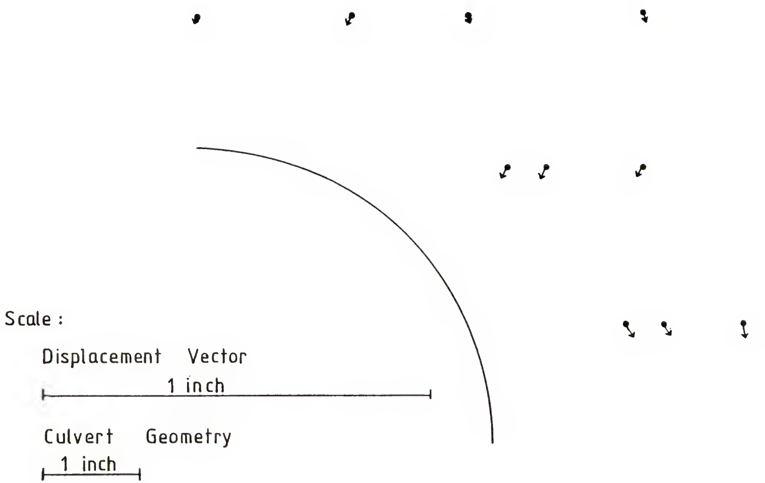

Figure 65. Soil Displacement Vectors, Low-Plasticity Soil

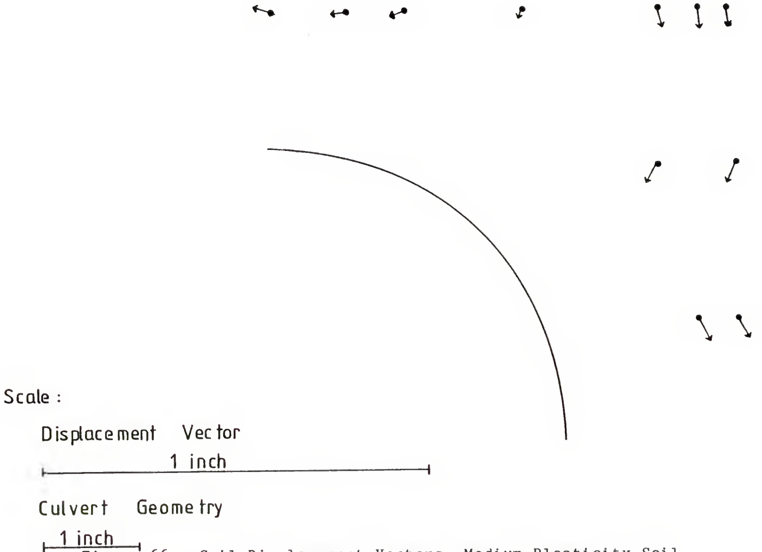

Figure 66. Soil Displacement Vectors, Medium-Plasticity Soil

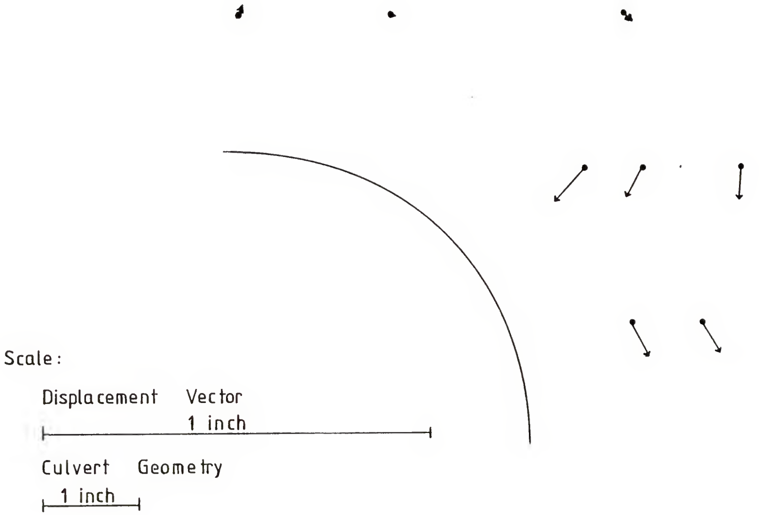

Figure 67. Soil Displacement Vectors, High-Plasticity Soil

increase as plasticity and compressibility of the soil increases.

High-Profile Arch

In this case (Figures 68-70) soil movement is similar to that of the low-profile arch. Soil particles move away from the structure at the springline and thrust beam layers. Downward movement is larger at the lower layers and increases with increasing plasticity.

Structure Deflected Shape

The deflected shapes of the structures are depicted in Figure 71. The semicircular arch moves inward at the thrust beam location whereas the other two shapes move outward. Furthermore, the crown of the semicircle rises whereas downward movement is observed for the other two shapes. Thus, the mode of failure will be different. The semicircle will fail by developing plastic hinges at the thrust beam and crown locations, whereas the other two shapes will fail due to continuous subsidence of the crown.

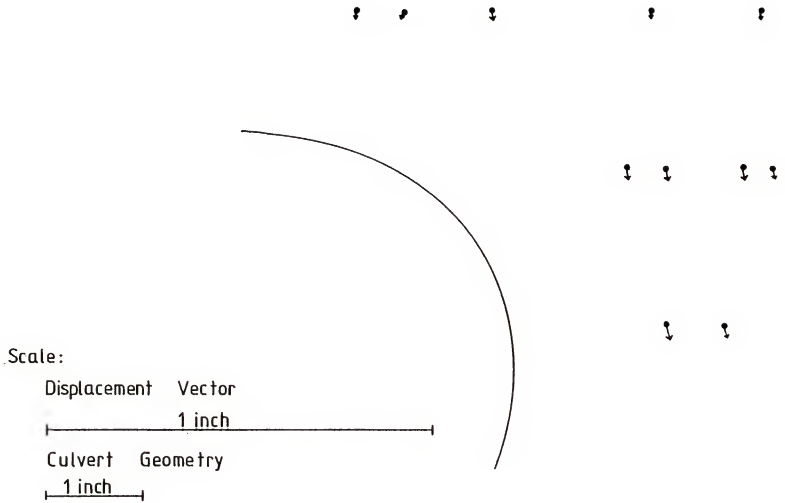

Figure 68. Soil Displacement Vectors, Low-Plasticity Soil

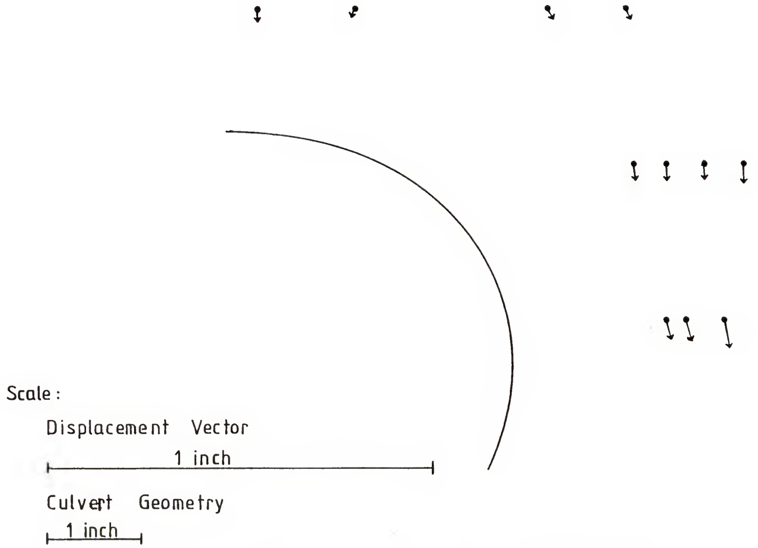

Figure 69. Soil Displacement Vectors, Medium-Plasticity Soil

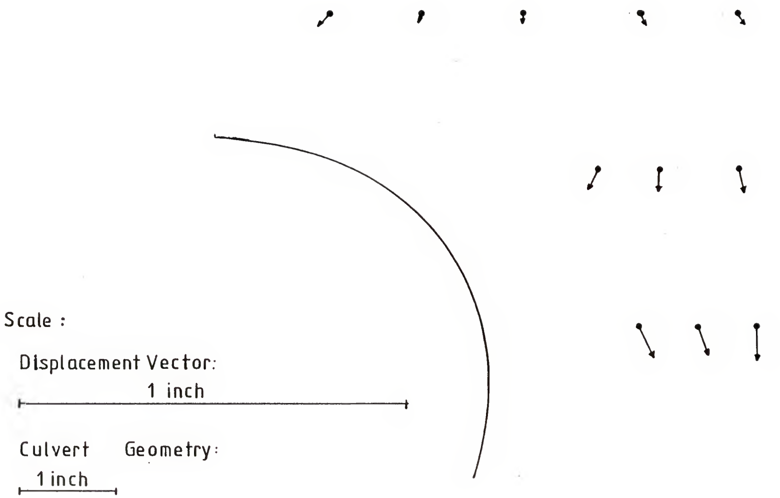

Figure 70. Soil Displacement Vectors, High-Plasticity Soil

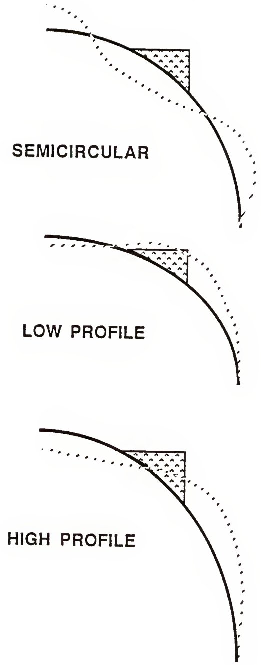

Figure 71. Deflected Shapes

CHAPTER NINE
LONG-TERM SOIL-STRUCTURE INTERACTION AND DESIGN OF LARGE-SPAN FLEXIBLE ARCH-SHAPED STRUCTURES

General

Experimental results have proven that structure geometry, embankment plasticity and consolidation are controlling factors in the response of the structure. In this chapter an attempt will be made to provide a justification of the soil-structure response as predicted by the centrifuge, along with a rational design recommendation which will incorporate the controlling parameters as well as the long-term effect.

Soil-structure interaction of large-span flexible culverts will be discussed in terms of structure geometry and backfill plasticity.

Structure Geometry

In general the experimental results have shown that the behavior of the low- and high-profile arches is similar in terms of axial stress distribution, deflected shape and bending moment diagram. On the contrary, the semicircular arch has unique behavioral characteristics. Thus, by inspection it is implied that the response of these structures is not primarily dependent on rise-to-span ratio but on some other geometric characteristic, or that the rise-to-span ratio is a controlling factor among others.

The semicircular arch due to its larger radius of curvature at the thrust beam is forced to deflect inward at this location during construction. The distortion of the shape is so excessive that large secondary bending stresses are generated which cause further inward flexure, the structure can no longer support the load as an arch, the distribution of axial and bending stresses is not efficient and therefore the structure experiences large stress concentrations at distinct locations.

On the contrary, the low- and high-profile arches are stiffer at the thrust beam location and therefore the inward deflection is not excessive during construction. Thus the net distortion from the original geometry is small, bending moments do not rise excessively and the axial stress distribution is approximately uniform.

Centrifuge maximum measured values are listed in Table 7. In the case of bending moments however, the maximum measured moment may not correspond to the actual maximum moment because of the complexity of the bending diagram and the limited instrumented locations. Previous comparisons with the finite element method have shown that the maximum measured value was approximately half of the actual maximum, thus the estimated maximum moment is twice the

Table 7
Maximum Axial Force and Moment
as Predicted by the Centrifuge

Case	Plasticity	Geometry	Axial Force (max measured) lbs	Moment (max measured) ft-kips/ft	Moment (max predicted) ft-kips/ft	
1	low	low-profile	31513	597	1194	
2	medium	low-profile	28213	745	1490	
3	high	low-profile	33988	1084	2168	
4	low	semicircular	39268	1232	2464	
5	medium	semicircular	33328	1620	3240	
6	high	semicircular	42073	2718	5436	
7	low	high-profile	33576	1011	2022	
8	medium	high-profile	28873	1282	2564	2661
9	high	high-profile	35308	1804	3608	3714

maximum measured values. Figures 72 through 75 show the variation of centrifuge axial force (maximum prototype axial force as predicted by the centrifuge model) and centrifuge moment (maximum prototype moment as predicted by the centrifuge model) with dimensionless geometric characteristics. Centrifuge moment versus rise-to-span ratio indicates no direct correlation (Figure 72). Centrifuge moment seems to be proportional to the square root of the ratio of the side arc radius to that of the top arc but the relationship is not linear. Figure 74 indicates that there is a linear relationship between centrifuge moment and the product of the two dimensionless ratios. It is evident that the value for the semicircle in high-plasticity soil falls out of the generalized pattern. This is due to the fact that this moment would cause the section to yield (yield moment = 4127 ft-kips/ft) and thus large bending strains would be generated. In an elastic stress analysis, large bending strains would imply large bending stresses (large moments); although it is evident that in this case, large strains are generated due to yielding of the section. Finally, Figure 75 depicts the variation of axial force with $\sqrt{R1/R2}$ which is linear.

Soil Plasticity

There are three aspects of soil-structure interaction that must be considered when discussing the effect of soil

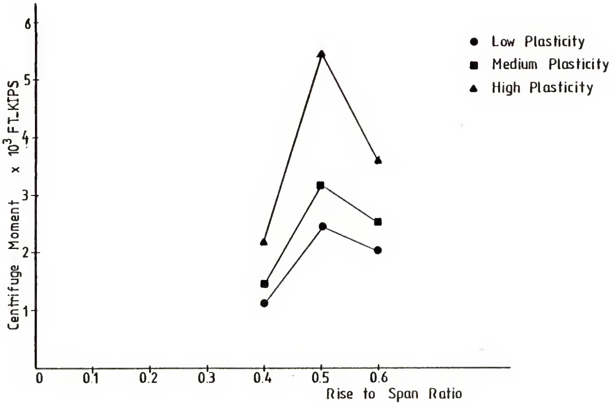

Figure 72. Variation of Moment with R/S

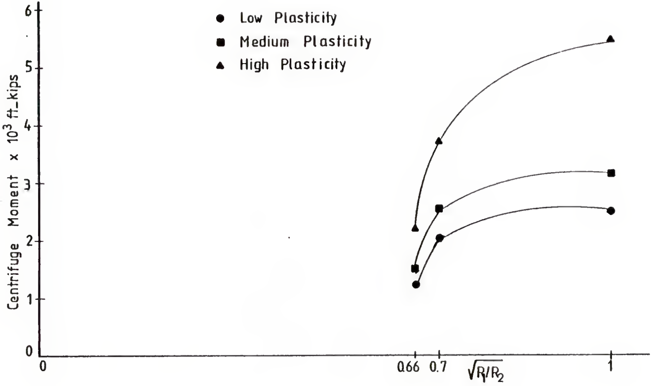

Figure 73. Variation of Moment with $\sqrt{R_1/R_2}$

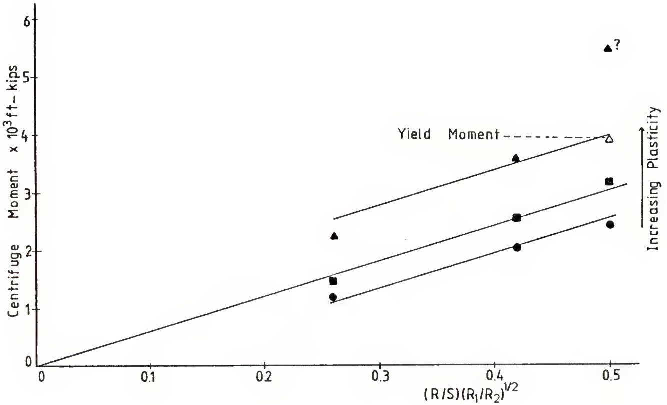

Figure 74. Variation of Moment with $(R/S)(\sqrt{R_1/R_2})$

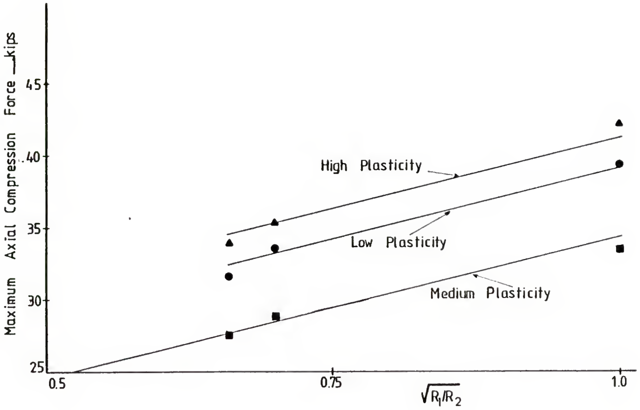

Figure 75. Variation of Axial Force with $\sqrt{R_1/R_2}$

plasticity and compressibility on subsurface flexible culverts: first is the compaction induced lateral pressure on the structure during backfilling against the sides; second is the lateral restraint due to development of passive pressures during placement of soil over the crown of the structure; and third is the consolidation of the embankment soil as time progresses. These soil-structure interaction aspects are dependent on soil plasticity and are controlling factors in the load carrying capacity of the structure.

Soil-structure interaction initiates with placement of soil against the structure which causes inward movement at the springline and upward movement at the crown. In general, compaction-induced lateral pressures approach passive earth pressure magnitudes (Duncan and Seed, 1986). In the case of small overburden weights (height of soil less than 8 ft.) the force due to passive pressure (Pp1) will be larger for more cohesive backfills (Table 8) and therefore the structure will tend to flex inward to a larger extent when interacting with this type of soil than with a cohesionless soil.

As soil placement continues over the crown the springline tends to move into the soil and therefore full passive pressures are mobilized. These pressures (Pp2) are larger for the less cohesive soils in this case (Table 8) and therefore restrain further lateral movement of the

Table 8
Passive Pressures

	ϕ	C psf	γ pcf	K_p	Pp1 lbs	Pp2 lbs
Low Plasticity	38	100	136.8	2.05	21676.86	58470.59
Medium Plasticity	34	300	126.4	1.88	23319.94	51911.82
High Plasticity	25	600	126.8	1.57	25073.57	45076.73

$$Pp = \int_0^H (2C\sqrt{Kp} + \gamma z Kp)$$

springline. Furthermore, the crown is not allowed to deflect downward and thus the structure is forced to carry the load in axial compression. Higher plasticity soils allow some outward movement of the springline as well as downward crown movement and thus some of the overburden weight is transferred to the soil.

As time progresses soil columns adjacent to the structure start to consolidate. Consolidation is larger for the more compressible soils and as it takes place, load transfer occurs from the soil to the structure and negative arching occurs.

The effect of each aspect of soil-structure interaction on the load transfer to the structure is depicted in Figure 76. Thus the net effect from soil plasticity is the superposition of the three and depends on the degree of significance of each one. Figure 77 depicts the variation of axial force with plasticity index as predicted by the centrifuge. It can be seen that for all shapes, axial forces are larger for the low- and high-plasticity soils. However, bending moments (Figure 78) are directly proportional to plasticity index.

Comparison with Current Design Procedures

In order to enhance our current perception of soil-structure interaction with particular emphasis to the controlling factors, a comparison is undertaken between

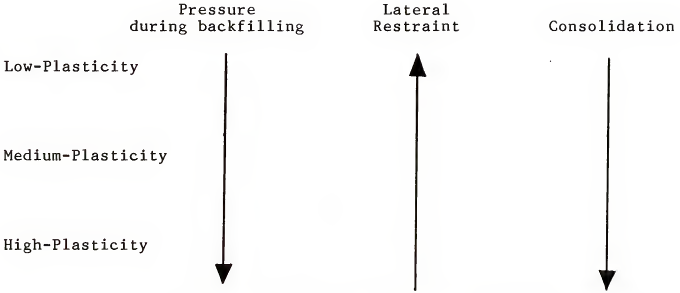

Arrow indicates load increase on the structure.

Figure 76. Effect of Each Aspect of Soil-Structure Interaction

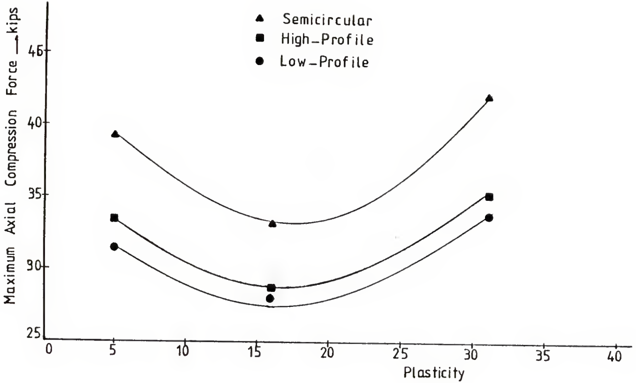

Figure 77. Variation of Axial Force with Plasticity Index

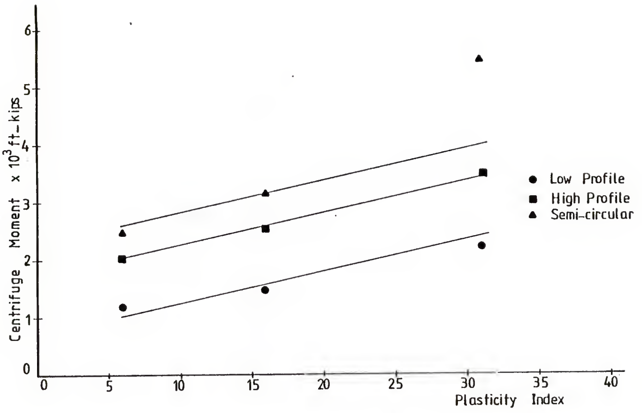

Figure 78. Variation of Bending Moments with Plasticity Index

predictions of axial forces and moments from the centrifuge and those from current design procedures. The methodology developed by Duncan (1979) as well as the ring-compression theory by White and Layer (1960) are being used.

Design Forces and Moments

The maximum axial compression force and maximum bending moment for each case were calculated using Duncan's methodology and are listed in Table 9. Similarly the ring-compression force for each case was also calculated using the formula proposed by White and Layer (1960) and the values are listed in Table 10. Ring-compression theory does not provide moment estimates.

Comparisons of Predictions

Table 11 provides a comparison of axial force and moment in the culvert wall. Axial forces calculated by Duncan's method exceed those calculated from ring-compression theory by 60-70% for the cases considered. On the contrary, centrifuge axial forces at the end of construction are within ± 17% of ring-compression theory values. Centrifuge axial forces after consolidation are in general larger than ring-compression forces by 0-50% for these shapes. Finally, axial forces calculated from Duncan's method exceed centrifuge values by 10-70%. Figure 79 presents the ratio of centrifuge maximum axial compression force to ring-compression force versus

Table 9
Predictions of Maximum Axial Force and Maximum Bending Moment Using the Methodology Developed by Duncan

Case	Plasticity Index	Density	Rise-to-Span Ratio	Es K/ft	P lps	M ft-k
1	6	136.8	0.4	150	50525	1461
2	16	126.4	0.4	100	46684	1751
3	31	126.8	0.4	50	46758	2441
4	6	136.8	0.5	150	49577	1686
5	16	126.4	0.5	100	45807	2021
6	31	126.8	0.5	50	45880	2817
7	6	136.8	0.6	150	48628	2023
8	16	126.4	0.6	100	44931	2425
9	31	126.8	0.6	50	45073	3385

Span = 27.5 ft.
Height of fill over crown = 16 ft.

Table 10
Ring-Compression Theory

Case	Plasticity	Geometry	Density	Axial Force
1	low	low-profile	136.8	30096
2	medium	low-profile	126.4	27808
3	high	low-profile	126.8	27852
4	low	semicircular	136.8	30096
5	medium	semicircular	126.4	27808
6	high	semicircular	126.8	27852
7	low	high-profile	136.8	30096
8	medium	high-profile	126.4	27808
9	high	high-profile	126.8	27896

Span = 27.5 ft.
Height of fill over crown = 16 ft.

$T = \gamma * H * D/2 = (136.8)*(16)*27.5/2 = 30{,}096$

Table 11
Comparisons of Predictions of Axial Force and Bending Moment

Case	Duncan/ Ring Compr.	Duncan/ Centrifuge	Centrifuge/ Ring Compre.	Centrifuge/ LT/EOC	Centrifuge/ Duncan Moment	Centrifuge EOC/ Ring Compr.
1	1.6788	1.6033	1.0470	1.1200	0.8171	0.9347
2	1.6788	1.6547	1.0145	1.1000	0.8509	0.9226
3	1.6788	1.3757	1.2203	1.2680	0.8882	0.9626
4	1.6472	1.2625	1.3047	1.1000	1.4612	1.1869
5	1.6472	1.3744	1.1985	1.4130	1.6033	0.8484
6	1.6472	1.0904	1.5105	1.4830	1.9299	1.0189
7	1.6157	1.4483	1.1156	1.1200	0.9992	0.9978
8	1.6157	1.5561	1.0382	1.2500	1.0573	0.8307
9	1.6157	1.2765	1.2677	1.4510	1.0657	0.8723

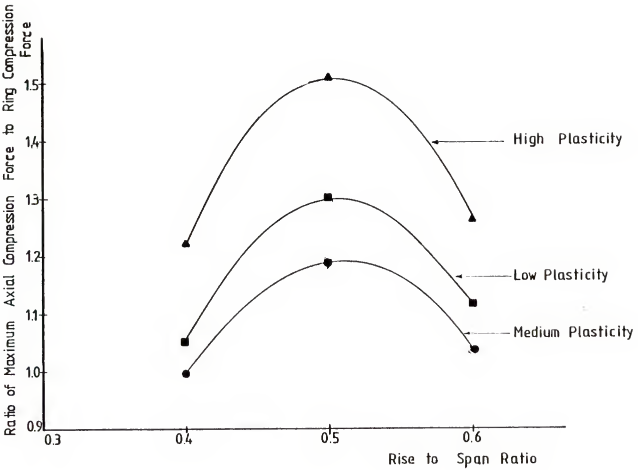

Figure 79. Ratio of Maximum Axial Compression Force to Ring-Compression Force vs R/S

rise-to-span ratio. The relationship is not linear and values for the semicircular arch are substantially higher.

In terms of bending moments it can be seen that centrifuge values are in good agreement for the low- and high-profile structures, whereas for the case of the semicircular arch centrifuge moments are substantially higher (46-93%) than Duncan's method. Figure 80 depicts the ratio of centrifuge moment to Duncan moment versus the ratio of the radii of curvature at the side and crown. It can be seen that there is good agreement between the two predictions for low ratios of radii of curvature but not for the semicircular arch (R1/R2=1). The value for the semicircular arch in high-plasticity soil falls outside the general pattern as expected since this moment causes the section to yield. Figure 81 shows that the ratio of centrifuge moment to Duncan moment increases with increasing plasticity index. Again the value for the semicircular arch in high-plasticity clay falls out of the generalized pattern.

Methodology for Predicting Long-Term Forces and Moments

General

Based on the conclusions which have been derived from the observed behavior of the centrifuge models as well as the comparisons with current design procedures, an attempt

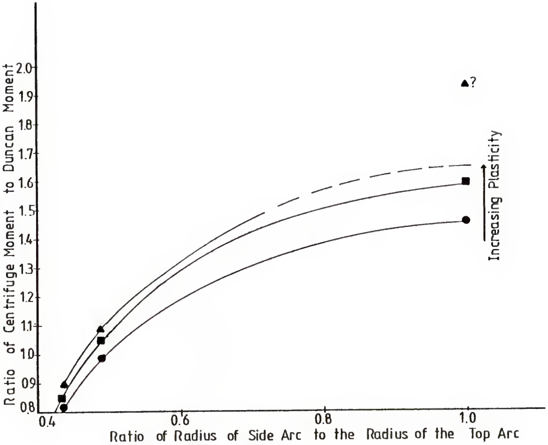

Figure 80. Ratio of Centrifuge Moment to Duncan Moment vs R_1/R_2

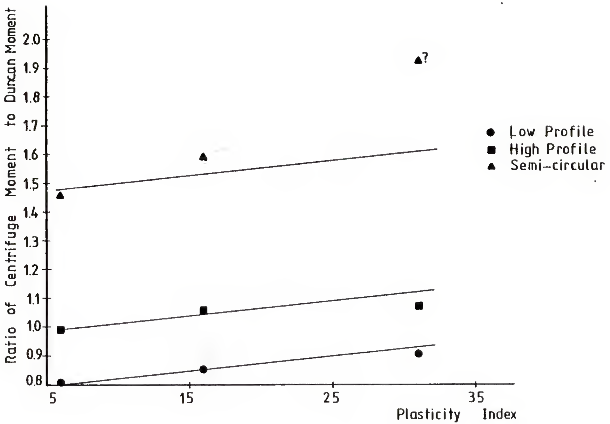

Figure 81. Ratio of Centrifuge Moment to Duncan Moment vs Plasticity Index

is made to provide a simple method that may be employed for estimating the long-term axial forces and bending moments to be used in the design of large-span culvert structures. The proposed method is applicable to large-span flexible (steel or aluminum) single-radius or double-radius arch structures with footings in deep cohesive backfills under static or quasistatic loading conditions where the effect of cyclic vehicular loading can be neglected. The method is not applicable for horizontal or vertical ellipses, circular pipes or pipe arches or structures with special features other than thrust beams or compaction wings. Dynamic effects of earthquakes and traffic loads are not considered.

Current design procedures which are based on past experience, experimental and numerical studies accept that the degree of load transfer from the embankment soil to the structure is dependent upon the following factors: the span of the structure (S), the density of the soil (γ), the height of cover over the structure (H), the rise-to-span ratio (R/S), the flexibility factor (Nf) which varies with the structure span, the secant modulus of the soil (Es), the moment of inertia of the structural plate (I), and the modulus of elasticity of the material (E). However, centrifuge results have shown that radii of curvature at the quarter point and at the crown are also important geometric characteristics and that embankment soil plasticity and compressibility and long-term consolidation should be accounted for in design.

A careful consideration of the results indicates that the maximum ring-compression forces (including long-term effects) determined from centrifuge experiments can be approximated by the following equation:

$$P_{max} = K_{\ell g}\, K_{\ell p}\, \gamma\, HS$$

where $K_{\ell g}$ = Coefficient for axial force to account for structure geometry (Figure 82)

$K_{\ell p}$ = Coefficient for axial force to account for soil plasticity and consolidation (Figure 83)

γ = Soil density

H = Height of soil cover over the crown

S = Culvert span.

Bending Moments

Maximum bending moments can be estimated using the equation

$$M_b = K_{\ell m}\, (R/S)\, \sqrt{R1/R2}\; \gamma\, S^3 = K_{mp}\, \sqrt{R1/R2}\; S^2\, R$$

where $K_{\ell m}$ = Coefficient for bending moment to account for soil plasticity and consolidation (Figure 84)

R = Culvert height

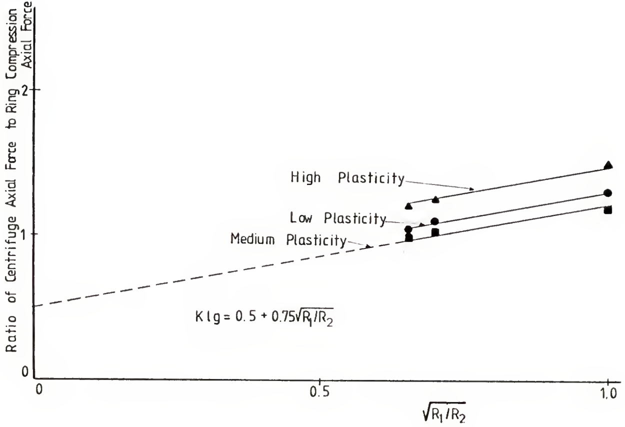

Figure 82. Ratio of Maximum Axial Compression Force to Ring-Compression Force vs $\sqrt{R_1/R_2}$

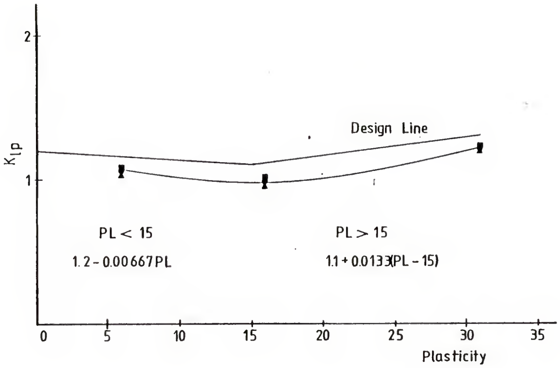

Figure 83. Coefficient of Axial Force to Account for Soil Plasticity and Consolidation

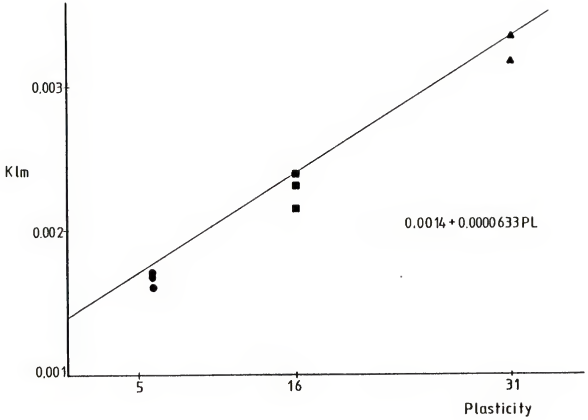

Figure 84. Coefficient of Bending Moment to Account for Soil Plasticity

S = Culvert span
R1 = Radius of curvature of side arc
R2 = Radius of curvature of top arc.

Limitations of Recommended Method

The methodology presented herein is not intended to replace current design methods and procedures which have been extensively used successfully, but rather to provide a tool for comparison with future long-term information with respect to forces and moments. However, the following limitations apply to the recommended methodology:

1. The values obtained, correspond to the specific drainage conditions that were encountered in the centrifuge study. The magnitude of these values may increase for drainage conditions which allow full dissipation of pore pressure.
2. The effect of the flexibility number was not investigated. However, the effect of this parameter is small for the range of structures considered.

CHAPTER TEN
CONCLUSION

Review of Objectives

The objectives of this study were described previously as follows:

1. to validate, improve and confer centrifuge modeling of large-span culverts
2. to provide insight to the long-term behavior of large-span culverts with emphasis on the effects of structure geometry and backfill plasticity
3. to recommend a method such that long-term forces and moments on large-span flexible culverts can be estimated.

Summary of Results

Validation of the Model

The comparison of the experimental model with the numerical model has shown reasonable agreement with respect to axial stresses and bending stresses in the culvert wall. The finite element analyses have shown that the axial stiffness is not a controlling parameter in the load transfer interaction phenomenon between structure and surrounding soil. Furthermore, there was very little difference between results of the finite element analyses in which the foundation connection was fixed from rotation and those in which it was free to rotate. Thus, in the case of the centrifuge model no significant errors are introduced in the simulation of the prototype due to this parameter.

Long-Term Soil-Structure Interaction

Stresses. The study has shown a definite increase of axial stresses and bending stresses with time. Increases of as much as 50% for axial stresses and 100% for bending stresses have been observed. Axial stresses increased uniformly from the crown to the springline for the low- and high-profile arches but a nonuniform distribution was observed in the case of the semicircular arch. In particular axial stress decreased at the thrust beam location while increasing at the crown and springline locations. This is associated with the large bending stress which develops at this location. In general maximum bending stresses occurred at the thrust beam location for all shapes.

The centrifuge study has shown axial stresses to be a function of $\sqrt{R_1/R_2}$ rather than rise-to-span ratio. Similarly, bending stresses have been shown to be a function of $(R/S)(\sqrt{R_1/R_2})$ rather than rise-to-span ratio only.

Three aspects of soil-structure interaction were defined in terms of soil plasticity. First, the compaction induced pressure during backfilling against the sides. Second, the lateral restraint due to passive pressure development during backfilling over the top and third, the consolidation effect. The effect of soil plasticity is manifested as the combination of these three aspects: axial stresses are larger for low- and high-plasticity soils while they reach a minimum for medium-plasticity soils. Bending stresses increase with increasing embankment soil plasticity. In general the distribution of stresses was found to be controlled by geometry whereas the magnitude was controlled by embankment soil plasticity and compressibility.

Deformations

Upward movement of the crown was observed during backfilling against the sides and downward movement during backfilling over the top. The low-profile arch experiences small crown movements while the high-profile arch experiences the largest crown movements. The magnitude of net upward and downward movement is controlled by soil plasticity for each shape. The low- and high-profile arches exhibit the same type of long-term behavior. The crown subsides as time progresses until it reaches equilibrium. In the case of the semicircular arch the crown rises as time progresses until it reaches equilibrium. The information obtained from the photographic technique concerning soil movement is compatible with LVDT information.

Pore Pressures

The shapes of the pore-pressure development and dissipation curves did not significantly differ from one geometry to another. Soil plasticity and compressibility are the most important factors concerning this phenomenon, as expected. A clear dissipation curve was not evident in the case of the high-plasticity soil due to the soil-structure interaction effect as discussed earlier. Pore-pressures became constant at approximately 2-4 psi indicating that full dissipation did not occur. This is due to the fact that water could not escape from the container. The long-term effect would be further accentuated if different drainage conditions existed that would allow full dissipation of pore pressure to take place.

Conclusions

The following conclusions were derived.

Evaluation of the Centrifuge Model

1. The centrifuge has been proven to be an excellent means of duplicating the complex soil-structure interaction of large-span flexible culverts.

2. The experimental model has been improved by modeling the bending stiffness of the structure rather than the moment of inertia. On the other hand axial stiffness and fixity of support did not significantly alter the system's response.

Soil-Structure Interaction

1. The distribution of axial and bending stresses is primarily dependent on structure geometry whereas the magnitude is dependent on soil compressibility.
2. The deformed shape of the structure is primarily dependent on geometry whereas the magnitude of deformations is dependent on both structure geometry and soil compressibility.
3. Bending stress concentrations were observed at the thrust beam location for all shapes. However, due to the different deflected shape in the case of the semicircular arch, the mode of failure for this structure is different than the other two. This shape will fail due to development of plastic hinges at the thrust beams and crown due to excessive inward movement at the thrust beam location and upward movement of the crown. Failure in the low- and high-profile arches will be due to continuous subsidence of the crown and outward movement of the thrust beam.

4. The time required for the structural changes to occur as well as the magnitude of these changes is dependent upon backfill permeability and compressibility as well as drainage conditions.

Design Recommendations

1. End of construction axial stresses as predicted by the centrifuge were closer to ring-compression theory values than Duncan's method predictions.
2. Axial stresses were found to be proportional to the square root of the ratio of radius of curvature of the side arc to that of the top arc rather than rise-to-span ratio. Maximum axial stresses occurred for the low- and high-plasticity soil.
3. Bending stresses were found to be proportional to $(R/S)(\sqrt{R_1/R_2})$ and to soil plasticity index.
4. Bending moments are, in general, in good agreement with Duncan's values for the low- and high-profile arches but not for the semicircular arch.
5. Maximum bending movements were observed at two time frames: first, during backfilling, when the height of backfill reaches the top of the crown; and second, at the end of long-term. However, the second case is more critical with respect to yielding of the section since it is accompanied by a larger axial force.

6. A limited methodology has been recommended to evaluate long-term forces and moments, based on centrifugal results.

Recommendations

1. Further research in this area is necessary to validate, improve or confer results from this study. Also, research into the influence of backfill depth and boundary drainage conditions must be undertaken.
2. Development of rate dependent constitutive models which will be incorporated in finite element analyses must be undertaken to study the long-term soil-structure interaction of large-span flexible culverts.
3. Finally, further full-scale instrumentation studies on prototypes for a long period of time are strongly recommended.

APPENDIX A
DIMENSIONAL ANALYSIS OF A SUBSURFACE LARGE-SPAN FLEXIBLE CONDUIT

The parameters which influence the behavior of the system were established and are listed in Table 12. There are three main categories of system parameters:

1. geometric parameters
2. material parameters
3. parameters describing the loading configuration.

The dimensional matrix is given in Table 13 and the dimensionless pi terms are listed in Table 14.

Similitude requires that the pi terms are equal in model and prototype, thus the following equations must be satisfied:

$$\frac{I_m}{D_m^3} = \frac{I_p}{D_p^3} \quad \therefore \quad \frac{I_m}{I_p} = \left(\frac{D_m}{D_p}\right)^3 \qquad (1)$$

$$\frac{t_m}{D_m} = \frac{t_p}{D_p} \quad \therefore \quad \frac{t_m}{t_p} = \frac{D_m}{D_p} \qquad (2)$$

$$\frac{h_m}{D_m} = \frac{h_p}{D_p} \quad \therefore \quad \frac{h_m}{h_p} = \frac{D_m}{D_p} \qquad (3)$$

Table 12
System Parameters

Parameter	Symbol	Dimension
Geometry		
Moment of inertia per unit length	I	L^3
Thickness of wall	t	L
Culvert span	D	L
Culvert height	h	L
Width of trench	B	L
Depth of cover	H	L
Material Properties of Culvert		
Young's modulus	E_m	FL^{-2}
Poisson ratio	ν	-
Tensile strength	F_y	FL^{-2}
Unit weight	W_m	FL^{-3}
Material Properties of Clay		
Grain diameter	d_c	L
Void ratio	e_c	-
Unit weight	W_c	FL^{-3}
Friction angle	ϕ_c	-
Material Properties of Sand		
Grain diameter	d_s	L
Void ratio	e_s	-
Unit weight	W_s	FL^{-3}
Friction angle	ϕ_s	-
Dependent Parameter		
Stress	σ	FL^{-2}

Table 12--continued.

Parameter	Symbol	Dimension
Reference Variables		
Culvert span	D	L
Unit weight of clay	W_c	FL^{-3}

Table 13
Dimensional Matrix

Symbol	Dimension of Reference Variable 1 (D)	Dimension of Reference Variable 2 (W_c)	
I	3	0	I/D^3
t	1	0	t/D
D	1	0	
h	1	0	h/D
B	1	0	B/D
H	1	0	H/D
E_m	1	1	E_m/W_cD
ν	0	0	ν
F_y	1	1	F_y/W_cD
W_m	0	1	W_m/W_c
d_c	1	0	d_c/D
e_c	0	0	e_c
W_c	0	1	W_c
ϕ_c	0	0	ϕ_c
d_s	1	0	d_s/D
e_s	0	0	e_s
W_s	0	1	W_s/W_c
ϕ_s	0	0	ϕ_s

Table 14
Pi Terms

π_1	I/D^3
π_2	t/D
π_3	h/D
π_4	B/D
π_5	H/D
π_6	E_m/W_cD
π_7	F_y/W_cD
π_8	W_m/W_c
π_9	d_c/D
π_{10}	d_s/D
π_{11}	W_s/W_c
π_{15}	σ/W_cD
π_{17}	ν
π_{18}	e_c
π_{19}	ϕ_c
π_{20}	e_s
π_{21}	ϕ_s

$$\frac{B_m}{D_m} = \frac{B_p}{D_p} \quad \therefore \quad \frac{B_m}{B_p} = \frac{D_m}{D_p} \tag{4}$$

$$\frac{H_m}{D_m} = \frac{H_p}{D_p} \quad \therefore \quad \frac{H_m}{H_p} = \frac{D_m}{D_p} \tag{5}$$

$$\frac{E_{mm}}{W_{cm} D_m} = \frac{E_{mp}}{W_{cp} D_p} \quad \therefore \quad \frac{E_{mm}}{E_{mp}} = \frac{W_{cm}}{W_{cp}} \frac{D_m}{D_p} \tag{6}$$

$$\frac{F_{ym}}{W_{cm} D_m} = \frac{F_{yp}}{W_{cp} D_p} \quad \therefore \quad \frac{F_{ym}}{F_{yp}} = \frac{W_{cm}}{W_{cp}} \frac{D_m}{D_p} \tag{7}$$

$$\frac{W_{mm}}{W_{cm}} = \frac{W_{mp}}{W_{cp}} \quad \therefore \quad \frac{W_{mm}}{W_{mp}} = \frac{W_{cm}}{W_{cp}} \tag{8}$$

$$\frac{d_{cm}}{D_m} = \frac{d_{cp}}{D_p} \quad \therefore \quad \frac{d_{cm}}{d_{cp}} = \frac{D_m}{D_p} \tag{9}$$

$$\frac{d_{sm}}{D_m} = \frac{d_{sp}}{D_p} \quad \therefore \quad \frac{d_{sm}}{d_{sp}} = \frac{D_m}{d_p} \tag{10}$$

$$\frac{W_{sm}}{W_{cm}} = \frac{W_{sp}}{W_{cp}} \quad \therefore \quad \frac{W_{sm}}{W_{sp}} = \frac{W_{cm}}{W_{cp}} \tag{11}$$

$$\frac{\sigma_m}{W_{cm}D_m} = \frac{\sigma_p}{W_{cp}D_p} \quad \therefore \quad \frac{\sigma_m}{\sigma_p} = \frac{W_{cm}}{W_{cp}}\frac{D_m}{D_p} \tag{12}$$

$$\nu_m = \nu_p \tag{13}$$

$$e_{cm} = e_{cp} \tag{14}$$

$$\phi_{cm} = \phi_{cp} \tag{15}$$

$$e_{sm} = e_{sp} \tag{16}$$

$$\phi_{sm} = \phi_{sp} \tag{17}$$

Assuming that the culvert span is scaled by a factor n, these equations are reduced to the following:

$$\frac{t_m}{t_p} = \frac{h_m}{h_p} = \frac{B_m}{B_p} = \frac{H_m}{H_p} = \frac{d_{cm}}{d_{cp}} = \frac{d_{sm}}{d_{sp}} = \frac{D_m}{D_p} = \frac{1}{n} \tag{18}$$

$$\frac{I_m}{I_p} = \left(\frac{D_m}{D_p}\right)^3 = \frac{1}{n^3} \qquad (19)$$

$$\frac{E_{mm}}{E_{mp}} = \frac{F_{ym}}{F_{yp}} = \frac{\sigma_m}{\sigma_p} = \left(\frac{W_{cm}}{W_{cp}}\right) \frac{D_m}{D_p} = \left(\frac{W_{cm}}{W_{cp}}\right) \frac{1}{n} \qquad (20)$$

Since we recognize that the same stress has to be stimulated in the model as in the prototype

$$\frac{\sigma_m}{\sigma_p} = 1 \quad \therefore \quad \frac{W_{cm}}{W_{cp}} \frac{1}{n} = 1 \quad \therefore \quad W_{cm} = n\ W_{sp} \qquad (21)$$

which means that the unit weight of the model soil must be increased by a factor n. This of course can only be achieved in an artificial gravitational field. The centrifugal acceleration due to circular motion is a most convenient type of such field and is simulated in the centrifuge. Equation 20 requires also that

$$\frac{E_{mm}}{E_{mp}} = \frac{F_{ym}}{F_{yp}} = \frac{\sigma_m}{\sigma_p} = 1$$

which means that the culvert model must have the same modulus of elasticity and yield strength as the prototype.

APPENDIX B
DESIGN OF ARTIFICIAL PROTOTYPE INSTALLATION

For numerical and centrifuge modeling purposes an artificial prototype installation was selected and designed based on an acceptable design methodology. The most common current procedure is that suggested by ARMCO.

The characteristics of the prototype installation are the following:

1. Height of cover, $H = 16$ ft.
2. Span, $D = 27.5$ ft.
3. Weight of soil, $W = 120$ lb/ft.

The equivalent dead load due to highway loading is negligible thus

$$Pv = K * DL = 1.0 * 16 * 120 = 1920 \text{ lb/ft.}$$

Compressive force $C = Pv * S/2 = 1920 * 27.5/2 = 26400$ lb/ft. The allowable wall stress is determined as

$$fc = fb/2$$

For a gage 5 plate $r = 0.690$ and $D/r = 478$. Therefore,

$fb = 21553$ psi, $fc = 10776$ psi and $A = C/fc = 2.5$ sq.in./ft. required. Gage 5 provides 3.199 sq.in./ft. of uncoated area. Handling stiffness is checked with the flexibility factor $FF = D/EI = (330)/30 * 10 * 0.1269 = 0.028 < 0.03$ which is the recommended AASHTO value. Therefore, a 6 x 2 gage 5 plate is selected, from the *Sectional Plate Handbook* of the Republic Steel Corporation (1977).

APPENDIX C
DATA REDUCTION

Stresses

Voltages from strain gages were recorded by an HP3497 data acquisition system and converted to strains. Due to the uniform section of the culvert along its longitudinal axis a plane strain condition exists in the soil-structure system. The longitudinal strain is given by

$$\varepsilon_z = \frac{1}{E}(\sigma_z - \mu\sigma_x) = 0$$

and subsequently the stress

$$\sigma_z = \mu\sigma_x$$

Lateral strains are found from the following equation:

$$\varepsilon_x = \frac{1}{E}(\sigma_x - \mu^2\sigma_x) = \frac{\sigma_x}{E}(1 - \mu^2) \qquad (1)$$

In general the culvert is undergoing both axial and bending stress; hence,

$$\sigma_x = \sigma_a + \sigma_b$$

where σ_a = axial stress

σ_b = bending stress.

Equation 1 may be reduced to

$$\varepsilon_x = \frac{\sigma_a}{E}(1 - \mu^2) + \frac{\sigma_b}{E}(1 - \mu^2)$$

or

$$\varepsilon_x = \varepsilon_a + \varepsilon_b$$

where

$$\varepsilon_a = \frac{\sigma_a}{E}(1 - \mu^2) \tag{2}$$

$$\varepsilon_b = \frac{\sigma_b}{E}(1 - \mu^2) \tag{3}$$

which means that the strain distribution in a section of the culvert wall is the superposition of axial strain and bending strain (Figure 85). Therefore, in the case of a pair of strain gages mounted on the outside and inside extreme fibers the strains are

$$\varepsilon_0 = \varepsilon_a - \varepsilon_b$$

$$\varepsilon_i = \varepsilon_a + \varepsilon_b$$

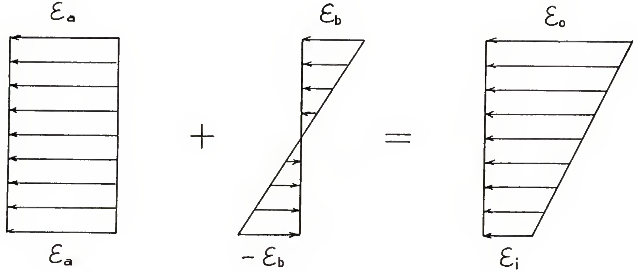

Figure 85. Strain Distribution in the Culvert Wall

where ε_o = outside strain

ε_i = inside strain.

As a result the summation of the readings from a pair of strain gages is

$$\varepsilon_o + \varepsilon_i = 2\varepsilon_a$$

or

$$\varepsilon_a = \frac{\varepsilon_o + \varepsilon_i}{2} \qquad (4)$$

Similarly

$$\varepsilon_b = \frac{\varepsilon_o - \varepsilon_i}{2} \qquad (5)$$

Equations 4 and 5 form the basis for the reduction of strain gage data into axial and bending strains, and equations 2 and 3 were used to obtain bending and axial stresses.

Deformations

Values were recorded by hand from the Doric transducer indicator 420. An initial reading was taken and subsequent readings were relative to the first reading. The differences between each reading and the initial reading were calculated and multiplied by the calibration factor for the LVDT. The calibration factor was determined prior to each test. All values of model crown deformations were multiplied by the scale factor in order to convert to prototype deformations.

Pore Pressures

Values were recorded by hand from a Doric transducer indicator 420. An initial reading was taken and pore pressures were calculated in a similar manner as in the case of deformations using a calibration factor.

Photographic Technique

Deformations of the embankment soil were measured using the photographic technique. The technique involved measurement of the coordinates of pins placed in the embankment soil relative to the constant coordinates of indelible marks on the transparent (plexiglass) side of the container. Photos were taken from the same location every time, such that the axis of the camera lens was perpendicular to the plexiglass. The coordinates of each pin were measured with a Swiss Kern DSR-1 device which is accurate to one micron. An inch long mark permanently drawn on the container was used to determine the scale of each photograph.

APPENDIX D
EQUIVALENT MODEL TIME DURING THE COMPACTION OF A LIFT

It has been shown earlier that diffusion time is scaled in the centrifuge with a factor of n^2. Hence,

$$t_p = n^2 t_m$$

Since acceleration increases linearly with time

$$n = \frac{A}{SUT} t_m$$

where n = acceleration at any time during start up

SUT = start up time duration

A = test acceleration level

t_m = model time.

As a result prototype time at any instant is

$$dt_p = n^2 dt_m = (\frac{A}{SUT} t_m)^2 \ dt_m$$

and prototype elapsed time at the end of start up duration

$$PET = \int_o^t (\frac{A}{SUT})^2 \ t_m^2 dt_m$$

which is the formula suggested by Bloomquist et al. (1984) to be used in order to account for start up time in the consolidation process. Considering the case of

$$A = 55 \text{ gs}$$

$$SUT = 3 \text{ min.}$$

$$PET = \left[\left(\frac{55}{3.0}\right)^2 \frac{t_m^3}{3}\right]_o = \left(\frac{55}{3.0}\right)^2 \frac{27}{3}$$

$$PET = 3025 \text{ min.}$$

Since acceleration level varies with time as shown in Figure 86, the prototype elapsed time to compact each lift is

$$3025 + (55)^2 \times 3.0 + 3025 = 15135 \text{ min.} = 10.5 \text{ days}$$

which is equivalent to 5 min. model time.

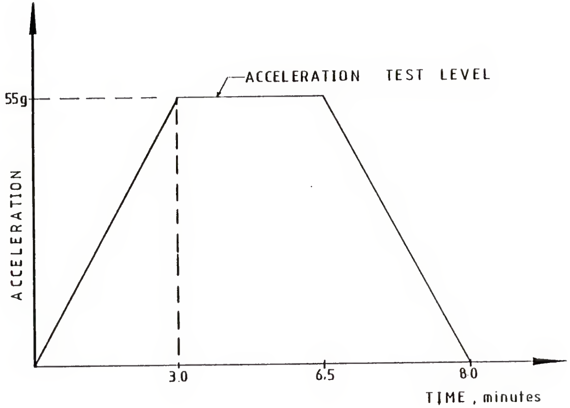

Figure 86. Variation of Centrifugal Acceleration Level During the Compaction of a Lift

REFERENCES

Abbott, P.A., "Arching for Vertically Buried Prismatic Structures," *Proc. ASCE*, Vol. 93, No. SM5, Sept., 1967, pp. 233-255.

Abel, J.F., and Mark, R., "Soil Stresses Around Flexible Elliptical Pipes," *Journal of the Soil Mechanics and Foundation Engineering Division*, ASCE, Vol. 99, No. SM7, July, 1973, pp. 509-526.

American Iron and Steel Institute (AISI), *Handbook of Steel Drainage and Highway Construction Products*, Author, Washington, D.C., 1967.

Armco Drainage and Construction Products, Inc., *Handbook of Drainage and Construction Products*, AISI, Middletown, Oh., 1958.

Arthur, J.R.F., and Roscoe, K.H., "An Examination of the Edge Effects in Plane-Strain Model Earth Pressure Tests," *Proc. 6th Int. Conf. on SM & FE*, Montreal, Vol. 2, 1965, pp. 363-367.

Avgherinos, P.J., "Centrifugal Testing of Models Made of Soil," Ph.D. Thesis, University of Cambridge, England, 1969.

Beal, B.D., "Field Tests of Long-Span Aluminum Culvert," *Journal of the Geotechnical Engineering Division*, ASCE, Vol. 108, No. GT6, June, 1982, pp. 873-889.

Beasley, D.H., "Centrifugal Modelling of Soft Clay Strata Subject to Embankment Loading," Ph.D. Thesis, University of Cambridge, England, 1973.

Bloomquist, D., "Centrifuge Modeling of Large Strain Consolidation Phenomena in Phosphatic Clay Retention Ponds," Ph.D. Dissertation, University of Florida, Gainesville, 1982.

Bloomquist, D., Davidson, J.L., and Townsend, F.C., "Platform Orientation and Start-Up Time During Centrifuge Testing," *ASTM Geotechnical Testing Journal*, Vol. 7, No. 4, 1984, pp. 195-199.

Brown, C.B., "Forces on Rigid Culverts Under High Fills," Proc. ASCE, Vol. 93, No. ST5, Oct., 1967, pp. 195-215.

Brown, C.B., Green, D.R., and Pawsey, S., "Flexible Culverts Under High Fills," Proc. ASCE, Vol. 94, No. ST4, April, 1968, pp. 905-917.

Buckingham, E., "On Physically Similar System: Illustrations of the Use of Dimensional Analysis," Phys. Rev., Vol. 4, 1914, pp. 345-376.

Chang, C.S., Espinoza, J.M., and Selig, E.T., "Computer Analysis of Newtown Creek Culvert," Journal of the Geotechnical Engineering Division, ASCE, Vol. 106, No. GT5, May, 1980, pp. 531-556.

Croce, P., "Evaluation of Consolidation Theories by Centrifuge Model Tests," M.Sc. Thesis, University of Colorado, 1982.

Davidson, J.L., and Bloomquist, D., "Centrifuge Modeling of the Consolidation/Sedimentation Process in Phosphatic Clays," Engineering and Industrial Experiment Station, Research Report 245 W6S, University of Florida, Gainesville, 1980.

Duncan, J.M., "A Design Method for Metal Culvert Structures Based on Finite Element Analyses," presented at Transportation Research Board Annual Meeting, Washington, D.C., Jan., 1976a.

Duncan, J.M., "Finite Element Analysis of Buried Flexible Metal Culvert Structures," Laurits Bjerrum Memorial Volume, N. Tambu, F. Jørstad and B. Kjoernsli, eds., Norwegian Geotechnical Institute, Oslo, Norway, 1976b, pp. 213-222.

Duncan, J.M., "Behavior and Design of Long-Span Metal Culverts," Journal of the Geotechnical Engineering Division, ASCE, Vol. 105, No. GT3, March, 1979, pp. 399-418.

Duncan, J.M., Byrne, P., Wong, K.S., and Mabry, P., "Strength, Stress-Strain and Bulk Modulus Parameters for Finite Element Analysis of Stresses and Movements in Soil Masses," Report No. UGB/GT/80-01, University of California at Berkeley, Aug., 1980.

Duncan, J.M., and Seed, B.R., "Compaction-Induced Earth Pressures Under Ko-Conditions," Journal of the Geotechnical Engineering Division, ASCE, Vol. 112, No. 1, Jan., 1986, pp. 1-22.

Duns, C.S., and Butterfield, R., "Flexible Buried Cylinders, Part 1--Static Response," Int. Journal Rock Mech. Min. Sci., Vol. 8, 1971, pp. 577-600.

Endicott, L.J., "Centrifugal Testing of Soil Models," Ph.D. Thesis, University of Cambridge, England, 1970.

ENR, "Culvert Failure Kills Five," Engineering News Record, Jan., 1983, p. 12.

James, R.G., "Some Aspects of Soil Mechanics Model Testing," Stress Strain Behaviour of Soils, Proc. Roscoe Memorial Symposium, Cambridge, England, G.T. Foulis, Henley-on-Thames, 1972, pp. 417-440.

Janbu, N., "Soil Compressibility as Determined by Oedometer and Triaxial Tests," Proceedings European Conference on Soil Mechanics and Foundation Engineering, Wisbaden, Germany, Vol. 1, 1963.

Katona, M.G., Forrest, J.B., Odello, R.J., and Allgood, J.R., "Computer Design and Analysis of Pipe Culverts," Interim Technical Report No. 51-040, Contract No. FHWA 3-1-1170, Civil Engineering Laboratory, Port Hueneme, Calif., Oct., 1974.

Katona, M.G., Smith, J.M., Odello, R.S., and Allgood, J.R., "CANDE--Engineering Manual--A Modern Approach for Structural Design and Analysis of Buried Culverts," Report No. FHWA-RD-77-5, Federal Highway Administration, Port Hueneme, Calif., Oct., 1976.

Kondner, R.L., "Hyperbolic Stress-Strain Response: Cohesive Soils," Proc. ASCE, Vol. 89, No. SM1, Feb., 1963, pp. 115-143.

Kondner, R.L., and Zelasko, J.S., "A Hyperbolic Stress-Strain Formulation for Sands," Proc. 2nd Pan-American Conf. on SM & FE, Brazil, Vol. 1, 1963, pp. 289-324.

Lambe, T.W., and Whitman, R.V., Soil Mechanics, John Wiley and Sons, Inc., New York, 1st Edition, 1969.

Larsen, H., "Earth Pressures Around Buried Pipes," Ph.D. Thesis, Cambridge University, England, 1977.

Lefebvre, G., Lalibrete, M., Lefebvre, L.M., Lafleur, J., and Fisher, C.L., "Measurement of Soil Arching Above a Large Diameter Flexible Culvert," Canadian Geotechnical Journal, Vol. 13, No. 1, Feb., 1976, pp. 58-71.

Leonards, G.A., Juang, C.H., Wu, T.H., and Stetkar, R.E., "Predicting Performance of Buried Metal Conduits," Transportation Research Record 1008, TRB, National Research Council, Washington, D.C., 1985, pp. 42-52.

Leonards, G.A., and Wu, T.H., "Predicting Performance of Buired Conduits," Report No. 6-36-62F, Final Report to Indiana State Highway Commission and FHWA, Engineering and Experiment Station, Purdue University, W. Lafayette, Ind., March, 1981.

Luscher, U., and Hoeg, K., "The Interaction Between a Structural Tube and the Surrounding Soil," Report RTD-TDR-63-3109, Air Force Weapons Lab, Kiutland Air Force Base, N.M., 1965.

Marston, A., "The Theory of External Loads on Closed Conduits in the Light of the Latest Experiments," Iowa Engineering Experiment Station, Bulletin 96, 1930.

McVay, M.C., "Evaluation of Numerical Modeling of Buried Conduits," Ph.D. Dissertation, University of Massachusetts, Amherst, 1982.

McVay, M., and Papadopoulos, P., "Long-Term Behavior of Buried Large-Span Culverts," Journal of the Geotechnical Engineering Division, ASCE, Vol. 112, No. GT4, April, 1986, pp. 424-442.

McVay, M.C., and Selig, E.T., "Performance and Analysis of a Long-Span Culvert," Transportation Research Record No. 878, Jan., 1982, pp. 23-29.

McVay, M.C, and Selig, E.T., "Predicted and Measured Response of East Liberty, Ohio Embankment Installation," Report No. ACP81-279I, Department of Civil Engineering, University of Massachusetts, Amherst, Ma., June, 1981.

Mikasa, M., and Takada, N., "Significance of Centrifugal Model Test in Soil Mechanics," Proc. 8th Int. Conf. on SM & FE, Moscow, Russia, Vol. 1.2, 1973, pp. 273-278.

Morris, D.V., "The Centrifugal Modelling of Dynamic Soil-Structure Interation and Earthquake Behavior," Ph.D. Thesis, Cambridge University, England, June, 1979.

Ovesen, N.K., "Modelforsøg Med Betonrør i Jor Udført i en Centrifuge," Engineering Academy of Denmark, Civil Engineering Department, 1971.

Papadopoulos, P.C., "Centrifuge Modeling of Long-Term Effects on Large-Span Flexible Culverts," M.Sc. Thesis, University of Florida, Gainesville, 1985.

Pokrovsky, G.I., and Fyodorov, I.S., "Studies of Soil Pressures and Soil Deformations by Means of a Centrifuge," Proc. 1st Int. Conf. on SM & FE, Harvard University, Vol. 1, 1936, p. 70.

Pokrovsky, G.I., and Fyodorov, I.S., "Centrifugal Model Testing in the Construction Industry," Stroiizdat, Moscow. In draft translation by Building Research Establishment (Aug., 1975), 1968.

Pokrovsky, G.I., and Fyodorov, I.S., "Centrifugal Model Testing in the Mining Industry," 'NIEDRA' Publishing House, Moscow. In draft translation by Building Research Establishment (Aug., 1975), 1969.

Sabnis, G.M., Harris, H.G., White, R.N., and Mivza, M.S., Structural Modeling and Experiment Technique, Prentice-Hall Civil Engineering and Engineering Mechanics Series, Prentice-Hall Inc., Englewood Cliffs, N.J., 1983.

Schofield, A.N., "Use of Centrifugal Model Testing to Assess Slope Stability," Cdn. Geot. J., Vol. 15, No. 1, 1978. pp. 14-31.

Scott, R.F., and Morgan, N.R., "Feasibility and Desirability of Constructing a Very Large Centrifuge for Geotechnical Studies," Report 760-170, Calif. Inst. of Tech. for NSF, 1977.

Sectional Plate Handbook, Republic Steel Corporation, Drainage Product Division, Canton, Oh., 1977.

Selig, E.T., "Instrumentation of Large Buried Culverts," Performance Monitoring for Geotechnical Construction, ASTM STP 584, American Society for Testing and Materials, 1975, pp. 159-181.

Selig, E.T., "Large Buried Metal Culvert Design and Construction," Proceedings 11th Ohio River Valley Soil Seminar on Earth Pressures and Retaining Structures, Clarksville, In., Oct., 1980.

Selig, E.T., "Review of Specifications for Buried Corrugated Metal Conduit Installations," Transportation Research Record 1008, TRB, National Research Council, Washington, D.C., 1985, pp. 15-21.

Selig, E.T., Abel, J.F., Kulhawy, F.H., and Falby, W.E., "Review of the Design and Construction of Long-Span Corrugated-Metal Buried Conduits," Report No. FHWA/RD-77-131, Federal Highway Administration, Washington, D.C., Aug., 1977.

Selig, E.T., Lockhart, C.W., and Lawtensleyer, R.W., "Measured Performance of Newtown Creek Culvert," Journal of the GT Division, ASCE, Vol. 105, No. 6T9, Sept., 1979, pp. 1067-1087.

Spangler, M.G., "Long-Time Measurement of Loads on Three Pipe Culverts," Highway Research Record No. 443, 1973, pp. 1-14.

Spangler, M.G., "The Structural Design of Flexible Pipe Culverts," Bulletin No. 153, Engineering Experimental Station, Iowa State College, 1941.

Spannagel, D.W., Davis, R.E., and Backer, A.E., "Effects of Method A and B Backfill on Flexible Culverts Under High Fills," Transportation Research Record No. 510, 1974.

Takada, N., Tohda, J., and Mikasa, M., "Model Test of Ditch Conduit in Centrifuge," Proceedings of International Symposium on Geotechnical Centrifuge Model Testing, Tokyo, April, 1984, pp. 1-6.

Terzaghi, K., Theoretical Soil Mechanics, John Wiley and Sons, Inc., New York, 1943.

Trott, J.J., Taylor, R.N., and Symons, I.F., "Tests to Validate Centrifuge Modeling of Flexible Pipes," The Application of Centrifuge Modeling to Geotechnical Design, University of Manchester Engineering Department, 1984, pp. 226-254.

Voellmy, A., "Eingebettete Rohre," Eidgenössischen Technischen Hochschule in Zürich, 1937.

White, H.L., and Layer, J.P., "The Corrugated Metal Conduit as a Compression Ring," Proceedings, Highway Research Board, Vol. 39, 1960, pp. 389-397.

Woodward, B.M., "Comparison of Centrifuge and Numerical Modeling of Large-Span Flexible Culverts in Sand," M.Sc. Thesis, University of Florida, Gainesville, 1986.

Zienkiewicz, O.C., The Finite Element Method, 3rd Edition, McGraw-Hill Book Co., London, England, 1977.

BIOGRAPHICAL SKETCH

I was born on the island of Cyprus in the Mediterranean Sea. I grew up in the city of Limassol where I attended school. After graduating in 1978, I joined the military forces for two years. Upon completion of my military service, I came to the University of Florida to pursue a bachelor and subsequently a master's degree in the area of civil engineering. I continued my studies for the doctorate degree. During this period, I became a member of the American Society of Civil Engineers, the American Concrete Institute and Tau Beta Pi.

My immediate goal is to return to Cyprus and work in civil engineering design.

I certify that I have read this study and that in my opinion it conforms to acceptable standards of scholarly presentation and is fully adequate, in scope and quality, as a dissertation for the degree of Doctor of Philosophy.

Frank C. Townsend

Frank C. Townsend, Chairman
Professor of Civil Engineering

I certify that I have read this study and that in my opinion it conforms to acceptable standards of scholarly presentation and is fully adequate, in scope and quality, as a dissertation for the degree of Doctor of Philosophy.

Michael C. McVay

Michael C. McVay, Cochairman
Associate Professor of Civil
Engineering

I certify that I have read this study and that in my opinion it conforms to acceptable standards of scholarly presentation and is fully adequate, in scope and quality, as a dissertation for the degree of Doctor of Philosophy.

John L. Davidson

John L. Davidson
Professor of Civil Engineering

I certify that I have read this study and that in my opinion it conforms to acceptable standards of scholarly presentation and is fully adequate, in scope and quality, as a dissertation for the degree of Doctor of Philosophy.

Duane S. Ellifritt

Duane S. Ellifritt
Professor of Civil Engineering

I certify that I have read this study and that in my opinion it conforms to acceptable standards of scholarly presentation and is fully adequate, in scope and quality, as a dissertation for the degree of Doctor of Philosophy.

Loukas G. Arvanitis

Loukas G. Arvanitis
Professor of Forest Resources
and Conservation

This dissertation was submitted to the Graduate Faculty of the College of Engineering and to the Graduate School and was accepted as partial fulfillment of the requirements for the degree of Doctor of Philosophy.

May, 1987

Hubert A. Bevis
Dean, College of Engineering

Dean, Graduate School